BIOINFORMATICS ANALYSIS OF CONTROL MECHANISMS OF BURN AND SEPSIS INDUCED INFLAMMATORY RESPONSE

by

MEHMET ALI ORMAN

A dissertation submitted to the

Graduate School-New Brunswick

Rutgers, The State University of New Jersey

In partial fulfillment of the requirements

For the degree of

Doctor of Philosophy

Graduate Program in Chemical and Biochemical Engineering

Written under the direction of

Dr. Marianthi G. Ierapetritou, Dr. Francois Berthiaume, and Dr. Ioannis P. Androulakis

and approved by

_____

_____

_____

_____

_____

New Brunswick, New Jersey

October, 2011

ABSTRACT OF DISSERTATION

Bioinformatics Analysis of Control Mechanisms of Burn and Sepsis Induced Inflammatory Response

By MEHMET ALI ORMAN

Dissertation Directors:

Dr. Marianthi G. Ierapetritou, Dr. Francois Berthiaume, and Dr. Ioannis P. Androulakis.

Burn injury and infections can lead to an uncontrolled and prolonged action of inflammatory response in the body, which increases the mortality rate of patients. To gain a more comprehensive understanding of these complex physiological changes and to propose therapeutic approaches to combat the deleterious consequences of burn and septic shocks, it is essential to develop animal models exhibiting patho-physiological behaviors similar to those of patients. This was addressed, in this study, by a systematic analysis of local and systemic responses -including the measurements of inflammatory mediators, gene expression and metabolic profiles of liver- in rat models receiving 20% total body surface area (TBSA) scald burn injury or cecal ligation and puncture (CLP) treatment.

All animal groups had 100% survival for at least 10 days following treatments. CLP caused a ~10% weight loss indicating an accelerated breakdown of skeletal muscle

protein. It was found that a certain number of cytokines and chemokines, such as MCP-1, GROK/KC, IL-12, IL-18, and IL-10, were significantly altered following the treatments including SCLP (control of CLP) which is a sterile surgical treatment where cecum is not ligated and punctured. Gene expression analysis elucidated that hepatic transcriptional response to burn injury was mainly related to pro-inflammatory and anti-inflammatory gene groups and genes involved in lipid biosynthesis and central carbon metabolism. Shortly after the CLP treatment, genes related to Toll like receptors and MAPK signaling pathway were significantly up-regulated. Significant changes in the genes associated with acute phase protein synthesis were also observed following the burn and CLP. Furthermore, perfusion experiments elucidated that hepatic metabolic response to burn injury and sepsis was characterized by an up-regulation of pathways including gluconeogenic reactions (sources of which are mainly lactate, aspartate, glycerol and glutamine), urea production from arginine, and serine-glycine inter-conversion. On the other hand, weight values of these pathways were dramatically decreased following the SCLP treatment. In summary, in this study, bioinformatics tools (clustering and metabolic network analysis algorithms) and animal models of burn and CLP were utilized to understand the various layers of regulation and capture the entire scope and complexity of the inflammatory response.

ACKNOWLEDGEMENT

I wish to express my sincere gratitude to my advisors Prof. Marianthi Ierapetritou, Prof. Ioannis Androulakis, and Prof. Francois Berthiaume for their continuous support, guidance and help throughout this study. I have understood from these worthy individuals that being inquisitive, explorative and hardworking is the most crucial thing for any research endeavor. This approach has further reshaped my outlook on life and for that I am extremely thankful. I would also like to thank to Dr. Jagadeeshan Sunderram for being a member of my thesis committee and for his valuable comments on my research proposal.

The financial support from NIH grant GM082974 is gratefully acknowledged. Moreover, I am grateful to my friends Nikisha Shah, Fani Boukouvala, Yijie Gao, Amalia Nikolopoulou, Shuliang Zhang, Vasilis Niotis, Pantelis Mavroudis, Jeremy Scheff, Nguyen Tung, Qian Yang, John Mattick, Sharareh Hashemi and Aina Andrianarijaona for their support, great friendship, advice and encouragement throughout my graduate program. I want to especially thank to Qian Yang, my collaborator who helped me to analyze gene expression data, and John Mattick for helping me in perfusion experiments.

Above all, I would like to thank to my family for loving, supporting and encouraging me all through my life. Without their precious and unwavering support, I would never reach this point.

DEDICATION

To my family

TABLE OF CONTENTS

LIST OF TABLES

LIST OF FIGURES

CHAPTER I

1 INTRODUCTION

Burns and infections result in a hypermetabolic state characterized by an accelerated breakdown of skeletal muscle protein in the patient which leads to muscle "wasting" and reduction of lean body mass. During the hypermetabolic state significant alterations in the utilization of amino acids, glucose and fatty acids, increased resting energy expenditure as well as a negative nitrogen balance at the whole body level take place (Bessey et al. 1989; Mizock 1995; Wolfe et al. 1987). Severe burn and trauma is generally associated with bacterial infections which cause more persistent inflammatory response with an ongoing hypermetabolic and catabolic state. Depending on the severity of the injury and septic complications, hyper-metabolism and other changes associated with the systemic inflammatory response can progress to multiple organ dysfunction syndromes, which can have a mortality rate as high as 90-100% (Beal and Cerra 1994).

Liver is one of the important players in systemic hyper metabolism since it is the main organ controlling circulating levels of metabolites and proteins. Moreover it is the major site for gluconeogenesis and disposal of amino acid nitrogen as urea. During catabolic state, muscle protein is converted into amino acids which are then released into the blood stream, where they are taken up by the liver. It is known that the hepatic response to severe injury and other stressors is characterized by a significant up-regulation of glucose, fatty acid, and amino acid turnover in the liver (Banta et al. 2007; Lee et al. 2000; Lee et al. 2003; Vemula et al. 2004). Yarmush and his co-workers (Yarmush et al.

1999) found that burn injury results in an increase in gluconeogenesis from lactate and the contribution of pyruvate to the oxaloacetate pool. Furthermore, up-regulation in the expression levels of genes involved in the urea cycle, gluconeogenesis, and the metabolism of several amino acids were also reported (Banta et al. 2007; Vemula et al. 2004).

Prior studies have analyzed the changes in gene expression levels (Banta et al. 2007; Jayaraman et al. 2009; Vemula et al. 2004) and metabolic fluxes (Banta et al. 2007; Lee et al. 2000; Lee et al. 2003) within liver after burn injury. The studies using perfused rat livers have identified intrinsic metabolic flux changes that were not only depend on the continual presence of elevated stress hormones and substrate loads. Therefore, it is essential to analyze the physiological behaviors of important players during the inflammation such as circulatory cytokines/chemokines concentrations as well as metabolic and gene expression profiles in the liver controlling the metabolic activity of the body and production of acute phase proteins. This is also critical to propose therapeutic approaches to combat the deleterious consequences of burn and septic shocks. However, nutritional and hormonal therapies that have been applied for patients are still partially effective. One of the main reasons of this is the lack of understanding of the integrated system as prior studies examined individual mediators/pathways in isolation from each other.

This research program mainly focused on the short term dynamic changes in systemic inflammatory mediators as well as liver gene expression levels and metabolic fluxes following the burn injury and CLP, which have been explained in subsequent chapters in great detail. In the second chapter, we briefly review the studies available in literature regarding the inflammatory mediators' (cytokines and chemokines) changes, and liver gene expression and metabolic flux alterations in burn and septic animals. We further provide a very profound review of basic concepts of metabolic network analysis which have been used to analyze the perfused liver metabolism in this study.

CHAPTER II

2 LITERATURE REVIEW

2.1 Inflammatory Mediators Following Burn and Sepsis

Inflammation is a complex biological response to injuries and infections, involving different inflammatory mediators, such as cytokines and chemokines, as well as nervous system reflexes, and hormones. Precise regulation and coordination of the processes linking them is necessary to mount an appropriate response enabling an eventual return to homeostasis (Tracey 2002). It is generally accepted that the severity of the inflammatory response and the involvement of the various components can vary depending on type and severity of the injury, infectious agent, as well as genetic and physiological factors (sex, body weight, preexisting conditions including immune system deficiencies).

Burn injury leads to denaturation of proteins and loss of membrane integrity of cells on injured area, which results in secretion of local mediators and endotoxins such as histamine, nitric oxide, oxygen-free radicals and cytokines such as IL-6, PDGF and TGF-α (Evers et al. 2010; Ono et al. 1995; Summer et al. 2008). This eventually recruits different blood cells including neutrophils, lymphocytes, macro-phages and fibroblasts to the injured area, thus causing a further increase in circulatory proteins and cytokines levels (Evers et al. 2010). A detailed analysis of experimental observations published in literature (Cannon et al. 1992; Damas et al. 1997; Debandt et al. 1994; Dehne et al. 2002; Drost et al. 1993b; Finnerty et al. 2006; Jeschke et al. 2007; Ono et al. 1995; Ozbalkan et

al. 2004; Struzyna et al. 1995; Summer et al. 2008; Vindenes et al. 1998; Yamada et al. 1996) reveals that at least one potential pre-inflammatory cytokine (for example TNF-α, or IL-1β) and one potential mediator or pro-inflammatory cytokine (such as IL-6 and IL-8) are elevated in the blood circulation after the injury. Pre and pro inflammatory cytokines also activates anti inflammatory reflex by up-regulating the secretion of anti-inflammatory cytokines such as IL-10 (Blackwell and Christman 1996). Inflammatory cytokines affects the afferent signals of nervous system which in turn increase the secretion of anti inflammatory stress hormones (Correa et al. 2007). Endotoxins and cytokines also activate the vagus efferent activity of nervous system inhibiting cytokine synthesis through cholinergic anti-inflammatory pathway (Tracey 2002).

Inflammation is known as a self limiting process but persistent response can lead to excessive tissue injury. Although burn wound is an important portal of entry for microbes (Church et al. 2006), pathogen originating from gastrointestinal tract is one of the most serious complications, which is not fully understood. Experimental observations demonstrate that there is a loss of physical barrier function in gastrointestinal tract after burn injury, which might be because of physical disruption of the mucosal barrier, intestinal over-growth of bacteria and suppression of the immune defense (Gosain and Gamelli 2005). Increasing endotoxin concentrations secreted by damaged tissues and inflammatory cytokines in circulation can behave as immunosuppressive agents which decrease T-cells population (Heideman and Bengtsson 1992; Kelly et al. 1999), and affect the mesenteric lymph (Olofsson et al. 1985; Olofsson et al. 1986). Decreases in

intestinal blood flow due to the vasoconstriction (Gosain and Gamelli 2005) and increase in nitric oxide and free radicals production stimulated by cytokines and endotoxin agents (Nadler and Ford 2000; Parihar et al. 2008; Wallace and Ma 2001) further damage the endothelial cells in gut/digestive system and minimize the mucosal barrier, which increase the intestinal permeability.

2.2 Alterations in Gene Expression Levels in Liver

Liver regulates metabolic activity of body and production of acute phase proteins (Vemula et al. 2004). Therefore, liver is one of the target organs to understand the underlying mechanisms of hypermetabolic state and to propose therapeutic techniques. Genetic studies show that inflammatory mediators activate important signaling pathways. Along with these mediators, metabolic changes in circulation systems might also result in persistent alterations in gene expression levels in liver.

There are numerous studies regarding the individual gene expression analysis where RT-PCR and immune-histochemical methods have been utilized. These studies reveal that many signaling pathways including MAPK, Jac/STAT, and Ik-B/NF-kB cascades which have key roles in expression of stress related enzymes and proteins as well as cytokines are activated in liver following burn and sepsis (Andrejko et al. 1998; Cho et al. 2004a; Klein et al. 2003; Ogle et al. 2000). Alterations in different and numerous signaling pathways in the cells are reasonable since burn and sepsis disrupt circulatory levels of hormones, cytokines, chemokines and endotoxins which interact with their corresponding receptors on the cell surface initiating signaling cascades at different levels. Moreover,

although a soluble factor might activate its specific transcription factor, upstream regulation of this specific transcription factor might also activate another transcript factor (Foteinou et al. 2009). Therefore, gene expression studies reveal that upregulation of some important receptors (such as CD14 receptors, protease activated receptors, histamine H-1 and H-2 receptors), transcription factors (NFk-beta, Stat3, and C/EBP-beta) and other proteins or kinases (such as ERK, JNK, and p38) involved in the MAPK, Jac/STAT, and Ik-B/NF-kB signaling pathways is observed in animals receiving burn injury and sepsis (Andrejko et al. 1998; Cho et al. 2004a; Cho et al. 2004b; Jeong et al. 2003; Jesmin et al. 2006; Klein et al. 2003; Masaki et al. 2005; Nishiura et al. 2000; Yang et al. 1999).

Although there are significant number of studies in the literature regarding the individual gene expression levels in the liver, microarray studies showing gene expression changes under stress condition are limited (Dasu et al. 2004; Jayaraman et al. 2009; Vemula et al. 2004). Vemula and co-workers (Vemula et al. 2004) analyzed the changes in gene expression in rat livers during the first 24 h after burn injury. Functional analysis of differentially expressed 339 genes revealed that metabolism and inflammation accounted for nearly 42 %. They showed that the inflammatory genes that were altered included several classic acute phase response markers, and other genes involved in the complement, kinin, clotting, and fibrinolytic protein systems. On the other hand metabolic genes showed that fatty acid and B-oxidation increased after burn to meet the enhanced energy demands. The same group (Jayaraman et al. 2009) also studied the gene

expression profiling of long term (1, 2, 4 and 7 day) changes in rat liver following burn injury. They identified that 60 % of 740 differentially expressed genes showed significant changes either on day 1 or on day 7 postburn. Detailed analysis of the data also revealed that fatty acids are used in the liver as energy substrates for the first 4 days after injury but not at later time point.

In the study of Banta and co-workers (Banta et al. 2007), systemic hypermetabolic response was induced in rats by applying a moderate burn injury followed 2 days later by cecum ligation and puncture (CLP) to produce sepsis. On fourth day after burn, alterations in gene expression levels in liver have been analyzed. Dual injury model revealed that mRNA levels of genes involved in the urea cycle, the respiratory chain, gluconeogenesis, the metabolism of some amino acid and the specific transporters of glutamine and arginine were significantly up-regulated.

Another interesting study published by Jayaraman and co-workers (Jayaraman et al. 2005) aimed to profile gene expression dynamics during IL-6 stimulated inflammation in hepatocytes maintained in stable, collagen double gel *in vitro* model system. They compared this response with that of an *in vivo* acute-phase response induced by burn injury (Vemula et al. 2004). Although they found that in vitro model captures many of the features of the in vivo setting at a systems level, significant differences in expression patterns of individual genes were observed including inflammatory signaling molecules (p38, SAPK) and transcription factors (STAT3 and C/EBP-beta). But, multiple mediators

in vivo compared with a single stimulus *in vitro* might result in significantly different results.

2.3 Metabolic Changes in Liver

Although metabolic changes at whole body level have been profoundly investigated, there are not many studies analyzing these changes at organ level. To analyze the metabolic activity of liver following the burn and sepsis, the isolated perfused liver model has been commonly used (Lee et al. 2000; Yamaguchi et al. 1997; Yarmush et al. 1999). Yamaguchi and co-workers (Yamaguchi et al. 1997) analyzed the glucose, urea and various amino acid concentration changes in perfusate medium during the isolated rat-liver perfusion after the burn injury. Their results showed that burn injury increased urea productions and oxygen consumption as well as net protein breakdown, but it did not alter the rate of gluconeogenesis. Yarmush and co-workers (Yarmush et al. 1999) determined fluxes in TCA cycle in perfused rat livers by supplying with labeled 13C-lactate. Isotopomer mass balance model of the TCA cycle showed that there was an increase in gluconeogenesis from lactate. Moreover, burn injury also resulted in an increase in the contribution of pyruvate to the oxaloacetate pool at the expense of non-TCA cycle sources.

Recently metabolic flux analysis has been used to determine the effects of burn injury and sepsis on the flux distribution through the major pathways in the liver associated with carbohydrate, fatty acid, and amino acid metabolism (Lee et al. 2000; Lee et al. 2003). Lee and co-workers (Lee et al. 2000) found that the fluxes in mitochondrial electron

transports, the TCA and urea cycles, gluconeogenesis, and pentose phosphate pathway significantly increased on day 4 post-burn in the rat liver. They also confirmed that glucose-6-phosphate was diverted into the PPP with the increase activity of glucose-6-phosphate dehydrogenase. The same group also profiled the dynamic changes of fluxes in the rat livers up to 7 days after burn injury (Lee et al. 2003). They observed that burn injury sequentially up-regulated the urea cycle, the PPP and the TCA cycle whereas no changes were observed in beta-oxidation and gluconeogenesis.

Banta and co-workers (Banta et al. 2007) compared the gene expression levels and metabolic fluxes in rat livers after burn and cecum ligation and puncture (CLP). The results showed that burn injury prior to CLP increased fluxes while metabolic gene expression levels were decreased. Conversely, CLP alone significantly increased metabolic gene expression, but decreased many of the corresponding metabolic fluxes. On the other hand both burn and CLP resulted in the most dramatic changes, where concurrent changes in fluxes and gene expression levels were observed.

2.4 Metabolic Network Analysis

Recently, metabolic engineering approaches developed for stoichiometric network analysis have been also applied to mammalian systems to gain a comprehensive understanding of metabolic network properties and to improve the existing processes or systems involving mammalian cells. These approaches are generally used (a) to reconstruct the metabolic networks (Terzer et al. 2009), (b) to identify metabolic flux

patterns using metabolic flux analysis (MFA) (Dauner 2010; Martens 2007; Niklas et al. 2010; Quek et al. 2010; Wiechert 2001; Zamboni) and flux balance analysis (FBA) (Kauffman et al. 2003; Raman and Chandra 2009), and (c) to characterize topology of the networks using pathway analysis (Klamt and Stelling 2003; Trinh et al. 2009) and other optimization based methods. In this section, we mainly focus on the basic techniques and principles of how stoichiometric network analysis used for mammalian systems.

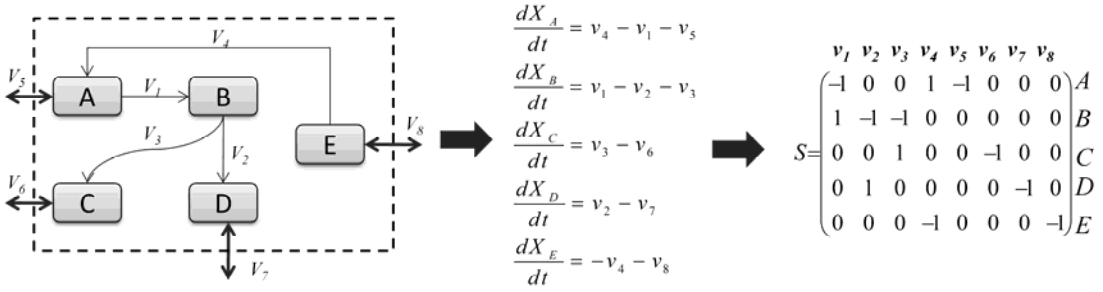

Figure 2.1. A small metabolic network.

*The network includes four internal reactions (v_1, v_2, v_3, and v_4) and four external reactions (v_5, v_6, v_7 and v_8) which are given as "output" fluxes. The stoichiometric matrix (**S**) is constructed according to material balance equations.*

2.4.1 Metabolic Flux Analysis (MFA)

Stoichiometric modeling framework is mostly characterized by metabolic flux analysis where a set of measured extracellular metabolite concentration rates of change are fitted to relatively simple mass balance models using the stoichiometric mass balance analysis

to derive comprehensive metabolic flux maps. Such quantitative maps have turned out to be extremely useful to compare the effects of various stressors on metabolism, as they provide a global picture and understanding of the changes in relevant metabolic pathways.

The flux distribution is calculated by using the basic idea of metabolic flux analysis (Varma and Palsson 1994) . The mass balances of all internal metabolites can be written as follows:

$$\frac{dX}{dt} = S.v \tag{2.1}$$

where **X** is vector of metabolite concentrations, **v** is the flux distribution vector, and **S** is the stoichiometric matrix where rows correspond to the metabolites and columns represent the reaction rates (**Figure 2.1**). It is generally assumed that the internal metabolites are at pseudo steady state, since metabolic transients are fast compared to environmental changes (Varma and Palsson 1994). Therefore, the mass balance is rewritten as follows:

$$S.v = 0 \tag{2.2}$$

The measured fluxes are used to reduce the possible solution space given in equation (2.2). Therefore, the vector of reaction **v** is divided into the vector of measured fluxes $\mathbf{v_m}$, and unknown fluxes $\mathbf{v_u}$. In the same way, the matrix **S** is partitioned in $\mathbf{S_m}$ and $\mathbf{S_u}$. So equation (2.2) can be rewritten in the following way:

$$S.v = S_u.v_u + S_m.v_m = 0$$
$$S_u.v_u = -S_m.v_m \tag{2.3}$$

The rank of the $\mathbf{S_u}$ determines the maximum number of the metabolite balances linearly independent. If the number of equations is less than the number of unknown fluxes, the system is undetermined implying that there are insufficient metabolite balances to determine the intracellular or unknown metabolic fluxes. For determined system where enough measurements are available, problem (2.3) can be easily calculated in order to determine the unknown fluxes uniquely. In over-determined or redundant system, the rank of $\mathbf{S_u}$ is greater than the number of unknown fluxes, which ensures to test statistical consistency of the measurements. To assess for the presence of measurement errors and consistency of the metabolic network, a test function that is generally assumed to have a Chi-square distribution is calculated. For over-determined system, unknown fluxes are usually identified by minimizing the sum of square errors between the measured and the estimated fluxes.

The null space of the stoichiometric matrix, $Nul(S) = \{v : Sv = 0\}$, determines the basis for the null space whose column vectors can give actual flux distribution when combined linearly. This analysis is also used to perform consistency validations of the considered metabolic network (Terzer et al. 2009). The dimension of the null space of the stoichiometric matrix also identifies the minimum number of fluxes (independent variables) required to determine the unknown fluxes (dependent variables) uniquely.

Independent reactions or fluxes should not be necessarily external fluxes, since determining all external fluxes may not necessarily result in the calculation of all the unknown fluxes because metabolic networks are very complex given the cyclic pathways or futile cycles (**Figure 2.3**). Therefore, to identify the flux distribution more accurately, fluxes of some internal reactions are measured. In this context, mass isotopomer analysis has been extensively used to quantify internal fluxes with substrates labeled with stable isotopes such as ^{13}C.

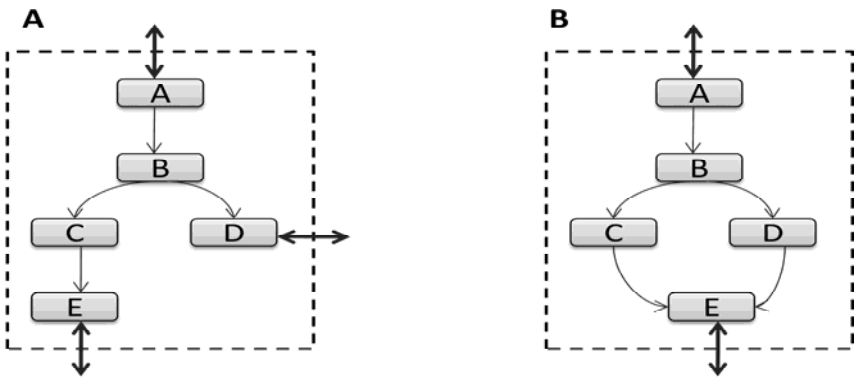

Figure 2.2. Nullspace of metabolic networks.

*Nullspaces of these two simplified metabolic networks have the same dimension which is equal to 2. This means that at least two independent variables or fluxes should be known in order to determine the flux distribution vector. Although any two external fluxes (represented by double arrows) in the metabolic network **A** can determine all unknown fluxes, those in network **B** can not identify the flux distribution vector due to the cyclic reactions. This can be determined by either isotope tracers or expanding the model by adding the material balances of energy metabolites such as ATP, NADH if they are associated with cyclic reactions (however this requires a complete metabolic network).*

In general, metabolic stationary conditions with constant intracellular fluxes are established during the carbon-labeling experiments. Then, NMR and MS techniques are utilized to obtain intracellular isotopomer distribution. Isotope balancing is very similar to metabolite balancing, i.e. the sum of labeled carbon atoms entering a given position of a metabolite has to equal the sum of labeled carbon atoms leaving this position (Christensen and Nielsen 2000). However, isotopomer balancing might be very complicated when the fraction of molecules having a certain combination of labeled carbon atoms is considered. For a metabolite consisting of n atoms which might be in labeled or unlabeled states (e.g. C atom in glucose), 2^n isotopomers are possible. Using a ^{13}C tracer, there are 64 carbon atom isotopomers of glucose, and 396 isotopomer models for simulating glucose labeling in the gluconeogenesis pathway (Antoniewicz et al. 2007). The number of isotopomer equations increases tremendously when different combinations of stable isotopes (such as ^{13}C, ^{2}H, ^{18}O) are used. In order to determine metabolic fluxes, the residuals between the experimental and the simulated isotopomer distribution is generally minimized. This technique has been described extensively in the literature and used in mammalian systems to characterize the metabolic networks under different environmental conditions and to provide information on specific metabolic pathways or key reactions being investigated (Bonarius et al. 2001; Bonarius et al. 1998; Goudar et al. 2010; Maier et al. 2009; Maier et al. 2008; Metallo et al. 2009; Munger et al. 2008; Portais et al. 1993; Santos et al. 2007).

2.4.2 Flux Balance Analysis

One of the common problems in solving problem (2.3) to obtain $\mathbf{v_u}$ is that the rank of $\mathbf{S_u}$ is generally smaller than the number of unknown fluxes which leads to an underdetermined system. Actually in most cases, the mass balance analysis typically does not yield a unique solution. To overcome this limitation, some metabolic engineering tools based on well known biological properties have been used in the literature. The solution space of steady state flux vectors can be reduced by incorporating additional constraints relying on well known regulatory mechanisms (Covert and Palsson 2002; Covert et al. 2001) or thermodynamic properties of biochemical reactions (Beard and Qian 2005; Nolan et al. 2006). Using flux balance analysis (Ibarra et al. 2002), it is also possible that a flux distribution can be uniquely determined when an objective function is defined such as maximization of biomass production (Ibarra et al. 2002) or minimization of ATP production (Ramakrishna et al. 2001).

FBA analysis has been widely used to calculate the intracellular fluxes by constructing an optimization problem having a specific objective function (z) restricted by mass balance equations, reaction reversibility constraints and other constraints. A typical optimization formula is given as following:

$$\begin{aligned} &Maximize / Minimize \quad z \\ &Subject\ to \quad S.v = 0 \\ &\qquad v_m^{\min} \le v_m \le v_m^{\max}, \qquad \forall m \in \{\text{measured fluxes}\} \\ &\qquad v_i \ge 0, \qquad\qquad \forall i \in \{\text{irreversible fluxes}\} \end{aligned} \tag{2.4}$$

The steady state solution space defined by linear equations and inequalities given in problem (2.4) is called flux cone and any programming method depending on the formulation of the problem can be used to choose an optimum point described by the objective function *z*. Various constraints can be incorporated to the stoichiometric modeling. For example, based on the measurement data from different *in vitro* or *in vivo* experiments, the external fluxes can be restricted by their minimum and maximum values. Thermodynamic or reaction directionality constraints can be further added to refine the steady state flux space. For example, pathway energy balance obtained from elementary modes weighted by Gibbs energy of reactions was used for hepatic metabolic network to reduce the feasible range of intracellular fluxes (Iyer et al. 2010a; Iyer et al. 2010b; Nolan et al. 2006; Yoon et al. 2007).

Flux balance analysis was used in the early 1990s for hybridoma cell lines by Savinell and Palsson to explore the optimum flux distribution corresponding to maximum growth rate (Savinell and Palsson 1992a; Savinell and Palsson 1992b). Recently, a significant number of studies utilized FBA to describe the metabolic network properties of mammalian cells. Wahl and co-workers (Wahl et al. 2008; Wahl et al. 2010) used the MDCK model to calculate a theoretical flux distribution representing an optimized cell that only consumes a minimum of carbon sources. Heino et al. (Heino et al. 2007) proposed an effective Markov chain Monte Carlo (MCMC) scheme to explore a two-compartment model for skeletal muscle metabolism. Tekir and co-workers (Tekir et al.

2006) investigated the human red blood cell (RBC) metabolism by performing FBA via optimization of alternative objective functions, and the maximization of production of ATP and NADPH. In order to observe the relative changes in the flux distribution of the deficient network, they applied two well known approaches, minimization of metabolic adjustment (MOMA) that minimize the Euclidean distance from a wild type flux distribution (Segrè et al. 2002) and regulatory on-off minimization (ROOM) that minimizes the number of significant flux changes with respect to wild type (Shlomi et al. 2005). Obrzut et al. (Obrzut et al. 2010) used FBA to characterize myocardial metabolic phenotypes among non-ischemic dilated cardiomyopathy (NIDCM) patients undergoing cardiac resynchronization therapy (CRT). Arterial and coronary sinus plasma concentrations of oxygen, glucose, lactate, pyruvate, free fatty acids, and 22 amino acids were obtained from 19 male and 2 female patients. Using a metabolic network of the cardiac mitochondria (189 reactions, 230 metabolites), an objective function maximizing ATP production was chosen for the calculations of unknown fluxes. They concluded that analysis of the myocardial metabolic network using FBA may provide unique and clinically useful prognostic information in patients with NIDCM undergoing therapy. Yang et al. (Yang et al. 2009b) demonstrated a proof of principle for the use of constraint-based modeling to achieve enhanced performance of liver-specific functions of cultured hepatocytes during plasma exposure by optimizing amino acid supplementation and hormone levels in the medium. FBA model was developed for the maximization of urea output. However since it is possible that alternative flux distribution exists that produces the same maximal output they applied a recursive mixed integer linear

programming (MILP) to enumerate all solutions. Uygun and co-workers (Uygun et al. 2007) investigated and identified possible metabolic objectives for hepatocytes cultured in vitro by a data-mining procedure including multi-level optimization based algorithm. The multi-level optimization problem formulated was to identify a minimum set of fluxes that are of major importance to the cells while minimizing difference between the fluxes measured and those predicted by the model and maximizing the summation of weighted fluxes. This problem creates a mixed integer nonlinear programming (MINLP) problem with multiple inner LPs, which is computationally challenging and requires a suitable algorithm for the solution. They solved the problem in an iterative scheme where different flux combinations are considered in the objective and tested for sufficient prediction accuracy.

Proposing an objective function for mammalian cells is a major obstacle for FBA. Mammalian cells exhibit various phenotypic states regarding the cell proliferation, differentiation, and organ-specific functions. Metabolic network properties of mammalian cells under different phenotypic states should be further investigated to provide clues regarding the metabolic objectives. Calik and Akbay (Çalik and Akbay 2000) determined the theoretical flux distributions in the fibrotic and healthy liver cells by maximizing respectively the collagen and palmitate synthesis in the objective function for the solution of the model. A mammalian cell type such as hepatocytes might exhibit multiple functions that need to be considered simultaneously when exploring the optimal fluxes. In this case, Pareto-optimal solutions satisfying all the objectives simultaneously can be

analyzed (Nagrath et al. 2007; Nagrath et al. 2010; Sharma et al. 2005). Nagrath and co-workers (Nagrath et al. 2007; Nagrath et al. 2010) developed a multi-objective optimization approach that couples the normalized Normal Constraint (NC) with both flux balance analysis (FBA) and energy balance analysis (EBA) to obtain multi-objective Pareto-optimal solutions. They investigated the Pareto frontiers in gluconeogenic and glycolytic hepatocytes for various combinations of liver-specific objectives (albumin synthesis, glutathione synthesis, NADPH synthesis, ATP generation, and urea secretion). Sharma et al. (Sharma et al. 2005) investigated the importance of amino acids in the supplementation and the criticality of the metabolic pathways using a Pareto optimal set of solutions corresponding to liver-specific functions of urea and albumin secretion in the metabolic framework using multiobjective optimization. Furthermore, they have used the concept of two stage stochastic programming to obtain robust solutions by considering extracellular variability. Since the metabolite measurements are subject to variability; uncertainty has to be integrated with system analysis to improve the prediction of hepatic function.

2.4.3 Metabolic Pathway Analysis (MPA)

Pathway analysis (based on stoichiometry of the network only) systematically characterizes the structure of a metabolic network and elucidates its important properties by decomposing the highly interconnected reactions into more organized pathways. Metabolic pathway analysis mainly based on extreme pathways and elementary modes has proven to be a useful tool (Klamt and Stelling 2003; Trinh et al. 2009) and has been extensively applied in the literature. Elementary modes consist of the minimum number

of reactions that exist as a functional unit whereas extreme pathways are the independent subset of elementary modes (Klamt and Stelling 2003). Pathway analysis identifies pathways which are important for desired products (yield analysis), evaluates how much of a flux is carried out by each pathway and to what extent an external metabolite taken by the cell affects the output of the pathway (Orman et al. 2011a). This analysis can elucidate important information about metabolic regulatory mechanisms and how dominant pathways are controlled.

It is noteworthy to mention that every flux distribution can be written as a linear combination of the elementary modes, or extreme pathways, thus a weight can be assigned to each corresponding pathway and can be interpreted as an indication of the importance of that pathway in the network (Llaneras and Picó 2007; Wiback et al. 2003):

$$\begin{aligned} & v = P.w \\ & w_k \geq 0, \ \forall k \in \{irreversible\ pathways\} \end{aligned} \tag{2.5}$$

where $\boldsymbol{w}$ denotes a vector involving the weight for each elementary mode; and $\boldsymbol{P}$ is the matrix of elementary modes. One of the main problems in pathway analysis is that the decomposition of a steady state flux vector into pathways is not always unique because for large networks the number of pathways is not usually equal to the dimension of the null space of the stoichiometric matrix (Schilling et al. 2000) (**Figure 2.3**). To provide a unique decomposition of the steady state flux distributions into elementary modes or pathways, different objective functions have been proposed in the literature including maximization of the number of elementary modes, minimization of the elementary mode

activity and the entropy maximization principle (Nookaew et al. 2007; Schwartz and Kanehisa 2005; Schwartz and Kanehisa 2006; Zhao and Kurata 2009).

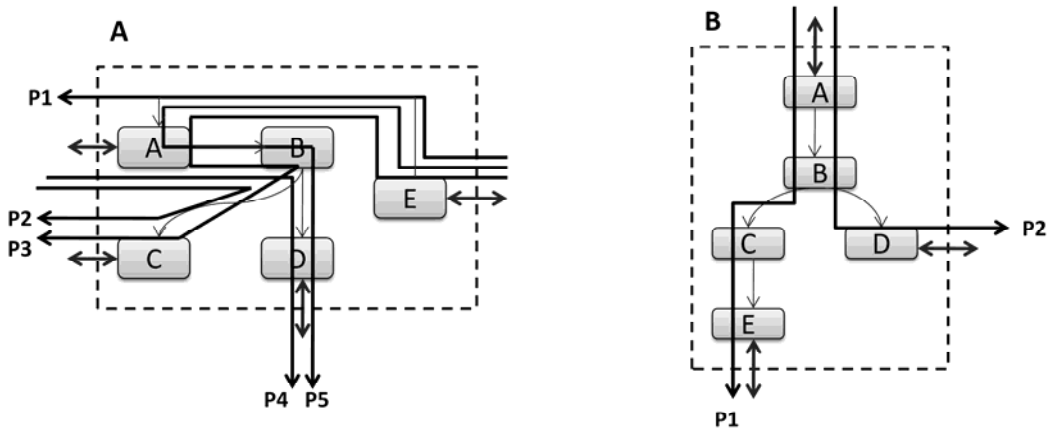

Figure 2.3. Metabolic pathways of two different networks.

A.*The number of pathways in this network is 5 which is greater than the dimension of the null space of the stoichiometric matrix (equal to 2). The system is redundant and the decomposition of the steady state flux vector into pathways is not unique. B. The number of pathways is equal to the dimension of the null space of the stoichiometric matrix, thus the decomposition method is unique.*

Pathway analysis has been used to characterize the red blood cell metabolism (Cakir et al. 2004; Price et al. 2003; Wiback et al. 2003; Wiback and Palsson 2002). Wiback et al. (Wiback and Palsson 2002) interpreted the extreme pathways of red blood cell metabolic network in a biochemical and physiological context and divided them into groups based on different criteria such as cofactor and by-product production, and carbon inputs. They

also described how physiological steady state solutions can be reconstructed from a network's extreme pathways by using a linear optimization problem which maximizes and minimizes the weights of a particular extreme pathway in the reconstruction to find a weight-spectrum (α-spectrum) (Wiback et al. 2003). The α-spectrum showed which extreme pathways can and cannot be included in the reconstruction of a given steady state flux distribution and to what extent they individually contribute to the reconstruction. Moreover it was also shown that accounting for transcriptional regulatory constraints can considerably reduce the alpha-spectrum (Wiback et al. 2003). Price et al. (Price et al. 2003) used singular value decomposition (SVD) method for extreme pathway matrix of human red blood cell. They observed that the first five eigenpathways, out of a total of 23, effectively characterize all the relevant physiological states of red blood cell metabolism. Moreover it was also shown that the dominant features of these first five eigenpathways described key metabolic splits regulated in the human red blood cell. Cakir et al. (Cakir et al. 2004) investigated five enzymopathies (G6PDH, TPI, PGI, DPGM and PGK deficiencies) in the human red blood cells using metabolic pathway analysis. They analyzed the elementary modes corresponding to each enzyme deficiency case given the functional capabilities.

The basic idea of metabolic pathway analysis was also utilized to characterize CHO and hepatic metabolic networks as well. Provost and Bastin (Provost and Bastin 2004) translated the elementary flux modes of CHO metabolism into a set of macro-reactions connecting the extracellular substrates and products. Then they built a dynamical model

using these macro-reactions. In order to provide weight values for all possible pathways within hepatic metabolic network, Orman et al. (Orman et al. 2011a) presented different approaches, considering the structural and physiological properties of metabolic network, aiming at a unique decomposition of the flux vector into pathways. These approaches based on optimization functions (including maximization of the number of elementary modes, maximization of the entropy of the system, and maximization of activity of short pathways, and the minimization of the elementary mode activity) were used to analyze the hepatic metabolism considering available data sets obtained from perfused livers of fasted rats receiving burn injury. Elementary modes were also used to formulate thermodynamic feasibility constraints for hepatic metabolic network to shrink the feasible range of intracellular fluxes (Iyer et al. 2010a; Iyer et al. 2010b; Nolan et al. 2006; Yoon et al. 2007). The underlying assumption behind pathway based energy balance is that an exergonic reaction can be a "driving-force" for an endergonic reaction if these two reactions are coupled in the same pathway.

CHAPTER III

3 COMPARISION OF THE CYTOKINE AND CHEMOKINE DYNAMICS OF THE EARLY INFLAMMATORY RESPONSE IN MODELS OF BURN INJURY AND INFECTION

Abstract

The inflammatory response, and its subsequent resolution, are the result of a very complex cascade of events originating at the site of injury or infection. When the response is severe and persistent, Systemic Inflammatory Response Syndrome can set in, which is associated with a severely debilitating systemic hypercatabolic state. This complex behavior, mediated by cytokines and chemokines, needs to be further explored to better understand its systems properties and potentially identify multiple targets that could be addressed simultaneously. In this context, short term responses of serum cytokines and chemokines were analyzed in two types of insults: rats receiving a “sterile” cutaneous dorsal burn on 20% of the total body surface area (TBSA); rats receiving a cecum ligation and puncture treatment (CLP) to induce infection. Considering the temporal variability observed in the baseline corresponding to the control group, the concept of area under the curve (AUC) was explored to assess the dynamic responses of cytokines and chemokines. MCP-1, GROK/KC, IL-12, IL-18 and IL-10 were observed in both burn and CLP groups. While IL-10 concentration was only increased in the burn

group, Eotaxin was only elevated in CLP group. It was also observed that Leptin and IP-10 concentrations were decreased in both CLP and sham-CLP groups. The link between the circulating protein mediators and putative transcription factors regulating the cytokine/chemokine gene expression was explored by searching the promoter regions of cytokine/chemokine genes in order to characterize and differentiate the inflammatory responses based on the dynamic data. Integrating multiple sources together with the bioinformatics tools identified mediators sensitive to type and extent of injury, and provided putative regulatory mechanisms. This is essential to gain a better understanding for the important regulatory points that can be used to modulate the inflammatory state at molecular level.

3.1 Introduction

Burns and infections lead to one or several of the following "primary" events in the inflammatory cascade: denaturation of proteins, loss of plasma membrane integrity, activation of complement proteins, and secretion of local mediators, such as histamine, nitric oxide, and reactive oxygen species (Evers et al. 2010; Ono et al. 1995; Summer et al. 2008). This is quickly followed by the production of pro-inflammatory cytokines (such as IL-1, TNF-α, IL-18, IL-6, and IL-12), and chemokines (such as Eotaxin, G-CSF, GM-CSF, GRO/KC, MCP-1, MIP-1, Rantes). The initial pro-inflammatory response also activates a modulating anti-inflammatory reaction consisting of anti-inflammatory cytokines (such as IL-4, IL-10, IL-13). Inflammatory cytokines also impact afferent signals to the nervous system which in turn increase the secretion of anti-inflammatory stress hormones (Correa et al. 2007) and activate the cholinergic anti-inflammatory

pathway (Tracey 2002). Although these different signals may result in distinct cellular responses depending on the type and severity of the injury, there is a large degree of overlap in the underlying signaling pathways, including MAPK, Jac/STAT, and Ik-B/NF-kβ activated during the inflammation.

Animal models of burn injury, cecal ligation and puncture, and endotoxin injection have previously been used to profile circulating mediator concentrations after an insult (Barber et al. 2008; Ertel et al. 1991; Finnerty et al. 2009; Gauglitz et al. 2008; Kataranovski et al. 1999; Klein et al. 2003; Shelley et al. 2003; Walley et al. 1996). Gauglitz et al. (Gauglitz et al. 2008) used male rats receiving a full thickness burn over 60% of the total body surface area (TBSA), where they observed that serum concentrations of several pro- and anti-inflammatory mediators (IL-1 beta, IL-6, IL-10, MCP-1, and CINC) were significantly elevated after burn. Barber et al. (Barber et al. 2008) studied the relation between burn size (20%, 30%, 40%, and 60% TBSA) and cytokine concentrations (TNA-alpha, IL-1 beta, and IL-6) at one time point (24 h) after burn injury, and observed burn size-dependent increases. Ertel et al. (Ertel et al. 1991) induced sepsis by CLP in male rats and analyzed the TNF, IL-1 and IL-6 cytokines profiles in serum within 20 hour time course after CLP. They observed a persistent elevation of plasma TNF until 10 hours, steadily increasing IL-1 plasma concentrations, and enhanced IL-6 plasma concentrations at all time points compared to the sham group.

It is noteworthy that these studies are limited to one type of insult or a limited number of cytokines. Chemokines and other inflammatory mediators including Leptin and IL18 are gaining more attention in the attempts to characterize the inflammatory responses. For example, elevated concentrations of IL-18, which is a proinflammatory cytokine involved in the regulation of cell-mediated and innate immune responses, have been reported to correlate with organ dysfunction after injury (Stassen et al. 2003). Peter et al. observed that GCSF, a chemokine mainly produced by monocytes and macrophages, modified the immune system by increasing the white blood cells and decreasing the TNF-α and IFN-γ concentrations in a rat animal model receiving 30 % TBSA burn injury (Peter et al. 1999). Leptin is also playing an important role in regulating energy metabolism. It was observed that Leptin reduced elevated tissue associated myeloperoxidase activity and microscopic damage scores in various tissues including liver, stomach, colon and kidney in rats receiving 30 % TBSA burn (ÇakIr et al. 2005).

In this study, we used nonlethal rat models of burn injury and cecal ligation and puncture (CLP) to profile the early temporal inflammatory response by measuring 23 different cytokines and chemokines. Moreover, the binding sites of promoter regions of the cytokines and chemokines whose concentrations were significantly altered in the treatment groups were explored to identify putative transcription factors. Comparison of the timing of cytokine/chemokine concentration changes among the groups revealed mediators sensitive to type and extent of injury. Connecting the cytokine/chemokine

dynamic patterns to transcription factor activation further provided insights on the regulatory mechanism of inflammation process.

3.2 Materials and Methods

3.2.1 Animals

Male Sprague-Dawley rats (Charles River Labs, Wilmington, MA) weighing between 150 and 200 g were used. The animals were housed in a temperature-controlled environment (25°C) with a 12-hour light-dark cycle and provided water and standard chow ad libitum. All experimental procedures were carried out in accordance with National Research Council guidelines and approved by the Rutgers University Animal Care and Facilities Committee.

3.2.2 Experimental Plan

Animals were randomly divided into four groups. Two different insults were investigated: a dorsal cutaneous burn (B) to mimic trauma with no infection, and cecal ligation and puncture (CLP) to mimic infection and sepsis. Control treatments included sham burn and sham CLP. In total four different groups of animals were investigated: sham-burn, burn, sham-CLP and CLP (labeled S, B, SCLP, and CLP, respectively).

3.2.3 Burn Injury

A full-thickness burn on the dorsal skin corresponding to 20% of the total body surface area (TBSA) was performed as described previously (Banta et al. 2007). This model was chosen because it has nearly 100% long-term survival, no evidence of systemic hypoperfusion, and no significant effect on the feeding pattern (Herndon et al. 1978).

Rats were anesthetized by intraperitoneal injection of 80 to 100 mg/kg ketamine + 12 to 10 mg/kg xylazine. All hair removed from the dorsal abdominal area using electric clippers. The animal's back was immersed in water at 100°C for 10 s to produce a full-thickness scald injury over 20% TBSA (**Figure 3.1**). Immediately after burns, the animals were resuscitated with 50 mL/kg of saline injected intraperitoneally. Sham burn controls consisted of animals treated identically but immersed in warm water (37°C). Rats were single caged after burn or sham burn and given standard rat chow and water ad libitum until sacrifice. No post-burn analgesics were administered, consistent with other studies with this full thickness burn model since the nerve endings in the skin are destroyed and the skin becomes insensate (Valenti et al. 2005). Furthermore, after the animals woke up, they ate, drank, moved freely about the cage, responded to external stimuli, and did not show clinical signs of pain or distress.

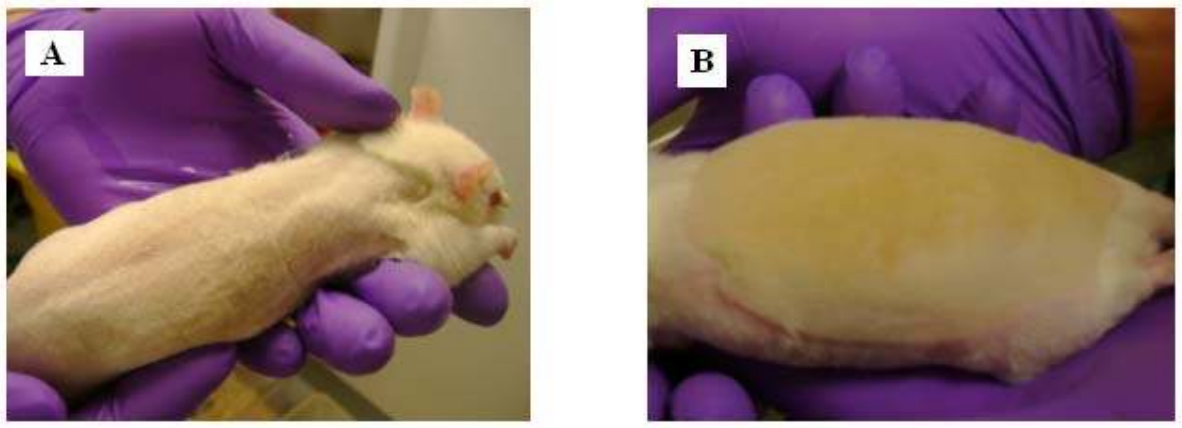

Figure 3.1. Experimental burn injury.

All hair is removed from the dorsal abdominal area (A), and the animal's back is immersed in water at 100°C for 10 s to produce a full-thickness scald injury (B).

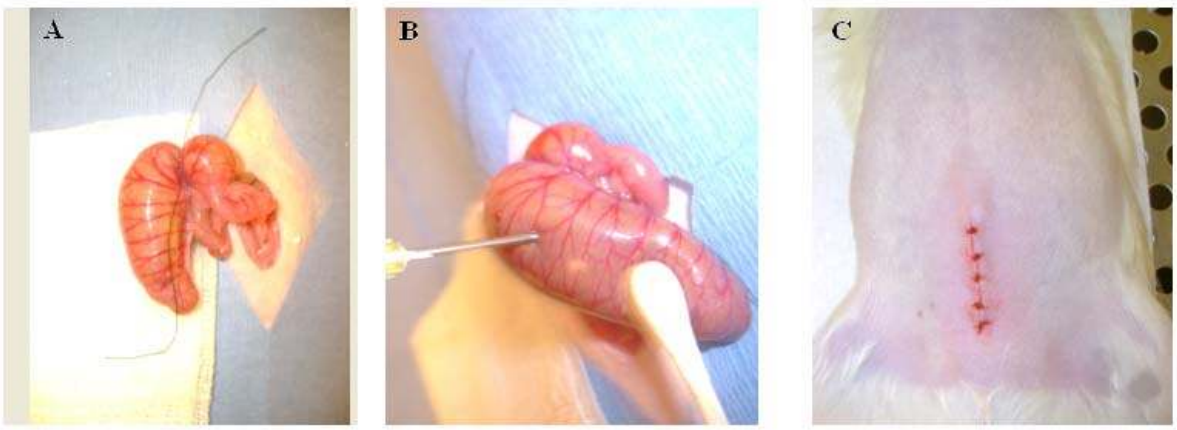

Figure 3.2. Experimental of CLP treatment.

The cecum is first ligated (A) and punctured using a 20 gauge needle (B). After replacing the cecum in the peritoneum, the abdominal incision is sutured (C).

3.2.4 Cecum Ligation and Puncture

CLP was used as an infection model because it is thought to closely mimic the physiological changes in human sepsis (Rittirsch et al. 2009). Rats were anesthetized and given the analgesic buprenorphrine subcutaneously at 0.01 to 0.05 mg/kg. Animals were then placed in supine position and hair was shaved on the abdomen. Bupivicaine (0.125% to 0.25%) was applied subcutaneously around the incision site for additional perioperative and postoperative analgesia. The abdominal cavity was cut open by a 2 cm midline incision. The cecum of the rat was exposed and ligated just below the ileocecal valve so as to avoid intestinal obstruction (**Figure 3.2 A**). Suture was passed between the body of the cecum and the main artery, so that the latter was not ligated. The cecum was punctured 4 times (not through and through) with a 20 gauge needle and replaced in the

peritoneum (**Figure 3.2 B**). The abdominal incision was then sutured in layers using interrupted monofilament sutures (**Figure 3.2 C**). The animal received 10 mL/kg saline intraperitoneally for resuscitation. Sham-CLP controls consisted of animals treated identically without receiving CLP, i.e. they were anesthetized, underwent laparotomy as described above, but no surgical manipulation of the cecum was performed. Rats were single caged after the treatments and given standard rat chow and water ad libitum until sacrifice.

3.2.5 Cytokine Analysis

Animals were anesthetized at different time points (2, 4, 8, 12, 16, 20, and 24) (n=3 per time point per group) post burn or CLP. Blood samples were immediately collected from the vena cava by heparinized catheters, kepted on ice, and then centrifuged at 4500 rpm for 3 min at 4 °C. The serum supernatant was collected and stored at -80 °C until analysis. A MILLIPLEX MAP Rat Cytokine/Chemokine Panel (Millipore) was used for the simultaneous quantification of 23 different cytokines (Eotaxin, G-CSF, GM-CSF, GRO/KC, IFN-γ, IL-10, IL-12 (p70), IL-13, IL-17, IL-18, IL-1α, IL-1β, IL-2, IL-4, IL-5, IL-6, IP-10, Leptin, MCP-1, MIP-1α, RANTES, TNF-α, VEGF) according to the manufacturer's guidelines.

3.2.6 Data Analysis

We recently developed an algorithm to estimate the area under the curve (AUC) of a variable baseline and compare it with the AUC of the response curve (Scheff et al. 2011).

This method was used to discover significant net responses such as transcriptional regulatory effects in gene expression data. Given the fact that cytokine production may be altered throughout the observation period, the concept of area under the curve can be used to assess the dynamic responses and the deviation from their baseline values (Heinzl 1996; Wolfsegger 2007). This method was selected here since it is proven to be more informative for experiments having high sampling frequencies after the experimental perturbations (Scheff et al. 2011). In this study, for each cytokine, the overall AUC (area under the cytokine concentration–time curve in treatment group, i.e. B and CLP groups) and baseline AUC (area under the cytokine concentration–time curve in control group, i.e. S group) were calculated numerically (Wolfsegger 2007). These values were then compared to determine if the overall AUC significantly deviates from the baseline AUC by identifying p-values using a t-distribution and Sattertwaite's approximation for degrees of freedom (Heinzl 1996). Finally, the algorithm proposed by Benjamini and Hochberg (Benjamini and Hochberg 1995) was used to determine a data-based p-value threshold controlling the false discovery rate at the level α (α=0.05 in this study).

Briefly, AUC was calculated by the trapezoidal rule using the means of replicates, $\bar{X}_{jk}$, at each time point t_j (Wolfsegger 2007) as follows:

$$
\begin{aligned}
AUC_k &= \sum_{j=1}^{m} w_j \bar{X}_{jk}, \quad k = 1.....f \\
\bar{X}_{ik} &= \frac{1}{n_{jk}} \sum_{i=1}^{n_{ik}} X_{ijk} \\
w_1 &= \frac{1}{2}\left(t_2 - t_1\right) \\
w_j &= \frac{1}{2}\left(t_{j+1} - t_{j-1}\right) \quad \text{for } 2 \le j \le m-1 \\
w_m &= \frac{1}{2}\left(t_m - t_{m-1}\right)
\end{aligned}
\tag{3.1}
$$

where m and f are the total number of time points and number of groups, respectively, and n_{jk} is the total number of replicates or animals at time points t_j and group k. The variance of linear AUC estimator is obtained as:

$$
V\left(AUC_k\right) = \sum_{j=1}^{m} w_j^2 \sigma_{jk}^2 n_{jk}^{-1} \tag{3.2}
$$

where σ_{jk} is the standard deviation of the concentration values at time j in group k. A test of null hypothesis of no difference between two AUCs has been presented by Heinzl (Heinzl 1996). The null hypothesis of equality among two AUC's (k=1, 2) is given as:

$$
H_o : E(AUC_1) - E(AUC_2) = \sum_{j=1}^{m} w_j \bar{X}_{j1} - \sum_{j=1}^{m} w_j \bar{X}_{j2} = 0 \tag{3.3}
$$

Assuming t-distribution and Sattertwaite's approximation, t value and degree of freedom, v, are calculated as follows in order to obtain p-value (t_{obs}, v):

$$t_{obs} = \frac{\sum_{j=1}^{m} w_j \bar{X}_{j1} - \sum_{j=1}^{m} w_j \bar{X}_{j2}}{\sqrt{\sum_{j=1}^{m} w_j^2 \sigma_{j1}^2 n_{j1}^{-1} + \sum_{j=1}^{m} w_j^2 \sigma_{j2}^2 n_{j2}^{-1}}} \tag{3.4}$$

$$v = \frac{\left(\sum_{j=1}^{m} w_j^2 \sigma_{j1}^2 n_{j1}^{-1} + \sum_{j=1}^{m} w_j^2 \sigma_{j2}^2 n_{j2}^{-1} \right)^2}{\sum_{j=1}^{m} w_j^4 \sigma_{j1}^4 \left(n_{j1}^2 \left(n_{j1} - 1 \right) \right)^{-1} + \sum_{j=1}^{m} w_j^4 \sigma_{j2}^4 \left(n_{j2}^2 \left(n_{j2} - 1 \right) \right)^{-1}} \tag{3.5}$$

Then, the calculated p-values are ordered, $p_{(1)} \le .... \le p_{(z)}$, where z is total number of cytokines. Using Benjamini and Hochberg approach (Benjamini and Hochberg 1995), $\hat{l}$ is calculated as:

$$\hat{l} = \max \left\{ 1 \le l \le z : p_{(l)} \le \alpha . \left(l / z \right) \right\} \tag{3.6}$$

If $\hat{l}$ exists, the first $\hat{l}$ null hypotheses are rejected, implying that the cytokines corresponding to $p_{(1)} \le .... \le p_{(\hat{l})}$ are significantly changed.

Heat maps were generated by the "clustergram" function in MATLAB, which was used to cluster the differentially produced cytokines and chemokines (hierarchical clustering). This further enabled to compare and analyze the dynamic patterns of the inflammatory mediators.

3.2.7 Predicting Putative Transcription Factors

In order to identify potential transcription factors (TFs) that regulate cytokine gene expression, we explored the basic underlying assumption of comparative genomics which states that functional regions evolve in a constrained fashion and therefore at a lower rate than non-functional regions (Doniger et al. 2005; Hardison 2000). It implies that conserved regions in a set of orthologous sequences survive due to their special functional implications i.e. TF families associated with binding sites identified on these conserved regions are more likely to function as transcriptional regulators. Promoters of cytokine genes of rats were extracted from the Genomatix database of promoter information with a default length (500bp upstream and 100bp downstream of the transcription start site) unless an experimentally defined length has been reported (Genomatix). Each promoter is characterized by a set of orthologous promoters from the same gene of other vertebrate species, if available (e.g. Homo sapiens, Macaca mulatta, Pan troglodytes, Mus musculus, Equus caballus, Canis lupus familiaris, and Bos Taurus). DiAlign TF (Genomatix) with default parameters (core similarity: 0.75, matrix similarity: optimal threshold for each position weight matrix suggested from MatBase (Genomatix)) was subsequently applied to identify conserved regions on promoter P and then transcription factor binding sites (TFBSs) that are enriched on corresponding conserved regions from the set of orthologous promoters with a common threshold (70% in this study). In addition, in order to increase the confidence of the predicted binding sites ModelInspector (Genomatix) was used to search for a list of cis-regulatory modules (L) from a library of functional, experimentally-verified, modules (MatBase(Genomatix))

that match on promoter P. Identified TFBSs on P are then scanned over L and only those that are present on modules in L are selected. Associated TF families with those selected TFBSs are inferred and considered as transcriptional regulators for corresponding cytokines.

3.3 Results and Discussion

3.3.1 Animal Weight Changes and Mortality

All animal groups had 100% survival for at least one week following treatment ($n \geq 3$ for each treatment). The time course of whole body weight changes was also monitored. CLP caused a ~10% weight loss, although after 24 hours, the animals started to regain weight at a rate similar to that observed pre-CLP (**Figure 3.3**). Sham-CLP did not cause any change in body weight gain rate. These observations are consistent with prior literature using a similar model (Banta et al. 2007). Burn injury and sham-burn did not result in any significant change in the rate of body weight gain (data not shown).

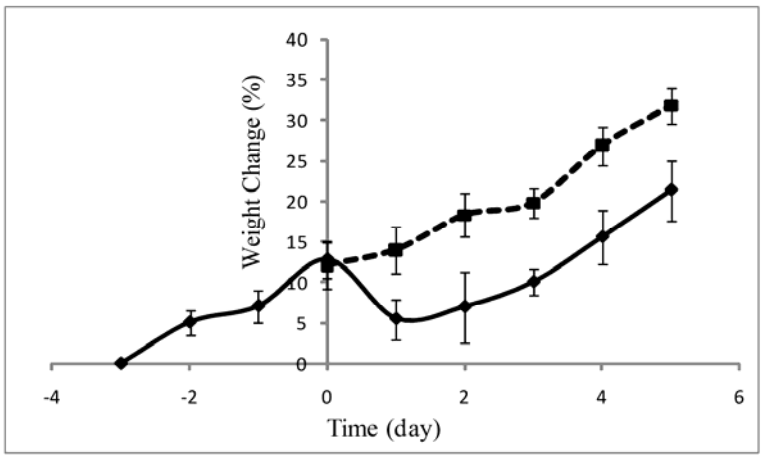

Figure 3.3. Body weight change (%) in CLP (solid line) and SCLP (dotted line) groups. n≥10.

CLP in rodents results in a hypermetabolic and catabolic state (Banta et al. 2007) and has been extensively used as a model of sepsis. While it is generally viewed as more realistic than endotoxin injection models, it is important to note that the response and mortality rate to CLP can vary depending on the specific procedural details (e.g. length of the cecum ligated, size of the needle, and the number of punctures) of the technique used, as well as rat strain (Otero-Anton et al. 2001; Rittirsch et al. 2009). In the procedure used herein, we took care to not ligate the cecal branch of the ileocecal artery, thus preserving viability of the cecum itself, which explains our high survival rate, consistent with observations published by Banta and co workers (Banta et al. 2007). We did not want high mortality since our purpose was to compare injury vs. infection induced systemic inflammatory responses in nonlethal and reversible conditions.

3.3.2 Cytokine Profiles

Cytokine profiles in the Sham group (which did not receive any injury or surgical manipulation) were used as reference to which the profiles obtained for all other groups were compared. **Table 3.1** shows the cytokines which have been filtered out by the AUC method incorporated with Benjamin and Hochberg false discovery rate correction. MCP-1 (Monocyte chemotactic protein), IL-18 (Interleukin-18), GCSF (granulocyte colony-stimulating factor), GRO/KC (growth related oncogene), IL-10 (Interleukin-10), IL-12P70 (Interleukin-12 or IL-12) and IL-1α (Interleukin-1α) were significantly altered in the animals receiving a 20% TBSA burn injury. Concentrations of the chemokines GRO/KC (P=0.003), MCP-1 (P=0.0002) and GCSF (P=0.0017) - which are chemotactic for leukocytes to injured areas- were increased in the burn group. GRO/KC showed a peak around t=8 h after the burn injury whereas MCP-1 steadily increased within 24 hours postburn (**Figure 3.4**). Similarly, IL-12 (P=0.004), which can be regarded as both a pro- and an anti-inflammatory cytokine, IL-10, an anti inflammatory cytokine (P=0.004), and IL-18 (P=0.0008), a pro inflammatory cytokine, reached a maximum at t=4h. On the other hand, IL-1α (P=0.007), a pro-inflammatory cytokine, seems to be down-regulated after burn.

SCLP, which involves laparotomy without ligation or puncturing of the cecum, caused changes in several markers. It was observed that some of the chemokines, including IP-10 (interferon gamma induced protein) (P=0.0001), GRO/KC (P=0.0004), and MCP-1 (P=0.0004) were significantly different from the Sham group (**Table 3.1**). GRO/KC and

MCP-1 peaked around t=8 h after SCLP treatment (**Figure 3.5**). On the other hand, IP-10 concentrations decreased (**Figure 3.5**). Similarly, some pro-inflammatory cytokines, including IL-1β, IL-17, and IFN-γ (P = 0.002, 0.01 and 0.01, respectively) and Leptin (P= 0.004), a hormone regulating energy intake and energy expenditure, were decreased after SCLP treatment.

Table 3.1. Differentially produced cytokines and chemokines.

Observed P values of cytokines obtained from AUC method which are filtered out by Benjamin & Hochberg criteria are only given.

S vs B		S vs SCLP		S vs CLP		SCLP vs CLP		Benjamin & Hochberg	
Cytokines & Chemokines	**P value (AUC)**	**Cytokines & Chemokines**	**P value (AUC)**	**Cytokines & Chemokines**	**P value (AUC)**	**Cytokines & Chemokines**	**P value (AUC)**	***l***	$p_l=\alpha.(l/z)$
MCP-1	0.00023 ($P \leq p_{l=1}$)	IP-10	0.00012 ($P \leq p_{l=1}$)	MCP-1	1.00E-05 ($P \leq p_{l=1}$)	IL-12P70	0.0005 ($P \leq p_{l=1}$)	*l=1*	*0.0022*
IL-18	0.0008 ($P \leq p_{l=1}$)	GROKC	0.00036 ($P \leq p_{l=1}$)	GMCSF	0.00037 ($P \leq p_{l=1}$)	IL-18	0.001 ($P \leq p_{l=1}$)	*l=2*	*0.0044*
GCSF	0.0017 ($P \leq p_{l=3}$)	MCP-1	0.0004 ($P \leq p_{l=3}$)	IP-10	0.0004 ($P \leq p_{l=3}$)	Eotaxin	0.0014 ($P \leq p_{l=3}$)	*l=3*	*0.0065*
GROKC	0.003 ($P \leq p_{l=4}$)	IL-1beta	0.0024 ($P \leq p_{l=4}$)	IL-18	0.0008 ($P \leq p_{l=4}$)	IL-4	0.009 ($P \leq p_{l=4}$)	*l=4*	*0.009*
IL-10	0.004 ($P \leq p_{l=5}$)	Leptin	0.004 ($P \leq p_{l=5}$)	IL-12P70	0.001 ($P \leq p_{l=5}$)			*l=5*	*0.011*
IL-12P70	0.004 ($P \leq p_{l=6}$)	IL-17	0.01 ($P \leq p_{l=6}$)	Leptin	0.0022 ($P \leq p_{l=6}$)			*l=6*	*0.013*
IL-1alpha	0.007 ($P \leq p_{l=7}$)	IFN	0.011 ($P \leq p_{l=7}$)	GROKC	0.012 ($P \leq p_{l=7}$)			*l=7*	*0.015*
				Eotaxin	0.012 ($P \leq p_{l=8}$)			*l=8*	*0.017*

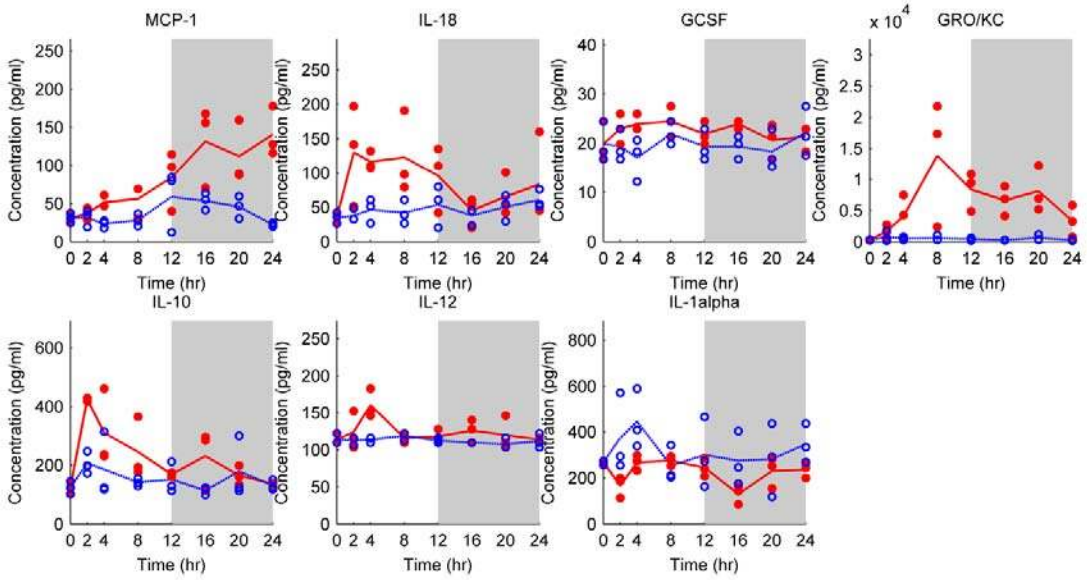

Figure 3.4. Cytokine and chemokine profiles in Burn (red dot) and Sham (blue circle) groups.

Each circle or dot represents an independent sample, and lines pass through average cytokine profiles at each time point. The white and grey colors represent light and dark cycles respectively.

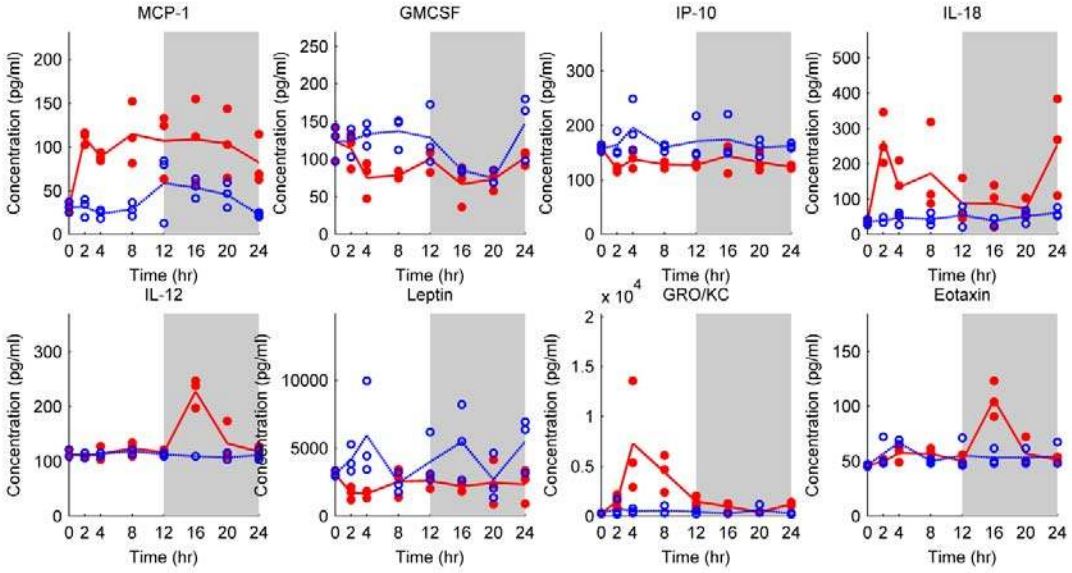

Figure 3.5. Cytokine and chemokine profiles in SCLP (red dot) and Sham (blue circle) groups.

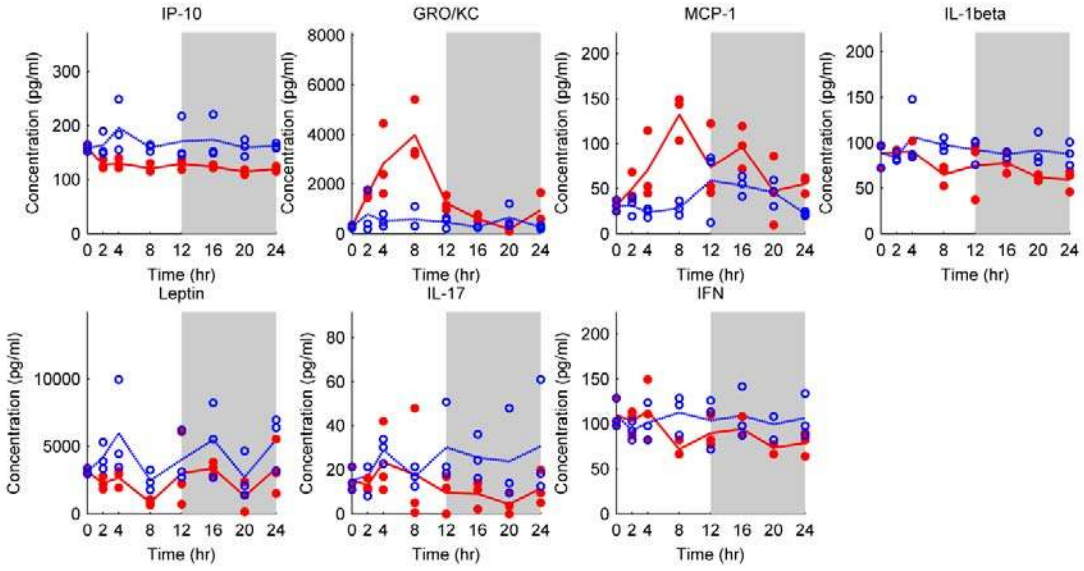

Figure 3.6. Cytokine and chemokine profiles in CLP (red dot) and Sham (blue circle) groups.

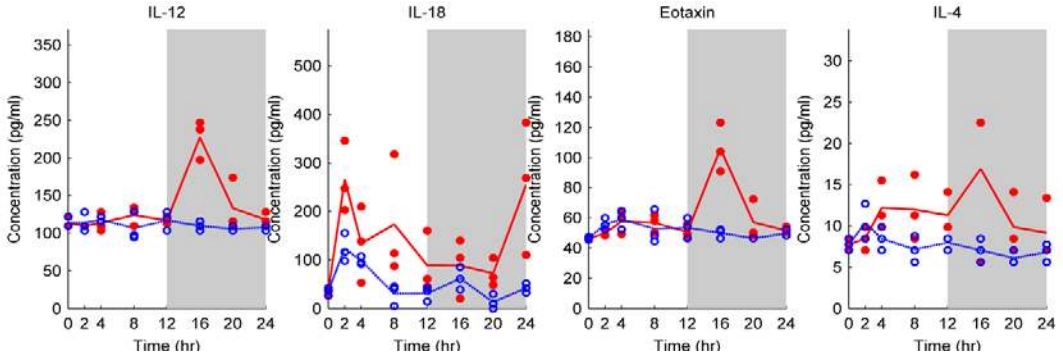

Figure 3.7. Cytokine and chemokine profiles in CLP (red dot) and SCLP (blue circle) groups.

MCP-1, GMCSF, IP-10, IL-18, IL-12, Leptin, GRO/KC and Eotaxin were significantly altered by CLP treatment compared to the Sham group (**Table 3.1** and **Figure 3.6**). IL-18, a pro inflammatory cytokine, was significantly elevated (P=0.0008) and demonstrated two peaks at around t=2 h and t=24 h. Similar to previous observations, GRO/KC peaked at 8 h post-CLP. On the other hand, IL-12 peaked later, at t= 16 h, which is also later than the observed IL-12 profile in the burn group (**Figure 3.4**). Eotaxin, a chemoattractant protein, also showed significant elevation at t=16 h (P=0.01). MCP-1 (P=0.00002) significant increased within the 24 h post-burn period. Other chemokines, namely GMCSF, IP-10, and Leptin, decreased after the CLP treatment.

Finally we compared the CLP group to the SCLP group to identify infection-specific effects. IL-12, IL-18, Eotaxin, and IL-4 were significantly different (**Table 3.1**). IL-4, an anti-inflammatory cytokine, was significantly decreased compared to the SCLP group

(P= 0.01) (**Figure 3.7**). On the other hand, IL-12, IL-18, and Eotaxin were increased in the CLP group compared to the SCLP group (as well as the Sham group).

When baseline values of the control group (S) were used for comparison to the injured animals (B, SCLP and CLP), we observed that GRO/KC and MCP-1 chemokine concentrations were significantly elevated in all treatment groups. Moreover, significant alterations in IP-10, Leptin and Eotaxin profiles in CLP and/or SCLP group (**Figure**s **3.5** and **3.6**) were also detected. Leptin is a hormone regulating food intake and metabolic functions, and its concentration was decreased in CLP and SCLP groups in this study. Although IL-1β and TNF-α contribute to the up-regulation of leptin production in animals, results from studies conducted in septic patients are contradictory since both up or down regulation in leptin production could be observed in the patients (Fantuzzi and Faggioni 2000). MCP-1 and Eotaxin are CC chemokines where the first two cysteines are adjacent to each other. They attract mononuclear cells to sites of chronic inflammation (Charo and Ransohoff 2006). GRO/KC and IP-10 are chemokines in CXC group (the first two cysteines are separated by an amino acid) which are neutrophil and lymphocytes chemo-attractants and induce granule exocytose, fibroblast differentiation and restrain angiogenesis (Charo and Ransohoff 2006).

IL-18, a pro-inflammatory cytokine, was increased in the early phase of inflammation in burn and CLP groups in this study. It has structural similarities with IL-1 family proteins (Arend et al. 2008) . It can be expressed by different cell types including macrophages,

Kupffer cells, keratinocytes and adrenal cortical cells (Lin et al. 2000). Similar to IL-1 and TNF-α pro inflammatory cytokines, IL-18 activates similar signaling molecules (Thomassen et al. 1998); thus, one can speculate that IL-18 might be functionally similar to TNF-α and IL-1β. In fact, Bohn and co-workers demonstrated that IL-18 is involved in the regulation of cytokine production during the early phase of bacterial infections and in the clearance of bacteria in mice (Bohn et al. 1998). IL-12 was another cytokine demonstrating increased concentrations in both the burn and CLP groups in this study. IL-12 plays an important role in the development of T helper (Th) 1 autoimmune responses (Lin et al. 2000). It is produced by monocytes, macrophages, dendritic cells, neutrophils and B cells (Paunovic et al. 2008). Administration of IL-12 in chimpanzees by intravenous injection induced increases in plasma concentrations of IL-15, IL-18, and IFN-γ, and a marked anti-inflammatory cytokine response (IL-10, IL-1 receptor antagonist) and secretion of different chemokines (Lauw et al. 1999). IL-10 is one of the most important anti-inflammatory cytokines which has been studied extensively to characterize the immune responses in different animal models. However, only in the burn group an increase in IL-10 concentration was detected. IL-10 is mainly synthesized by CD4+ Th2 cells, monocytes and B cells (Opal and DePalo 2000). IL- 10 is regarded as modulator of the pro- inflammatory response by inhibiting production of TNF-α and IL-1β. IL-10 is also capable of decreasing the IL-18 mRNA expression in monocytes (Marshall et al. 1999).

Table 3.2. Grouping the cytokines and chemokines based on their concentration changes in three injury models.

Some mediators (MCP-1 and GRO/KC) are observed in more than one group whereas some are specific to an injury type.

Cytokines/Chemokines	Sham vs Burn	Sham vs CLP	Sham vs SCLP
GCSF	√		
IL-10	√		
IL-1A	√		
GMCSF		√	
EOTAXIN		√	
IL-17			√
IFN			√
IL-1beta			√
IL-18	√	√	
IL-12	√	√	
IP-10		√	√
LEPTIN		√	√
MCP-1	√	√	√
GRO/KC	√	√	√

3.3.3 Comparison of Injury Models

In this study three different injury models were analyzed. When these are compared, certain mediators exhibit insult-specific behavior whereas others exhibit similar response across all animal groups (**Table 3.2**). GCSF, IL-10 and IL-1alpha were only identified in the burn group, whereas GMCSF and Eotaxin were specific to CLP. IL-17, IFN and IL-1beta were only observed in Sham-CLP group which received a sterile surgical treatment. A significant number of overlapping cytokines/chemokines between CLP and other groups were identified, including IL-18, IL-12, IP-10, Leptin, MCP-1 and GROKC

(**Table 3.2**). Among them, MCP-1 and GROKC are the only mediators observed in all groups.

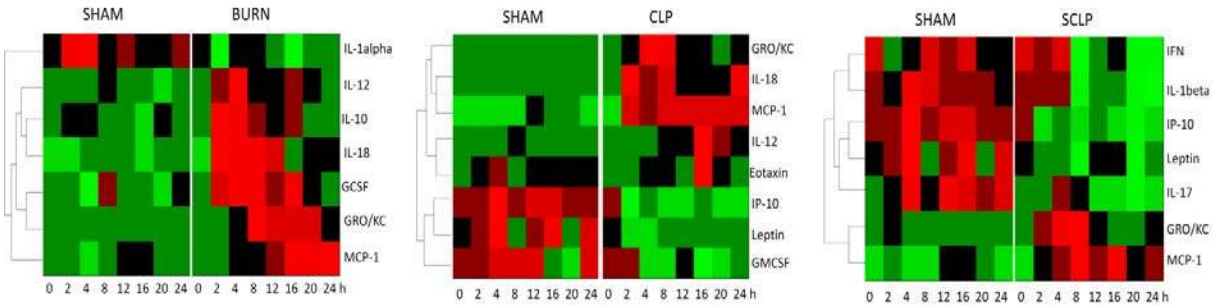

Figure 3.8. Heat maps comparing the treatment groups (Burn, CLP and SCLP) with the control group (Sham).

Green indicates the lowest level while red indicates the highest and black average level.

We further clustered the temporal profiles of the differentially produced cytokines in all three groups and represented them as heat maps (**Figure 3.8**) to elucidate and compare the dynamic patterns. IL-1alpha was down regulated in the burn group whereas GMCSF, Leptin and IP-10 concentrations decreased following the CLP treatment in a similar fashion. In SCLP group, additional cytokines and chemokines were down-regulated including IFN, IL-1beta, IP-10, Leptin and IL-17. In the burn group, IL-12, IL-10, IL-18 and GCSF were up-regulated at the early stage while GRO/KC and MCP-1 at the late stage around t=8-12 h. Similarly, early up-regulation of IL-10 concentration was also

reported by Gauglitz et al. (Gauglitz et al. 2008) whereas they showed MCP-1 concentration was increased at the early stage in the rat model receiving 60 % TBSA burn. Finnerty et al. (Finnerty et al. 2009) also elucidated an early up-regulation in GRO/KC concentration in mice following the 35 % TBSA burn. The chemokine/cytokine dynamic patterns in the burn group (**Figure 3.8**) were not observed in SCLP or CLP groups in this study. MCP-1 and GRO/KC concentrations were increased at the early stage and moreover MCP-1concentration showed a persistent elevation in both groups. It is noteworthy that IL-12 profile peaked early around 4 hour postburn, while it peaked much later, at 16 hours following CLP (**Figure 3.8**). Similarly, Eotaxin concentration was only increased in the CLP group and also exhibited a peak around t=16 h. However concentrations of both Eotaxin and IL-12 were up-regulated for a short period of time in CLP group.

In this study, we did not observe any significant change in the concentration of TNF-α, IL-1 β and IL-6, in either burn or CLP groups. Similarly, Murphy et al. (Murphy et al. 2005) observed no significant differences between sham and burn (25 % TBSA) mice in the plasma concentrations of TNF-α, IL-6 and IL-10 after the injury. In fact, conflicting observations regarding the cytokine expressions in animal models have been extensively reported in literature. It is obvious that variations in experimental procedures, and size and severity of injuries as well as utilizing different species might result in different consequences in cytokine profiles. Barber and co-workers (Barber et al. 2008) observed that cytokine concentrations significantly increased when burn size increased in rats.

Walley et al. (Walley et al. 1996) used mice and three needle sizes (18 GA, 21 GA and 26 GA) for CLP treatments. They observed that as the diameter of the CLP needle decreased, the TNF-α and IL-6 concentrations decreased and IL-10 concentration increased. Klein and co-workers (Klein et al. 2003) used rats for 30% TBSA burn, and observed that IL-1 beta and TNFalpha increased after burn. On the other hand, Gauglitz and co-workers (Gauglitz et al. 2008) utilized rats receiving full thickness burn of 60% TBSA. They observed that serum concentrations of TNF-α were not found to be significantly different although other cytokines or chemokines including IL-10, MCP-1 and GRO (CINC-1) were significantly elevated after burn. We also observed significant elevations in IL-10, MCP-1 and GRO concentrations in rats receiving 20 % TBSA burn injury. Conflicting observations were also reported in the studies conducted in burn or septic patients or human subjects. Interestingly in some studies, a transient increase in TNF-α concentration was observed in burn patients (Vindenes et al. 1998). It has been also shown that IL-1β was not detected in the plasma of burn patients (Debandt et al. 1994) although its plasma concentration generally increases after burn injury with septic shocks in human or it is positively correlated with burn size (Drost et al. 1993b).

3.3.4 Putative Transcription Factors

By searching the conserved regions of promoters, we identified putative transcription factors (TFs) of the significantly altered cytokines that might participate in the regulation of their corresponding genes (**Table 3.3**). It is well known that many signaling pathways including MAPK, Jac/STAT, and Ik-B/NF-kβ cascades where NF-kβ, Stat, and C/EBP-β transcription factors play key roles are activated in various tissues in the early phase of

burn and septic shocks (Andrejko et al. 1998; Cho et al. 2004a; Klein et al. 2003; Ogle et al. 2000). NF-kβ, Stat, and C/EBP-β are well known regulators involved in cytokine production. These were also identified in our analysis (**Table 3.3**) and were found to be associated with GRO/KC, MCP-1, Eotaxin and IL-10. It is also remarkable to say that cytokines or chemokines produced by these TFs eventually trigger the signaling pathways activating the similar TFs. IL-18, IL-12 and most of the chemokines activate JAK/STAT and MAPK signaling pathways (Soriano et al. 2003). IL-10 (which was significantly elevated in the burn group in our study) induces STAT activation which promotes the transcription of Suppressor of Cytokine Signaling 3 (SOCS3), a negative feedback regulator inhibiting many inflammatory cytokines such as TNF-α, IL-6, and IL-1. There are also other putative TFs identified (**Table 3.3**) such as ETS, SP1, GATA and VTBP which have been known to regulate the function of immune system and play important role in the inflammation. ETS transcription factors activate immunity-related genes including promoters of IL-12 and IL-18 (Gallant and Gilkeson 2006).

Table 3.3. Putative transcription factors of some cytokines and chemokines observed in burn and CLP groups.

Transcription factors	GRO/KC	MCP-1	Eotaxin	Leptin	IL-18	IL-12	IL-10
ETSF (Human and murine ETS1 factor- E-twenty six family)	√	√			√	√	
MYOD (Myoblast determining factors)	√						√
NFKB (Nuclear factor kappa B/c-rel)	√		√				
PBXC (PBX1 - MEIS1 complexes)	√						
SORY (SOX/SRY-sex/testis determining and related HMG box factors)	√						
STAT (Signal Transducer and Activator of Transcription)		√	√				√
PARF (PAR/bZIP family)			√				
CEBP (CCAAT-enhancer-binding proteins)			√				√
SP1F (GC-Box factors SP1/GC)			√	√	√		
EREF (Estrogen Response Element family)							
VTBP (TATA binding protein factor)			√		√		√
BRNF (Brn POU domain factors)					√		
CAAT (CCAAT binding factors)					√		
CREB (cAMP response element-binding)					√		
FKHD (Fork head domain factors)					√		
HNF1 (Hepatocyte nuclear factor 1)					√		
NF1F (Nuclear Factor 1)					√		
OCT1 (Octamer-binding transcription factor 1)					√		
GATA (GATA binding factors)				√		√	
HAND (Twist subfamily of class B bHLH transcription factors)						√	
KLFS (Krupple like factor family)				√			

***Note**: These are transcription factor families, each of which includes several TFs that have similar binding sites.*

Although more complicated experimental analysis is required to identify the functional transcription factors regulating cytokine expression levels, bioinformatics analysis like the one presented in this work provides insights on the signaling system and identifies possible targets for the experimental researches. It is well known that NF-kβ regulates the expression of a number of cytokines and chemokines including IL-1, TNF and IL-6 (Pahl 1999). It is also known that the transcription factor CREB might show an anti-inflammatory behavior by inhibiting NF-kβ signaling (Wen et al. 2010). We identified that CREB is a putative TF of IL-18 whose concentration was elevated in both burn and CLP groups. On the other hand, IL-1, TNF and IL-6, mainly regulated by NF- kβ, were not identified in burn and CLP groups in this study. Another interesting finding is that ETS1 factors might have potential to regulate the MCP-1 and GRO/KC chemokines which had similar temporal profiles. It has also been reported in literature that inhibition of ETS1 up-regulates IL-10 concentration (Russell and Garrett-Sinha 2010). IL-10 was significantly elevated at the early phase of the inflammatory response in the burn group. However, MCP-1 and GRO/KC concentrations were elevated when IL-10 concentration decreased in the burn group (see **Figure 3.8**). On the other hand, in CLP and SCLP groups, we did not observe significant changes in IL-10 concentration, but GRO/KC and MCP-1 were increased at the early stage and more persistent elevated MCP-1 was observed in CLP and SCLP groups when compared to the burn group (**Figure 3.8**). Due to the high interdependency of physiological processes, integrating multiple sources together with the bioinformatics tools in attempt to answer the question to what extend transcription factor activation affects the circulatory inflammatory mediators provide an

overview of the global regulation. This is also crucial to elucidate important regulatory points that can be used to modulate the inflammatory state at molecular level.

It is interesting that there is a certain number of putative TFs that might regulate the same cytokine (**Table 3.3**). Similarly, a TF might also regulate more than one cytokines. It should be noted that the tissue specificity was not considered in this study to determine the binding sites in the promoters. The sequence of the promoter regions of the cytokine genes was only analyzed to determine the putative TF binding sites. Although a set of TFs has potential to regulate the same cytokine, the question is whether, and how, this affects cytokine expression patterns in different injury models. It should be kept in mind that peripherally circulating cytokines are secreted by various tissues or cells including leukocytes, glial cells and liver, etc. It is well known that inflammatory response of a tissue might be different than that of another tissue, and similarly the host response depends on type of the injury (Feezor et al. 2005). Temporal and quantitative differences in the activation of TFs in various injury models explain the diversity of cytokines' patterns.

Complex interactions of cytokines or chemokines through the signaling network is a big challenge for studies aiming at determining new therapeutic targets to eliminate deleterious effects of chemokine or cytokine related disease states. Inhibition of certain mediator receptor interactions might be required in order to eliminate the negative effects of disorders caused by inappropriate mediator receptor regulations. However, this might

lead to activation or deactivation of undesired upstream signaling pathways. For example, using inhibitors or animal models deficient in certain chemokines-receptors including CXCR2 or CCR1 demonstrated improvement in sepsis formation and sepsis related lethality in animals (Ness et al. 2004; Ness et al. 2003). On the other hand, inhibiting chemokine receptors might also weaken antibacterial resistance of host by up-regulating the IL-10 (Feterowski et al. 2004). Consequently, a comprehensive understanding of underlying mechanisms of the inflammatory response is essential to have a more control over the proposed therapeutic approaches.

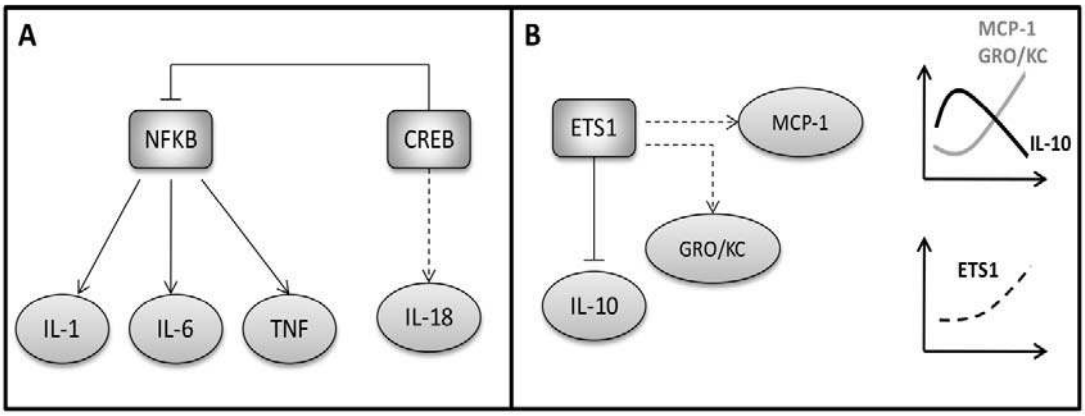

Figure 3.9. Putative regulatory mechanisms.

A. *The regulatory mechanism between NF-kβ and CREB. In burn and CLP groups, only IL-18 of which CREB is a putative TF was elevated, however no changes in IL-1, IL-6 and TNF concentrations were observed in both treatment groups.* ***B****. The regulatory mechanism of ETS1. ETS1 was identified as a putative TF of MCP-1 and GRO/KC. In burn group, these two cytokines' concentrations were increased while IL-10*

concentration was decreased. Note that straight lines indicate known regulatory mechanisms (based on literature) and dashed lines represent putative mechanisms estimated from this study based on experimental observations and TF analysis.

The mammalian regulatory landscape is highly complex and redundant conferring highly robust characteristics to the host (Carninci et al. 2005; Tan et al. 2008). Although very preliminary, the results of our TF analysis begin to point towards the direction of elucidating the structure and networks of transcription factors as these emerge as major contributors to regulation (Kyrmizi et al. 2006). The idea of inferring functional interactions by observing the dynamics of regulated signals has been previously explored in the context of liver-specific responses to soluble signals (King et al. 2007), whereas we recently demonstrated how the regulated dynamics can begin to elucidate implicit upstream interactions among transcription factors (Yang et al. 2007a; Yang et al. 2009a). In this context the information generated through our preliminary analyses enables the initial formulation of putative injury-specific modules of regulatory interactions (**Figure 3.9**). Undoubtedly, a lot of work still remains to be accomplished, but we wish to demonstrate that it is indeed plausible to integrate in vivo responses and bioinformatics tools towards the ultimate goal of describing testable hypotheses related to critical regulatory interactions.

3.4 Conclusions

In this study, we characterized the circulating cytokine profiles in the first 24 hours following 20% TBSA burn injury, SCLP, and CLP. Burn injury alone was used to investigate the effect of a systemic but "sterile" pro-inflammatory insult. CLP was used to investigate the effect of a bacterial infection, also a pro-inflammatory, but different, stimulus. Since CLP involves laparotomy, a surgical procedure, it was also necessary to include a SCLP group to ascertain the effect of the surgical procedure vs. that of the infection itself. While none of the insults caused mortality, CLP caused a transient decrease in body weight. We found that a certain number of cytokines and chemokines, belonging to the pro- and anti- inflammatory types, were altered by these insults. Furthermore, each insult was associated with a different cytokine signature profile.

Experimental observations can be very noisy. Problems can always arise in multiplex assays because of potential interactions between different antibodies and cytokines, and the presence of varying dynamic mutual-effects between rare and abundant cytokines in the samples (Zhou et al. 2010). The limited number of replicates in animal experiments can be also an additional complicating factor. In serial sacrifice designs where only one sample is taken from each animal, significant differences in the physiologic concentrations of circulatory proteins between the samples can be observed. Moreover, cyclic fluctuations (or circadian rhythm) in cytokine expressions, which affects the inflammatory response of the body (Holzheimer et al. 2002), can display 24 h period and even persist in the absence of external timing information (Keller et al. 2009). Therefore,

due to the dynamic behaviors and fluctuations observed in physiological processes, it was important to utilize an appropriate statistical approach to identify differentially expressed proteins over a time course. Although existing statistical methods such as ANOVA test are more appropriate for static sampling designs, these might not be applicable for time course experiments where detecting differences in the physiological behaviors of two or more groups over time is essential (Storey et al. 2005). The AUC is considered as an important indicator for drug availability and assessing the net pharmacological response of a given dose of drug (Heinzl 1996; Wolfsegger 2007). We recently explored this method to analyze gene expression time course data (Scheff et al. 2011). Similarly, the same concept can be applied for temporal experiments aiming at identifying differentially expressed proteins. This provides a quantitative estimate of overall exposure to cytokines which can be obtained by integrating the concentration curve over time. This also considers the temporal variability in the cytokine concentrations of control groups.

In conclusion, we analyzed the early stage (first 24 hours) serum cytokine and chemokine profiles in moderately injured rats receiving 20 % TBSA burn injury and CLP treatment. We identified cytokines and chemokines which were significantly elevated in the burn and CLP groups. Determining cytokine expression patterns in different animal models receiving different injuries would provide critical insights regarding the complex interactions of those inflammatory mediators at the cellular level enabling a better characterization of the inflammatory response.

CHAPTER IV

4 DYNAMICS OF SHORT TERM GENE EXPRESSION PROFILING IN LIVER FOLLOWING THERMAL INJURY AND SEPSIS

Abstract

Severe trauma, including burns and infections, triggers a systemic response that significantly impacts on the liver, which plays a key role in the metabolic and immune responses aimed at restoring homeostasis. While many of these changes are likely regulated at the gene expression level, there is a need to better understand the dynamics and expression patterns of burn injury or sepsis induced genes in order to identify potential regulatory targets in the liver. Herein we characterized the response within the first 24 h in a standard animal model of burn injury or sepsis induced by cecum ligation and puncture (CLP) using a time series of microarray gene expression data.

The clustering method of expression data identified 621 burn-responsive probesets in 4 different co-expressed clusters. Functional characterization revealed that these 4 clusters are mainly associated with pro-inflammatory response, anti-inflammatory response, lipid biosynthesis, and insulin-regulated metabolism. Cluster 1 pro-inflammatory response is rapidly up-regulated (within the first 2 h) following burn injury, while Cluster 2 anti-inflammatory response is activated later on (around 8 h post burn). Cluster 3 lipid biosynthesis is downregulated rapidly following burn, possibly indicating a shift in the

utilization of energy sources to produce acute phase proteins which serve the anti-inflammatory response. Cluster 4 insulin-regulated metabolism was down-regulated late in the observation window (around 16 h postburn), which suggests a potential mechanism to explain the onset of hypermetabolism, a delayed but well-known response that is characteristic of severe burns and trauma with potential adverse outcome.

Following the CLP treatment, three major clusters have been identified. The first cluster which is enriched by the genes involved in Toll like signaling and MAPK signaling pathways are activated around 2 h following the treatment. The gene expression profile of CLP group in the second cluster is activated around 4h and peaks around 12h, later than that of SCLP. This group is mainly related to genes involved in acute phase protein synthesis. The third cluster is slightly down-regulated following the CLP, which is associated with the genes in transcription system.

Simultaneous analysis and comparison of gene expression profiles for both burn and sham control groups provided a more accurate estimation of the activation time, expression patterns, and characteristics of a certain burn-induced response based on which the cause-effect relationship among responses were revealed.

4.1 Introduction

Thermal injury, one of the most severe forms of trauma, triggers a number of physiological responses including local and systemic inflammation, hyper-metabolism,

immune-suppression, and eventually organ dysfunction (Dasu et al. 2004). Severe burn injuries are generally associated with bacterial infections trans-located from gastrointestinal tract to circulatory system, which results in an ongoing hyper-metabolic state in the body. Cecal ligation and puncture (CLP) model is an animal model that mimics the physiological changes of human sepsis, which is considered as the gold standard for sepsis researches (Wichterman et al. 1980). Following CLP, animals generally develop bacteremia, hypothermia, hypotension, and hyper-metabolic and catabolic state at whole body level. Clinical studies have shown that an uncontrolled and prolonged action of inflammatory cytokines, which is evidenced by a sustained release of acute phase proteins, may contribute to detrimental complications (Drost et al. 1993a). Liver is an important player in the modulation of the inflammatory response since it largely controls circulating levels of metabolites and the production of acute phase proteins. It is known that inflammatory mediators as well as metabolic changes in the circulation result in alterations in gene expression levels in the liver (Dasu et al. 2004; Vemula et al. 2004). Therefore, understanding the liver response at the molecular level is critical to understand the systemic inflammatory disease, as well as its potential as a target for therapeutic approaches.

Prior studies using classical RT-PCR to analyze gene expression in liver have shown that inflammation upregulated specific receptors (such as CD14 receptors, protease activated receptors, histamine H-1 and H-2 receptors), transcription factors (NF-κβ, Stat3, and C/EBP-β) and other proteins or kinases (such as ERK, JNK, and p38) involved in the

MAPK, Jac/STAT, and Ik-B/NF-kB signaling pathways (Andrejko et al. 1998; Cho et al. 2004a; Cho et al. 2004b; Jeong et al. 2003; Jesmin et al. 2006; Klein et al. 2003; Masaki et al. 2005; Nishiura et al. 2000; Yang et al. 1999). Recently, microarray technology and transcriptional profiling have been used to elucidate genome-wide changes in the liver following the burn injury (Dasu et al. 2004; Jayaraman et al. 2009; Vemula et al. 2004) and CLP (Chinnaiyan et al. 2001; Cobb et al. 2005; Li et al. 2007).

In general, unsupervised hierarchical clustering was applied in order to identify specific patterns of gene expression in the liver associated with burn injury or CLP. A limitation of the aforementioned studies is that the control group was defined as the initial pre-treatment condition corresponding to the 0 h time point. However, gene expression in a healthy animal liver naturally fluctuates over time due to circadian rhythms (Almon et al. 2008). In order to obtain a better resolution of the dynamics of the injury response, it is therefore necessary to account for the dynamics of the control group as well.

In this study, we used a standard burn injury model of the rat to compare the dynamics of gene expression in liver in burn vs. sham burn (control of burn) and CLP vs. sham CLP (control of CLP) conditions during the first 24 h. The differentially expressed genes between control and treatment conditions over time whose expression patterns were significantly altered following the treatment were identified and clustered. Simultaneous analysis of the expression profiles of these groups enabled to characterize the dynamic patterns of both groups and reveal a comprehensive picture regarding the temporally

coordinated inflammatory and metabolic changes in the liver following burn injury or CLP.

4.2 Materials and Methods

4.2.1 Animal Model

Male Sprague-Dawley rats (Charles River Labs, Wilmington, MA) weighing between 150 and 200 g were used. The animals were housed in a temperature-controlled environment (25°C) with a 12-hour light-dark cycle and provided water and standard chow ad libitum. All experimental procedures were carried out in accordance with National Research Council guidelines and approved by the Rutgers University Animal Care and Facilities Committee.

Animals were randomly divided into four groups. Two different insults were investigated: a 20% total body surface area scald burn injury (B) to mimic trauma with no infection, and cecal ligation and puncture (CLP) to mimic infection and sepsis. Control treatments included sham burn and sham CLP. Detailed explanation regarding the experimental injury models and methodology was provided in previous sections.

Microarray experiments to generate liver gene expression data have been explained elsewhere (Vemula et al. 2004). Briefly, animals were sacrificed (starting at 9am) at different time points (0, 2, 4, 8, 16 and 24hr post-treatment) and liver tissues were collected, snap frozen in liquid nitrogen and stored at -80ºC (n=3 per time point per

group). The tissues were lysed and homogenized using Trizol, and the RNAs were further purified and treated with DNase using RNeasy columns (Qiagen). Then cRNAs prepared from the RNAs of liver tissues using protocols provided by Affymetrix were utilized to hybridize Rat Genome 230 2.0 Array (GeneChip, Affymetrix) comprised of more than 31,000 probe sets.

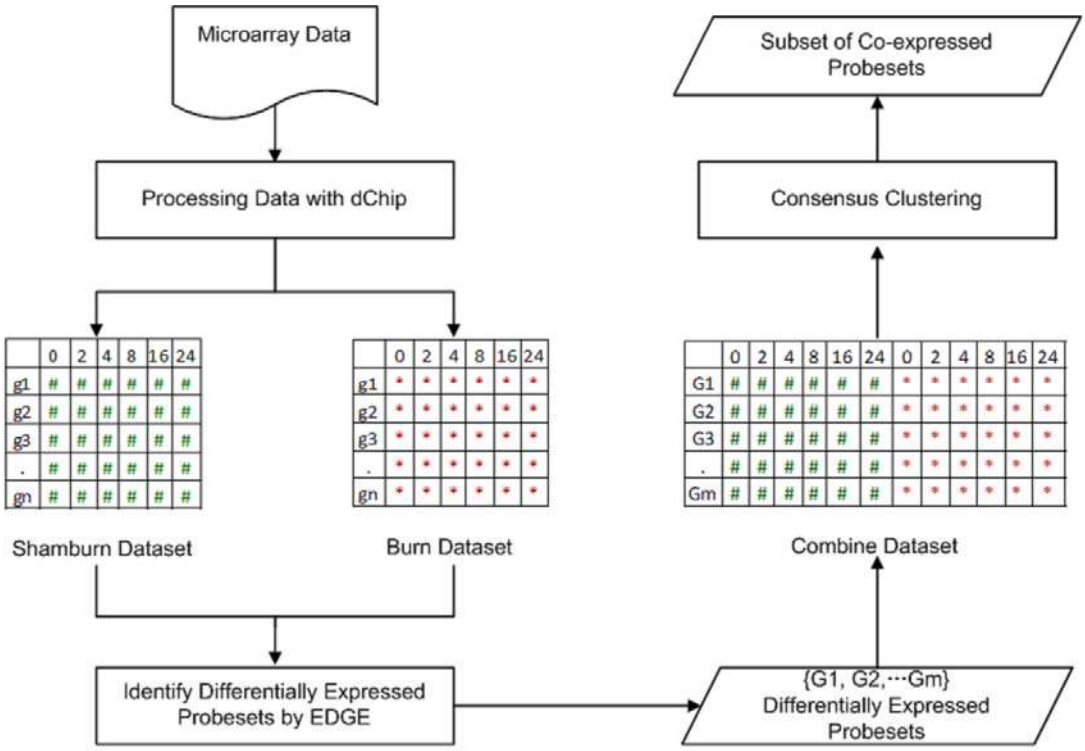

Figure 4.1. Schematic overview of the microarray data analysis.

Microarray data was preprocessed by using dChip. Then, two data sets corresponding to burn and sham groups, respectively, were analyzed to identify the differentially expressed probesets by using EDGE with 'between classes' option under the statistical threshold $q<0.01$, $p<0.01$. Finally, the data sets corresponding to those differentially expressed

probesets in burn and sham groups were combined to form one single matrix, which was then clustered using the approach of "consensus clustering" with threshold p<0.01.

4.2.2 Data Analysis

In this study gene expression data analysis includes data preprocessing, filtering for "between class temporal differential expressions", combining the datasets and clustering as seen in **Figure 4.1**. First, DNA chip analyzer (dChip) software (Li and Wong 2001) was used with invariant-set normalization and perfect match (PM) model to generate expression values. Microarray outlier filter analysis (Yang et al. 2007b) identified that there were approximately 10% outliers in the gene expression data sets, which is typically observed in a microarray data. The outliers were replaced by the mean of the replicates (Pearson et al. 2003). Then the data sets corresponding to treatment and control groups were investigated to identify the differentially expressed probesets by using the method (EDGE) proposed by Storey et al. (Leek et al. 2006). The statistical test used is analogue to an F statistics which compares the goodness of fit of the model under the null hypothesis to that under the alternative hypothesis. The null hypothesis model is obtained by fitting a time-dependent curve to the two or more groups combined, and the alternative hypothesis model is obtained by fitting a separate curve to each group. The significance threshold for this analysis was set as *q-value* <0.01 and *p-value*<0.01. This step determined a set of probesets whose expression patterns were significantly altered following the treatment considering the temporal differences between the control and

treatment groups. Finally the data sets corresponding to those differentially expressed probesets in either treatment and/ or control groups were combined to form one single matrix, which was then clustered using the a approach "consensus clustering" (Nguyen et al. 2009), in an unsupervised manner. This provided a set of burn (or CLP) responsive genes, which is significantly different than that of control group. We further applied one-way ANOVA test (p<0.01) independently for each gene in each cluster and animal group in order to verify if the gene has been differentially expressed across the time only. Moreover, t-test was used additionally for pair-wise comparison of burn and sham genes (or CLP and SCLP genes) identified in the clusters at each time point in order to estimate the activation time of a certain response related to injury. We characterized the biological relevance of the intrinsic responses by evaluating the enrichment of the corresponding gene subsets using the KEGG database through ARRAYTRACK (Tong et al. 2003) as well as analyzing the functions of each individual gene (Twigger et al. 2002).

4.3 Results and Discussion

4.3.1 Gene Expression Profiles Following the Burn Injury

We examined the gene expression levels at 0, 2, 4, 8, 16, and 24 h in the livers of rats after a 20% total body surface area (TBSA) burn injury or sham-burn (control of burn) by using microarray measurement. Differentially expressed burn responsive genes with their short term dynamic profiles were identified considering the time-dependent variations in the gene expression profiles of control group in this study. 1534 probe sets in burn group

exhibit altered gene expression patterns over time compared to the corresponding sham control. Consensus clustering further determined 4 statistically significant clusters composed of 62, 82, 404, and 73 probe sets respectively. The average expression patterns of the 4 clusters are depicted in **Figure 4.2** (right panel) while a heat map of all probe sets is shown in the left panel. ArrayTrack as well as single gene ontology analysis was used to further elaborate the functional annotations of burn injury responsive genes.

Cluster 1 (**Figure 4.2**, cluster 1) exhibits an early up-regulation during the first two hours following thermal injury. One-way ANOVA ($p<0.01$) indicates that the majority of the probesets in this cluster are not differentially expressed in the sham-burn condition over time while all the probesets in the burn group show time-dependent expression variability. Burn injury induced a rapid, but transient, up-regulation of the genes in this cluster in the early post-burn stage (solid line). However, within less than 8 hours, this response returned to baseline implying that the pro-inflammatory response returns to homeostasis.

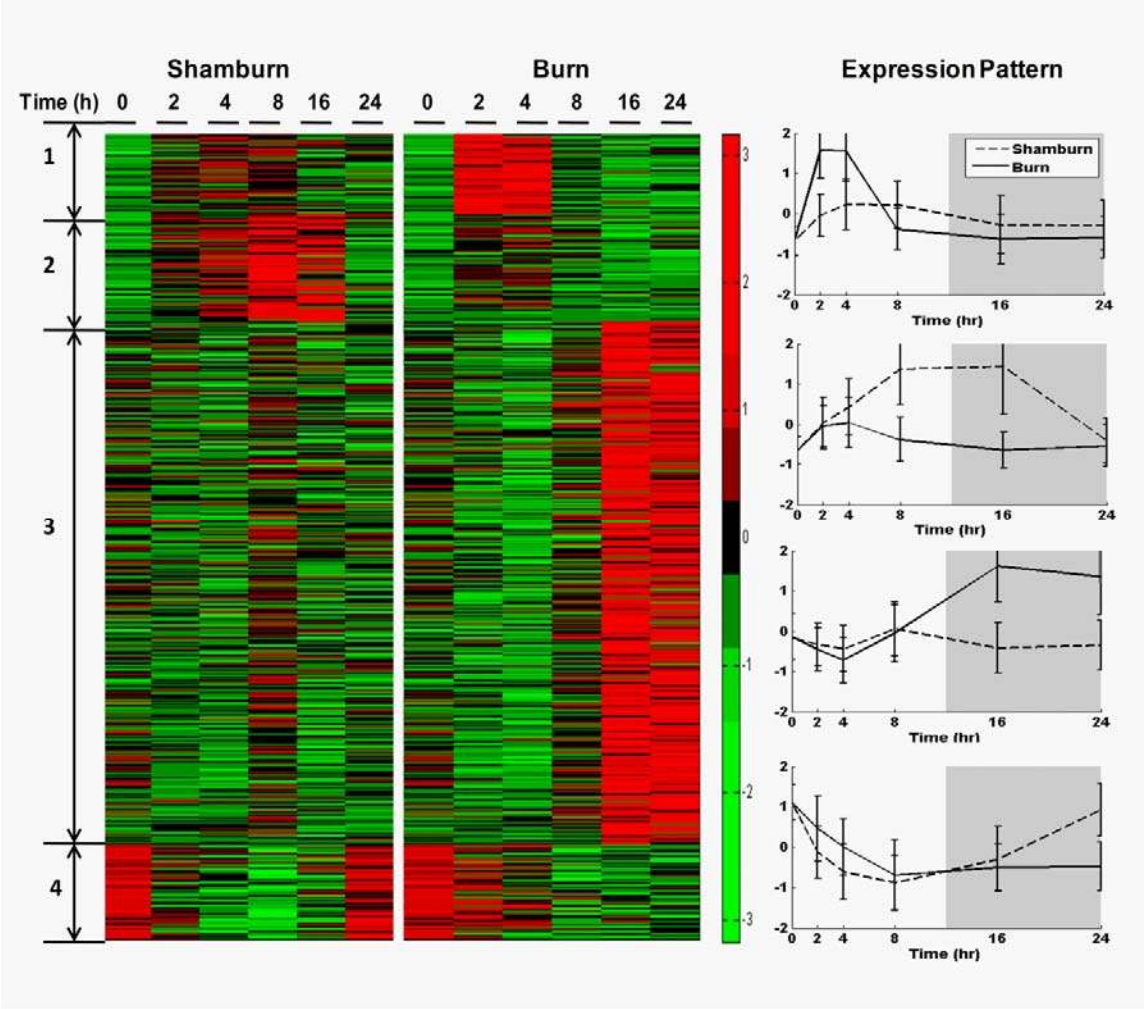

Figure 4.2. Gene expression profiles of rat livers in response to sham-burn or burn injury.

Left Panel, expressions of 62, 82, 404 and 73 probesets in 4 clusters in sham-burn rats and burn rats at 0, 2, 4, 8, 16, 24 h post-treatment are exhibited in a heatmap.

Right Panel, the expression patterns are shown by plotting the average normalized (z-score) expression values of 62, 82, 404 and 73 probe sets in 4 clusters in sham-burn and burn groups (displayed as the means ± SEM)

A group of inflammatory genes are involved in this cluster including cytokines, chemokines and chemokine receptors (*Il1a, Cxcl16, Ccl11 and Ccl9*), as well as genes related to the modulation of innate and adaptive immune responses (*Ceacam1*). IL-1α is a pro-inflammatory cytokine which plays central role in the regulation of the immune response by binding to the IL-1 receptor (Dinarello 1989). In the liver, cutaneous burn injury induced marked elevations of pro-inflammatory cytokines such as IL-1α which exhibits a peak in the early stage of inflammatory response (Mester et al. 1994). Chemokine (C-X-C motif) ligand 16 (CXCL16) is a chemoattractant belonging to the CXC chemokine family. Expression of *Cxcl16* is induced by the inflammatory cytokines IFN-γ and TNF-γ (Abel et al. 2004). Chemokine (C-C motif) ligand 11 (CCL11) is also an inflammatory mediator belonging to the CC chemokine family that is known as Eotaxin-1. Chemokine (C-C motif) ligand 9 is known as macrophage inflammatory protein (MIP)-1γ which is constitutively expressed in macrophages (Youn et al. 1995). The systemic inflammatory response encompasses the release of numerous pro-inflammatory cytokines postburn which are the primary mediators of inflammatory reaction to trauma of severe burn injury. Pro-inflammatory cytokines were thought to trigger and enhance inflammatory response and to mediate catabolic effects (Gauglitz et al. 2008).

Cluster 2 can be considered to be down-regulated following burn injury (**Figure 4.2**, cluster 2). The majority of the probesets in this cluster were not temporally differentially expressed over time following burn injury, while almost all of them pass the ANOVA

test (p<0.01) in the sham-burn condition. This indicates that the expression of the genes in the sham-burn group varies with time, and burn injury appears to disrupt this expression pattern. The sham-burn cluster exhibited an early and sustained upregulation until 16 h and a late downregulation around 24 h post-burn. Burn injury significantly suppressed the expression of the genes in this cluster starting around 2 h post-burn. A Student t-test (p<0.01) reveals that the most significant suppression occurred at 8 h and 16 h.

The genes in this cluster are involved in the unsaturated fatty acid biosynthetic pathway (*Acot1, Acot2, and Acot3*), fatty acid metabolism (*Acaa2, Cpt1a, Dci*), and synthesis of ketone bodies (*Hmgcs2*). Many other genes in this motif also participate in lipid metabolism and lipid transport such as *Eci1, Pigo, cyp4b1, Adfp, Pnpla8, Pank4, Crot, Etfdh*. Phosphatidylinositol glycan anchor biosynthesis, class O, is encoded by *Pigo* which plays a role in the synthesis of glycosylphosphatidylinositol (GPI), a glycolipid. CYP4B1 is a member of the cytochrome P450 superfamily, and one of its functions is to catalyze reactions involved in lipid synthesis (Motamed-Khorasani et al. 2007). Adipose differentiation related protein encoded by *Adfp* gene is an intrinsic lipid storage droplet protein. It is suggested that ADFP protects neutral lipids from degradation by lipases (Xu et al. 2005). The absence of Pnpla8 is linked to reduced biosynthesis of lipid mediators *in vivo* (Yoda et al. 2010). Pank4 encodes a key enzyme in the biosynthesis of coenzyme A (CoA) in bacteria and mammalian cells. CoA is well known for its role in the synthesis and oxidation of fatty acids. HMGCS2 participates in ketone body biosynthesis. The

enzyme carnitine octanoyl transferase encoded by *Crot* gene is responsible for the transfer of fatty acids from peroxisomes to mitochondria. Previous observations elucidating the circadian rhythmicity in the gene expression patterns of rat liver indicated that the genes mainly related to fatty acid biosynthesis were up-regulated in the late afternoon and early evening hours (Ovacik et al. 2010). Our results, consistent with their observation, showed that fatty acid biosynthesis in the sham-burn group undergo a daily oscillation and returns to the starting level at 24 h. However, following burn injury, it was observed that the genes in this cluster lost rhythmicity and were suppressed early (~2 h post burn) compared to the dynamic gene expression profiles of the control group. Vemula et al. reported that expression of genes involved in the synthesis of mono-unsaturated fatty acid (FA) and the precursor for FA biosynthesis were both significantly reduced between 16-24 h postburn (Vemula et al. 2004). Fatty acid biosynthesis associated enzymes are observed to be downregulated following the burn, possibly implying an enhanced energy demand.

In addition, genes related to cell-cell junctions are also found in this cluster. ABLIM3 is a molecular component of adherence junctions (AJs) which can be detected in liver. It is thought that ABLIM3 is a novel component of adherens junctions with actin-binding activity (Matsuda et al.). Alkaline ceramidase 2 encoded by A*cer2* was recently reported to play an important role in regulating β1 maturation and cell adhesion mediated by β1 integrins (Sun et al. 2009). Cadherin 17 is a Ca(2+)-dependent cell-cell adhesion molecule expressed in liver and intestine which plays a role in the morphological

organization of liver and intestine (Berndorff et al. 1994). Genes participating in cell-cell junctions are associated with the integrity of the barrier function of hepatocytes linings and were suppressed around 2 h postburn. Though no direct report on the damage of the liver hepatocytes cells by burn injury is available, many studies reveal that intestinal permeability is increased in burn patient shortly after the injury partly due to the junction integrity alterations (Bjarnason et al. 1995). Thus, the suppression of probe sets functioning as cell-cell junctions and membrane structural integrity may be indication of the damage on the liver caused by the burn injury.

Cluster 3, is activated later, around 8 h post-burn as seen in **Figure 4.2**, cluster 3. ANOVA (p<0.01) revealed that almost all the probesets were differentially expressed after burn injury while the most majority of these probesets were not differentially expressed over time in the sham group. The probesets in both groups show similar expression patterns in the early time period (from 0 to 8 h post treatment). However, burn injury significantly activated the probesets in this cluster starting around 8 h and the maximum deviation between the groups was observed at 16h and 24h postburn (two-sample t-test, p<0.01).

Genes in this major temporal class are important in the complement and coagulation cascade pathways (*C2, C4bpa, C8a, Cfh, Masp1, and Serping1*), N-Glycan biosynthesis pathway (*B4galt1, Dad1, Ddost, Dpagt1, Ganab, and Man1b1*), ribosome (*Rps25*, *Rps2*), Jak-STAT signaling pathway (*Il13, Il4, Il7, Jak3*). Ribosome is the component of the cell

that produces protein from mRNA. N-linked glycans are extremely important in proper protein folding in eukaryotic cells (Helenius and Aebi 2001). All the proteins encoded by the genes in complement and coagulation cascades are important positive acute phase proteins (APP) which are diffusible anti-inflammatory mediators (Tracey 2002). It is also well known that the anti-inflammatory response is induced by the suppressor of cytokine signaling proteins (SOCS) activated by Jak/STAT signaling pathway. Thus these gene groups represent the anti-inflammatory response resulting in an increase in the synthesis of the acute phase proteins and important anti-inflammatory cytokines. Moreover, many other genes in this group participate in various processes such as transcription (*Brca1, Mcm7, Tcf25, Kdm1, Nfyb, Tef, Cited4, Otx1, Sox4, Acvr1, Tbx2, Zfhx2, Dmrt2, Tsc22d1, Ccdc101*), translation (*Atpif1, Mrps21, Rps25, Rps2, Mrps11*), protein folding (*Dnajb11, Ppib, Hyou1, Edem2, Sep15, Pdia6, Dnajc3, Pdia3, Ugcgl1, Sec63, Mlec, Mecp2*), protein degradation (*Pcolce, Cpn1, caspase 12, Cdc34, Spink3, Hspa5, RGD1306508, Erlec1, Aph1a, Derl2, Os9, Rnf20, Ppp2r5c, Aurkaip1, Prss32, Prepl, Tbl1xr1, St14, P4hb*) and protein target (*Tmed3, Ssr4, Tram1, Sec61a1, Rrbp1, Arfgap2, Gabarap, Erp29, Ssr3, Rrbp1, Sec61a1, Derl1, Gosr2, Cope, Tmed2, Copz1, Copg, Sec13, Abcb10, Kdelr1, Kdelr2, Tram1, Serp1, Ssr3, Atp6v0d1, Rabac1, Vps28*). Protein synthesis is a complex multistep process including transcription, translation in ribosome, post-translational modification and protein folding, and protein targeting. Thus, taken together these observations are consistent with the notion that the protein machinery is activated to produce APPs following burn injury.

The most significant feature of this response is the enhanced production of APPs because approximately 20% of all differentially expressed probesets in this study are associated with this function. It was previously reported that the increase in the levels of APPs produced by the liver is a prominent characteristic of the acute phase response following thermal injury, which is believed to be critical for the adaptation of the body to stress (Kataranovski et al. 1999). In addition, the transcription of APPs is activated in the late phase starting around 8 h post-burn, consistent with previous observations that the level of amyloid A, a APP, is not increased until the concentration of IL-6, a late phase cytokine, increases (Plackett et al. 2007). The requirement of the energy and amino acids (AA) to produce large amount of APP in liver are satisfied by the increased flux of amino acids from the periphery to the liver, especially from the accelerated breakdown of muscle proteins (Hasselgren et al. 1988). The alterations in nitrogen and protein metabolism represent a major threat for the organism, as it leads to a debilitating loss of lean body mass (Windsor and Hill 1988). Thus, a sustained or exaggerated acute phase response has been shown to be an indicator of a potentially life threatening uncontrolled and prolonged action of proinflammatory cytokines leading to multiple-organ failure.

Critical cytokines in this cluster are well known anti-inflammatory cytokines such as IL-13 and IL-4. IL-13 inhibits the ability of host immune cells to destroy intracellular pathogens by recruiting a large number of Th2 cells while IL-4 induces differentiation of naive helper T cells (Th0 cells) to Th2 cells. IL-4 promotes the activation of macrophages into repair macrophages which is coupled with secretion of IL-10 and TGF-beta that

result in the diminution of pathological inflammation. It is reported that the anti-inflammatory cytokines, such as IL-4, are released later on in an attempt to counter-regulate the effects of the pro-inflammatory cytokines (Finnerty et al. 2009). Moreover, following the burn injury, a state of immunosuppression occurs whose intensity and duration is closely related to morbidity and mortality in burn patients (Moran and Munster 1987). Interestingly, the inflammatory response after burn injury may play a role in the induction of adaptive immunosuppression. Both in *vivo* and *in vitro* studies manifest the altered adaptive immunity after burn which have shown that there is a decreased production of Th1- type cytokines (IL-2 and IFN-γ) and an increased production of Th2- type cytokines (IL-4 and IL-10) (Lederer et al. 1999). In the current study, the gene expression of Th2- type cytokines, IL-4 and IL-13, is enhanced starting from 8 h post burn, which may imply the onset of the host immunosuppression.

Our results reveal that the gene expression of critical proteins (IRAK1, LBP, and TRAF3) in the TLR4 signaling pathway is upregulated at 8 h post burn injury (**Figure 4.2**, cluster 3). The TLR4 signaling pathway is critical for Gram-negative bacterial infections. It is well known that patients with severe burn injury are exceedingly susceptible to bacterial infections. Not only bacterial infection from the injured area but also bacterial translocation from the gut cause septic complications in the hosts. Mesenteric lymph nodes and liver indeed contain bacteria after burn injury in mice (Maejima et al. 1984). It is generally accented that the decreased resistance to infection and enhanced secondary inflammatory response following serious injury is associated

with abnormalities of both natural and adaptive immunity. Fang et al. (Fang et al. 2002) observed that thermal injury can markedly up-regulate lipopolysaccharide-binding protein (LBP) gene expression in various organs. LBP, a soluble acute-phase protein, binds to bacterial LPS to facilitate the immune response. Excessive LBP mRNA expression may be associated with enhanced synthesis and release of TNF-α stimulated by burn induced-endotoxin. Paterson et al. demonstrated that burn injury significantly increased TLR2- and TLR4-induced IL-1, IL-6, and TNF- α production by liver cells as early as 1 day after injury and they were found to be persistent for at least 7 days (Paterson et al. 2003). Thus, the alteration of the TLR4 signaling pathway may imply that burn injury primes the innate immune system for enhanced TLR4-mediated responses to subsequent infection and provides evidence to suggest that an augmented Toll-like receptor signaling pathway might contribute to the development of increased systemic inflammation following severe burn injury.

Finally, a number of bile acid production related genes were also identified in this cluster including *Idi1*, *tmem97*, *Npc2*, and *Hsd17b4*. Isopentenyl-diphosphate delta isomerase 1 encoded by *Idi1* is an enzyme participating in the cholesterol biosynthesis pathway. TMEM97 is identified as a novel transporter binding to the NPC1 protein in the regulation of endosomal uptake of cholesterol from LDL particles (Bartz et al. 2009). Niemann-Pick type C2 encoded by *Npc2*, a small soluble cholesterol-binding protein, is a key molecule for normal intracellular trafficking of cholesterol. It is proposed that NPC2 is secreted from the liver into bile, where it may play a functional role in cholesterol

transport (Klein et al. 2006). It was revealed that HSD17B4 functions in peroxisomal β-oxidation and bile acid metabolism in mouse (Baes et al. 2000). Bile acids are end products of cholesterol and the major driving force for bile formation, and the major excretory products of cholesterol. Previous studies revealed that bile acid production increased following burn injury (Vemula et al. 2004). The main function of bile acids is to promote the formation of micelles, which facilitate fat digesting and absorption. Therefore, the enhanced production of bile acids may also reflect the demand of the energy from food intake. In fact, nutritional therapy is commonly used with burn patients (Chan and Chan 2009). This approach attempts to compensate for burn injury-induced metabolic abnormalities although it is limited given that it does not address the underlying mechanisms that are responsible for hypermetabolic and catabolic induction. Although nutritional supplements partially alleviate the hyper-catabolic condition, it cannot reverse it or completely restore the nitrogen balance.

Finally, cluster 4 is downregulated around 16 h post burn (**Figure 4.2**, cluster 4). The probesets of this cluster in both sham and burn groups exhibit an early down-regulation. Although the control group seems to recover their expression within 24 h, persistent downregulation is observed in the burn group. The maximum deviation between the sham-burn and burn groups occurs at 24 h postburn (two sample t-test, $p<0.01$).

The genes in this cluster are involved in the insulin signaling pathway (*Gck, Irs1, Mknk2, Trip10*), phenylalanine metabolism (*Ddc*), glycine, serine and threonine metabolism (*Bhmt*), and galactose metabolism (*Gck*). The insulin signaling pathway is activated through the phosphorylation of insulin receptor substrate-1(IRS-1) at a critical tyrosine residue after insulin binds to its receptor. IRS-1-deficient mice exhibits generalized pre- and post- natal growth retardation, as well as insulin resistance in peripheral tissues (Tamemoto et al. 1994). Glucokinase encoded by Gck catalyzes the phosphorylation of glucose to glucose-6 phosphate, which has a major impact on glucose homeostasis. It plays a critical role in the regulation of carbohydrate metabolism by acting as a glucose sensor, facilitating storage of glucose as glycogen. Hepatic glucokinase activities are reported to be controlled primarily at the transcriptional level, mainly regulated by insulin and glucagon (Jung et al. 2006). The expression of genes associated with amino acid metabolism are reported to be regulated by the circadian rhythm in rat liver (Ovacik et al. 2010). Consistent with this observation, the insulin and amino acid metabolism-related genes in the sham-burn group also exhibited daily oscillation reaching a nadir at the interface of the light and dark phases. However, this daily oscillation was disrupted and suppressed maximally 24 h postburn, as demonstrated by the dynamic gene expression profile of the burn group (**Figure 4.2**, cluster 4). Among the downregulated genes in this cluster are IRS-1 and GK, which are known to play a major role in the insulin signaling pathway and insulin resistance. Gauglitz and co-workers previously reported that total IRS-1 transcriptional expression was noticeably decreased at 24, 72 and 192 h postburn. In addition, the significantly impaired insulin signaling pathway was associated with an

inactivation of signaling molecules acting downstream of IRS-1, leading to significantly decreased mRNA expression of GK (Gauglitz et al. 2009). Insulin is an anabolic hormone which promotes the storage of substrates in liver by stimulating lipogenesis, glycogen and protein synthesis (Saltiel and Kahn 2001). Thus, downregulation of the genes involved in the insulin signaling pathway suggests a potential mechanism to explain the onset of a hypercatabolic state which is characteristic of hypermetabolism.

4.3.2 Gene Expression Profiles Following the CLP

Consensus clustering analysis determined 3 important groups composed of 202, 456 and 214, probe sets respectively when CLP group was compared to SCLP group. ArrayTrack as well as single gene ontology analysis was used to further elaborate the functional annotations of CLP injury responsive genes.

Cluster 1 (**Figure 4.3**) shows an early up-regulation during the first 2 hours following CLP treatment. The majority of the probesets in this cluster are not differentially expressed following SCLP treatment while almost all probesets show time-dependent expression variability in CLP group (one way-ANOVA $p<0.01$). The SCLP-response was slightly up-regulated around 2 hours while CLP treatment results in a significant up-regulation in this cluster which peaks around 4h. However, within less than 8 h, this response goes back to baseline values corresponding to SCLP induced response. According to t-test, the most significant difference occurs around 4h.

The genes in this cluster participate in Toll-like receptor signaling pathway (*Cxcl10, Il1b, Map3k8, Nfkbia*), MAPK signaling pathway (*Dusp14, Gadd45a, IL1b, Map3k8, Nr4a1, Tgfb2*), complement and coagulation cascades (*Plaur, Serpina5, Thbd*) and chemokine signaling pathway (*Cxcl10, Foxo3, NFkbia*). Increasing evidence suggest that Toll-like receptors (TLRs) play a key role in the mediation of systemic responses to invading pathogens during sepsis. TLRs are from a family of transmembrane receptors which interacts with relevant pathogen-associated molecular patterns and an intracellular Toll/IL-1 receptor domain involved in signaling. It has been demonstrated that the expression of TLR-2 and TLR4/MD-2 in hepatic macrophages is significantly up-regulated in mice with experimental peritonitis induced by CLP (Tsujimoto et al. 2005). Williams et al. also demonstrated that TLR-2 and TLR-4 mRNA expression in liver of CLP mice were significantly up-regulated as compared with that in sham-operated mice, which occurred as early as 1h after the onset of peritonitis (Williams et al. 2003). It is likely that the expression and function of TLRs greatly influence the quality and control of innate immune response in patients with infectious disease. TLRs are essential for triggering the host's immune response, acting as a sensor against invading pathogens (Tsujimoto et al. 2005). Besides, MAPK pathway, another critical signaling pathway, can be activated by a wide variety of different stimuli acting through diverse receptor families, including LPS, leading to transcription of cytokines genes (Kyriakis and Avruch 2001).

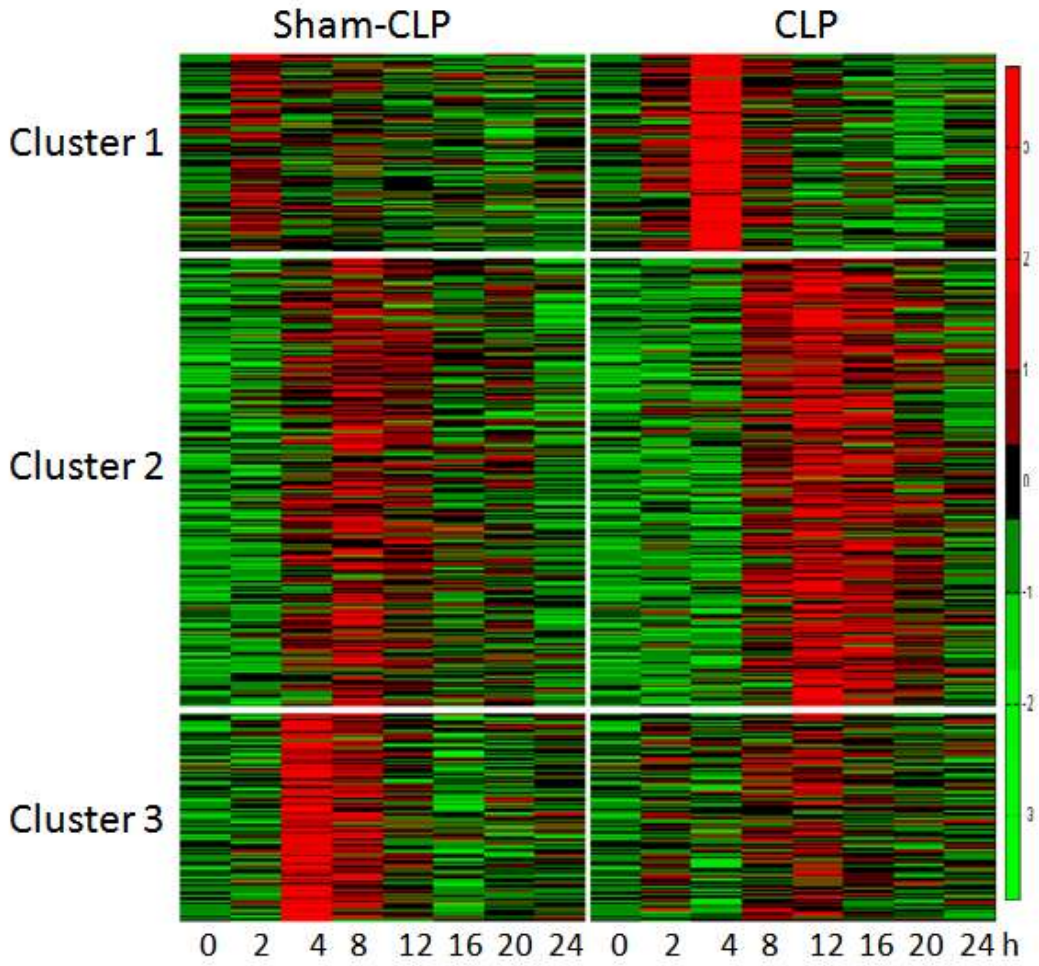

Figure 4.3. Gene expression profiles of rat livers in response to sham-CLP and CLP.

In addition to the important immune related signaling pathway, the genes activated by CLP stimulus in this cluster are highly related to pro-inflammation and immune system including *Il1b, Cebpd, Cish, cxcl10, Ikba, Plscr1, Tgfb2,* and *CD44*. IL-1β is a well-known marker of pro-inflammation and important mediator of inflammatory response which participates in a variety of cellular activities. The expression of IL-1β in the liver is significantly increased post CLP treatment (Salkowski et al. 1998). C/EBPδ encoded by

Cebpd gene is involved in the regulation of genes participating in immune and inflammatory responses, which is shown to discriminate between transient and persistent TLR4- induced signals in response to LPS induced infection (Litvak et al. 2009). CISH belongs to the suppressor of cytokine signaling (SOCS), whose expression is upregulated by LPS. The transcription of this inhibitor is upregulated as a feedback response to immune activation by a variety of immune cytokines and by LPS (Wormald and Hilton 2007). CXCL10 is an IFN-γ induced cytokine which has been attributed to several functions including chemoattraction for diverse immune cells. CXCL10 was shown to be an early marker of sepsis. CXCL10 is identified to play a critical role in host defense during polymicrobial sepsis by increasing neutrophil recruitment and function in a low lethality sepsis model (Kelly-Scumpia et al.). And in CLP induced sepsis, CXCL10 protected mice from sepsis-induced mice lethality (Ness et al. 2003). Vcam1, a cell surface antigen and adhesion molecule, whose gene was upregulated from 4 to 24h after LPS stimulation (Saban et al. 2001). IkBα, encoded by *Nfkbia*, is a member of cellular proteins that function to inhibit the NF-κB transcription factor. Phospholipid scramblase 1 encoded by *Plscr1* is an IFN- inducible protein which is localized in nucleus or cell membrane with a role in antiviral effect. PLSCR1 offers mechanisms for amplifying and enhancing the IFN response through increased expression of a selected subset of potent antiviral genes (Dong et al. 2004). TGF-β2 is a cytokine which plays roles in wound healing. Alterations in the regulation of CD44 expression play a key role in modulating cell migration, adhesion and inflammation. The activation of CD44 expression is a critical event in the monocytic cells migration to sites of inflammation or injury. LPS has

the ability to enhance CD44 expression which may modulate CD44- mediated biological effects in monocytic cells during inflammation and immune responses (Gee et al. 2002).

In Cluster 2 (**Figure 4.3**), SCLP induced response is up-regulated around 2h and reaching its maximum at 8h post SCLP, however, the response in CLP group is activated later, around 4h post –CLP surgery and peaks around 12h. Genes in this major temporal class are critical in ubiquitin mediated proteolysis (*Herc2, RGD69425, Rchy1, Ube2e3, Ube2q2, Ube4a*), antigen processing and presentation (*Canx, Ciita, Ctsb, Hspa5, Lgmn*), ribosome (*Rpl22l1, Rpl23a, Rol27, Rps15a*), N-Glycan biosynthesis (*Dad1, Man1b1*), and complement and coagulation cascade (C9, Fga). Ribosome is the component of the cell that produces protein from mRNA. N-linked glycans are important for proper protein folding in eukaryotic cells (Helenius and Aebi 2001). All proteins encoded by the genes in complement and coagulation cascades are important positive acute phase proteins (APP) which are diffusible anti-inflammatory mediators (Tracey 2002). Moreover, many other genes in this group participate in various processes such as translation (*Rpl22l1, Serp1, Rpl23a, Rpl27, Rps15a, Srp9, Rps4x, Serp1*), protein folding (*Txndc4, Fkbp14, Canx, Sgtb, Tra1*), protein degradation (*Spink3, Tmem67, Spink3, Usp54, Ube4a, Man1b1, Usp33, Lgmn, Derl1, Rchy1, Serpini1, Solh, Ubxd4, Usp32, Yme1l1, Hspa5, Ubxd4, Herc2*) and protein target (*Tmed2, Chmp5, Synrg, Bet1, Ppp3ca, Fxc1, RGD1560633, Stx5, Nsf, Wipi1, Ssr3, Arl2bp, Tmed3, Tmed10, Ssr3, Rab33b*). One characteristics of the metabolic response to trauma and sepsis is acute- phase protein synthesis in liver. Hepatic uptake of amino acids is stimulated and protein synthesis in the

liver are enhanced. It is assumed that the synthesis of the acute-phase proteins is beneficial to the host (Gabay and Kushner 1999).

Many important genes induced by CLP found in this clusters are also involved in antimicrobial responses (*Lcn2, Reg3b, Hepcidin, Fgr*) or in anti-inflammatory response (*Sels, Ebi3, cxcl3, cxcr4, Osmr*), or protective effect (*sod2*). The transcription of lipocalin 2 (*lcn2*) is markedly increased in macrophages in response to LPS stimulation. Recently, it is reported that this protein is required to mediate an innate immune response to bacterial infection. During the infection, the transcription, translation and secretion of lipocalin2 is stimulated in immune cells upon encountering invading bacteria to limit bacterial growth (Flo et al. 2004). Thus, the induction of lipocalin is required to protect host from bacterial infection. Reg3b is a lectin-related protein which may be involved in stress response to control bacterial proliferation during acute pancreatitis. Hepcidin encoded by Hamp is found primarily in the liver with the role in inflammation and antimicrobial defense (Park et al. 2001). Fgr is involved in defense response to Gram-positive bacterium. Selenoprotein S, as a modulator of inflammatory response in infectious and autoimmune disease, plays a pivotal role in the anti oxidative and anti-inflammatory action (Duntas 2009). EBI3 plays a role in regulating cell-mediated immune response. EBI3 mRNA is induced by LPS whose maximal expression level is between 12 and 24 h in human monocytes (Pflanz et al. 2002). CXCL3 is involved in cytokine-cytokine receptor interaction and inflammatory response which is reported to be up-regulated by LPS (Selleri et al. 2008). Chemokine receptor 4 (Cxcr4) is involved in

regulation of cell migration and viral infection. Though Surface expression of neutrophil CXCR4 is down-modulated by bacterial endotoxin, Cxc4r4 gene expression is gradually up-regulated in neutrophiles cultured with LPS (Kim et al. 2007). OSMR is a member of the type I cytokine receptor family whose expression can be induced in monocytes treated with LPS. Superoxide dismutase 2, mitochondrial (sod2), a key antioxidant enzyme in inflammatory condition is elevated in the whole liver under LPS stimulation (Shilo et al. 2008). The upregulation of SOD2 is considered to protect the cell against damage by superoxide radicals (Tian et al. 1998). LPS resulted in a higher level of ADAM8 expression in immature dendritic cells (Richens et al. 2007). S100a9 is phagocyte- specific calcium-binding protein belonging to the S100 family. Recent studies have shown that phagocyte-specific S100 proteins play an important role in the regulation of the innate immune response. Binding of S100A 8 /S 100A9 complexes to carboxylated N-glycan on endothelial cells enhances the subsequent adhesion of phagocytes to the vascular endothelium (Srikrishna et al. 2001). In addition, S100A8 and S100 A9 have been identified as potent chemoattractants for neutrophils and macrophages (Ryckman et al. 2003). The expression of S100a9 is induced by LPS (Zhang et al. 2007).

Given the control gene profile, the cluster 3 (**Figure 4.3**) can be considered to be down-regulated following CLP injury. Almost all of the probe sets pass the ANOVA test ($p<0.01$) in the SCLP group, while the majority of the probesets in this cluster are not differentially expressed over time following CLP injury. This indicates that the expression of the gene in the SCLP varies with time, and CLP surgery appears to exhibits

a further downregulation effect. The SCLP induced expression is activated around 2h and peak at 4h, while the gene profile in CLP is constantly expressed overtime with a slight upregulation at 12h. The most majority of the genes in this cluster are related to transcription system including *Iqwd1, Tshz1, Jmjd5, Trps1, RGD1304792, LOC682097, Zfp112, Nr1d2, Znf688, Pou1f1, Tshz1, Nr1d2, Phf3, Nr1d2, Kdm5b, Narg1, Tbpl1, LOC680222, RGD1560762, Elk1, Ctr9, Otx1, Hey2, Fzd7, Epc1, Med23*. Many of these genes have been reported to be downregulated following LPS stimulus in previous studies. Nr1d1 (Rev-erbA alpha) and Nr1d2 (Rev-erbA beta) are highly expressed in liver participating in both circadian regulation and inflammation. It has been reported that *in vivo* CLP suppresses Nr1d expression in human peripheral blood leukocytes (Haimovich et al. 2010). Mcl1 is identified to be decreased in LPS-stimulated monocytes (Suzuki et al. 2000). Egln1component of transcriptional complex that plays a central role in mammalian oxygen homeostasis is reported to be downregulated in human whole blood incubated with LPS (Ghielmetti et al. 2006).

4.4 Conclusions

We have shown a short-term liver gene expression profiling in response to thermal injury or sepsis. The analysis characterizing the dynamic patterns of both burn and sham groups elucidated that temporal changes in the expression levels after the injury are mainly associated with the pro-inflammatory response, fatty acid biosynthesis, the anti-inflammatory response, and insulin-regulated metabolic responses. The network of dynamic changes in gene expression observed in this study revealed the possible links between the diverse burn-induced responses. Based on our results, the pro-inflammatory

response is activated immediately around 2 h following burn treatment which triggers the anti-inflammatory response starting around 8 h postburn. The biosynthesis of unsaturated fatty acid starts to be suppressed around 2 h which may imply the preservation of the energy sources for the synthesis of APPs whose genes were activated later around 8 h post burn. In addition, the impaired insulin signaling pathway, starting from around 16 h postburn and putatively as a result of the alterations in inflammatory gene expression, is expected to further strengthen the catabolic response. A Suppression of fatty acid synthesis and enhanced production of bile acids were also observed, but were not likely due to the impaired insulin signaling because of the discrepancy in the dynamics of these responses. The analysis of CLP treatment revealed that Toll-like receptor signaling pathway, MAPK signaling pathway, acute phase protein synthesis and the genes involved in transcription system were activated in the liver following the induction of sepsis. Toll-like receptor signaling pathway is essential for triggering the host's immune response, acting as a sensor against invading pathogens. MAPK pathway, another critical signaling pathway, can be activated by LPS, which leads to transcription of cytokines and chemokines. In conclusion, simultaneous analysis of treatment and control groups' expression profiles enables to characterize the dynamic patterns of both groups. Our results reveal critical gene expression pattern changes triggered by the injuries, which reflects host physiological and biological alterations and provides a more comprehensive understanding of the pathophysiology of the disease state.

CHAPTER V

5 METABOLIC FLUX ALTERATIONS IN LIVER FOLLOWING BURN AND SEPSIS

Abstract

Isolated liver perfusion systems have been used to characterize intrinsic metabolic changes in liver as a result of various perturbations, including systemic injury, hepatotoxin exposure, and warm ischemia. Most of these studies were done using hyperoxic conditions (95% O_2) but without the use of oxygen carriers in the perfusate. Prior literature data do not clearly establish the impact of oxygenation, and in particular that of adding oxygen carriers to the perfusate, on the metabolic functions of the liver. Moreover, these studies were performed utilizing fasted animals prior to perfusion so that a simplified metabolic network could be used in order to determine intracellular fluxes. However, fasting-induced metabolic alterations might interfere with disease related changes. Therefore, there is a need to develop a "unified" metabolic flux analysis approach that could be similarly applied to both fed and fasted states.

First, in this study we explored a methodology based on elementary mode analysis to determine intracellular fluxes and active pathways simultaneously. In order to decrease the solution space, thermodynamic constraints, and enzymatic regulatory properties for

the formation of futile cycles were further considered in the model, resulting in a mixed integer quadratic programming problem.

Then the effects of oxygen delivery in the perfusion system on liver metabolism were investigated by comparing three modes of oxygenation. We found that perfused livers consumed oxygen up to the rate of 400 μmole/g liver/h when the perfusate contained RBCs. Even when using 95% O_2, in the absence of oxygen carriers, oxygen uptake was significantly reduced; urea and ketone body production were significantly decreased, and metabolic pathway analysis suggests that significant anaerobic glycolysis occurred.

Using red blood cells in the perfusate which facilitate the oxygen utilization rate, we further analyzed the effect of fasting on the liver metabolism of burn animals. Rats first received a 20% total body surface area (TBSA) scald burn injury or sham-burn treatment. The livers were perfused 4 days after the treatment. One day prior to liver perfusion experiments, some animals in burn and sham groups were fasted for 24 h, whereas the rest were not. It was found that fasting further increased the urea production and amino acid uptake rates including glutamine, arginine, methionine and glycine in burn animals, which was not observed in sham-burn animal group. It also increased lactate uptake in sham-treated animals, but not in burned animals. These results showed that fasting did not result in parallel responses in burn and sham-burn animals, therefore care must be taken to define the nutritional state of the animal model used in such studies.

Finally, we investigated the effects of burn injury or CLP treatment on liver metabolism. The animals were sacrificed 24 h after the treatment. Animals were not fasted and the livers were perfused with perfusate which contained RBCs at 10 % Htc. It was observed that burn injury increased gluconeogenic reactions while the opposite was observed following the SCLP. Moreover, most of the pathways in burn and CLP groups were found to have significantly higher weight values compared to other groups.

5.1 Introduction

The liver has many complex physiological functions including detoxification, lipid, protein, and carbohydrate metabolism, as well as bile and urea production. It also plays a major role in the onset and maintenance of aberrant "hyper-metabolic" patterns associated with various disease states, such as burns, infections and major trauma, which are characterized by an accelerated breakdown of skeletal muscle protein, increased resting energy expenditure, and a negative nitrogen balance. Isolated organ perfusion systems have been used to characterize the related metabolic changes at the individual organ level, including liver (Arai et al. 2001; Banta et al. 2007; Banta et al. 2005; Lee et al. 2000; Lee et al. 2003; Orman et al. 2010; Yokoyama et al. 2005). Normothermic liver perfusion systems are also being developed as an alternative to cold preservation techniques in the context of liver transplantation (Schon et al. 2001). A better understanding of the metabolic pattern in such systems may be helpful to assess the status of a liver graft before transplantation.

While the isolated perfusion approach enables one to determine the intrinsic changes in the organ by removing external influences, an obvious drawback is the artificial ex vivo environment of the perfusion which may potentially induce artifactual metabolic patterns. In particular, adequate oxygen transport and delivery is critical to correctly assess the metabolic state of organs that are suspected to undergo increased energy expenditure as a result of systemic inflammation due to disease and/or injury. Inadequate oxygenation could by itself alter gene expression levels (Rosmorduc and Housset 2010) and/or promote anaerobic pathways, including glycolysis, and would obviously limit the ability to observe a putative increase. However, the majority of liver perfusion studies were done without oxygen carriers, and it was also claimed that hyperoxic oxygenation without the use of oxygen carriers was adequate to support perfused rat liver function (Bessems et al. 2006). The importance of using oxygen carriers in liver perfusion studies remains controversial, and the full ramifications of the impact of oxygenation have not been well characterized.

Several isolated liver perfusion studies have identified relevant changes in the hepatic central carbon and nitrogen metabolism following systemic injury as well as infection. In this approach, livers were isolated from animals at different time points after injury, the rates of uptake/release of a panel of ~30 metabolites were measured during ex vivo normothermic perfusion, and the data used as input to a metabolic network model accounting for mass balance constraints of the major biochemical pathway reactions to derive a metabolic flux map distribution. A limitation of these studies is that animals

were typically fasted overnight prior to liver perfusion. In this case, one could assume that glycogen storage was depleted and there was inhibition of all strictly glycolytic enzymes, thus reducing the number of unknown fluxes as well as eliminating potential futile metabolic cycles (Banta et al. 2007; Lee et al. 2000; Lee et al. 2003). This allowed a relatively simple metabolic network model and a unique flux distribution could be generated solely based on mass balance constraints. However, the effect of superimposing fasting on injury has not been investigated, while there is likely to be some interaction between these stimuli because they are both known to impact on many of the same reactions within glucose and nitrogen metabolism.

We recently applied a mass balance analysis on the perfused rat liver system to identify the metabolic fluxes in both fed and fasted conditions using a more comprehensive metabolic network including all liver specific pathways (Orman et al. 2010). Since the stoichiometric model was underdetermined given the experimentally determined external fluxes, the flux spectrum or variability approach which returns a range of values for each flux that is consistent with external flux measurements was used. However, the calculated flux ranges for both states were too large to determine the most distinctive patterns between the two states. Therefore, more comprehensive stoichiometric based mathematical approaches should be explored to estimate the steady state flux distribution vectors which are necessary to identify distinctive features of experimental conditions investigated.

Flux balance analysis (FBA) is a very powerful metabolic engineering tool which uniquely determines the flux vector by formulating an objective function. Pathway analysis based on extreme pathways and elementary modes is another approach used to characterize the structure of the metabolic network and elucidate important topological and physiological properties. Since every flux distribution can be written as a linear combination of the elementary modes or extreme pathways, the solution space of steady state flux vector can be also described by these more organized pathways. The solution space obtained from pathway analysis or flux balance analysis can be further reduced by incorporating additional constraints relying on well known regulatory mechanisms (Covert and Palsson 2002; Covert et al. 2001) or thermodynamic properties of biochemical reactions (Beard and Qian 2005; Nolan et al. 2006). Thermodynamics has been applied to many areas of biology. Beard and Qian (Beard and Qian 2005) used optimization based methodology with thermodynamic and enzyme activity constraints to determine the concentration profiles of metabolites in a relatively small scale hepatic metabolic network. Recently, elementary modes have been also used to formulate thermodynamic feasibility constraints for metabolic network models (Boghigian et al. 2010; Iyer et al. 2010a; Iyer et al. 2010b; Nolan et al. 2006; Yang et al. 2011; Yoon et al. 2007). In these studies, Gibbs free energy change across the systematically enumerated pathways/modes were forced to be less than or equal to zero.

The decomposition of a steady state flux vector into pathways is not always unique because for large networks the number of pathways is not usually equal to the dimension

of the null space of the stoichiometric matrix (Schilling et al. 2000). Proposing an appropriate objective function is necessary to obtain a unique solution, however this is one of the obstacles in mammalian systems because of lack of knowledge regarding metabolic properties of these complex systems. Schwarz and his co-workers (Schwarz et al. 2005) discussed the importance of short pathways in elementary mode analysis and they assumed that short pathways are the modes which contribute most to gene expression (Stelling et al. 2002; Wagner and Fell 2001). By examining amino acid biosynthetic pathways across 48 sequenced organisms, Rutter and Zufall (Rutter and Zufall 2004) investigated whether the evolutionary properties of a metabolic network could be determined by the network characteristics such as the pathway length. They showed that longer pathways exhibit lower rates of change in pathway structure than shorter pathways. They suggested that short pathways with high variability in structure across the organisms can also be regarded as important properties since they are specific to the organism, which has been developed as a result of adaptive responses to environmental changes. We have previously presented different optimization problems based on different underlying assumptions (such as maximizing the activity of short pathways, maximizing the activity of pathways including glucose and/or urea production, etc) to decompose the flux vectors into pathways (Orman et al. 2011a). The methods were applied to the hepatic network and data set obtained from perfused livers of rats receiving various treatments. It was found that short pathways have higher weights given the topological properties of hepatic metabolic network and flux distribution obtained from perfusion experiments.

In this chapter, we first developed a stoichiometric based optimization methodology incorporating (1) flux balance and metabolic pathway analyses (elementary mode analysis) in order to identify the intracellular fluxes and active pathways simultaneously; (2) pathway based thermodynamic analysis to reduce the solution space and eliminate thermodynamically infeasible pathways; (3) a mixed integer binary formulation to represent the formation of futile cycles. Then, the effects of three modes of oxygen delivery to perfused livers: normoxic (arterial) perfusate (21% O_2), hyperoxic perfusate (95% O_2), and hyperoxic perfusate with oxygen carriers (95% O_2 + 10% hematocrit using bovine red blood cells) were compared to identify the most adequate oxygenation condition which improves the perfused livers functions. Thirdly, we investigated the effect of fasting on the metabolic flux distribution in perfused livers isolated from rats 4 days after being subjected to systemic burn injury or "sham"- burn control treatment. Totally four animal groups were compared: *Sham+Fed*, *Sham+Fasted*, *Burn+Fed*, *Burn+Fasted*. Finally, the flux distributions were identified in the livers from the animals 24 h after being subjected to burn injury or CLP using modified network model and experimental strategies.

5.2 Materials and Methods

5.2.1 Animal Model and Perfusion Experiments

Male Sprague-Dawley rats (Charles River Labs, Wilmington, MA) weighing between 150 and 200 g were used. The animals were housed in a temperature-controlled environment (25°C) with a 12-hour light-dark cycle and provided water and standard chow ad libitum. All experimental procedures were carried out in accordance with National Research Council guidelines and approved by the Rutgers University Animal Care and Facilities Committee.

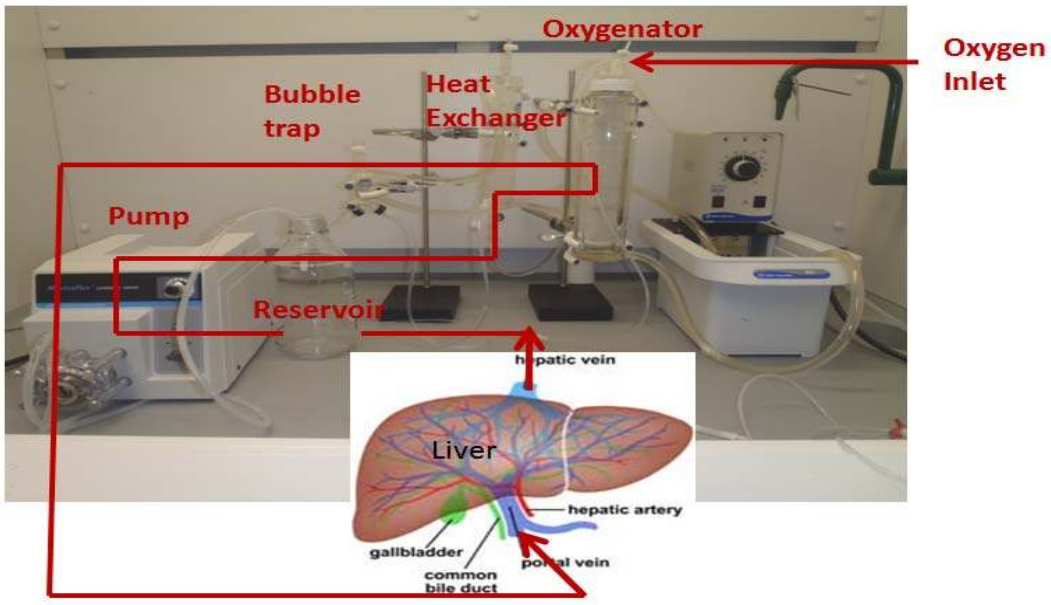

Figure 5.1. Perfusion system.

The isolated perfused rat liver studies for all animals were performed following a modification of Mortimore's methods as described previously (Yamaguchi et al. 1997) (**Figure 5.1**). The rats were anesthetized with an intraperitoneal injection of ketamine (80

to 100 mg/kg) and xylazine (12 to 10 mg/kg). The abdominal cavity was opened and heparin (1000 U/kg) was injected by transphrenic cardiac puncture, and then the liver was perfused *in situ* via the portal vein at a constant flow rate by a peristaltic pump. The hepatic artery and the suprarenal vena cava were ligated, and the liver outflow from the hepatic vein collected through the catheter which was cannulated into the inferior vena cava via the right atrium. After blood was washed out from the liver by flushing with perfusate for 10 minutes, the end of the tube connecting to the outflow catheter was placed into the perfusate reservoir to initiate the recirculating perfusion. In all perfusion experiments, the perfusion pressure was kept below 15cm H_2O while the flow rate was set to 3.0 ml/min/g liver. The perfusate consisted of Dulbecco's Modified Eagle's Medium (DMEM, Gibco BRL) used as basal medium supplemented with 3% w/v bovine serum albumin (Fraction V; Sigma-Aldrich, St. Louis, MO). The concentrations of nutrients (lactate, glucose, amino acids, etc) in the perfusate (500 ml total volume) have been reported elsewhere (Yamaguchi et al. 1997). The pH of the perfusate solution was initially adjusted to 7.3, but reached the target pH of 7.4 after filling the perfusion system. Throughout the perfusion pH was close to 7.4 entering the liver but slightly lower at around 7.3 exiting the liver presumably due to production of acidic metabolites such as CO_2 and lactate. Gas exchange in the oxygenator and the buffering capacity of the perfusate were sufficient to return the perfusate to the desired pH before reentering the liver, therefore no adjustments (i.e. addition of NaOH or the like) were necessary. The temperature of the heating fluid in the heat exchanger was set to a temperature higher than 37°C to account for heat losses between the heat exchanger and the liver inlet. The

temperature of the liver was frequently measured during the perfusion by inserting a thermocouple between the lobes, and the range was 37±0.5°C. Perfusate samples were taken from the reservoir every 10 minutes for 1 hour to measure the metabolite concentrations (Arai et al. 2001; Banta et al. 2007; Banta et al. 2005; Lee et al. 2000; Lee et al. 2003; Yokoyama et al. 2005). Samples were also withdrawn every 20 minutes for 1 hour from ports adjacent to both cannulae to measure the O_2 concentrations across the liver.

In order to investigate the effect of oxygen delivery mode on liver metabolism, rats were divided into three experimental groups (n=4 for each group). The groups consisted of *Group 95% O_2*, *Group 95% O_2+10% Hct* and *Group 21% O_2*. For *Group 95%O_2*, the perfusate was oxygenated by passing through 3 m of silicone tubing in contact with a 95% O_2 / 5% CO_2 gas mixture. For *Group 95% O_2+10% Hct*, the perfusate was supplemented with washed bovine red blood cells (RBCs) (Lampire, Pipersville, PA) at 10% hematocrit and otherwise oxygenated with the same 95% O_2 / 5% CO_2 gas mixture. For *Group 21% O_2,* perfusate medium was oxygenated using room air.

In order to investigate the effect of fasting on burn animals, the rats were first randomized into two groups of equal size. The first group received scald burn injury (described further below) and the second group received a sham burn injury. Three days post injury, food was removed from half of the animals in each group to initiate fasting. One day later (four days post injury), animals underwent isolated liver perfusion (also described further

below). Thus, totally four groups were investigated: *Sham+Fed*, *Sham+Fasted*, *Burn+Fed*, *Burn+Fasted* (n≥3 for each group).

Finally, the effects of burn injury and sepsis on carbohydrate and amino acid metabolism were investigated. More specifically, rats were subjected to a full-thickness scald burn or CLP. Some animals received a "sham-burn," where animals were anesthetized and prepped but not burned, as well as a "sham-CLP" where animals underwent laparotomy but no cecal damage. Totally four different groups were investigated: Sham-burn, Burn, Sham-CLP and CLP. 24 h after the treatment, the animals were sacrificed for liver perfusion experiments.

The concentrations of metabolites (glucose, urea, lactate, glutamine, glutamate, β-hydroxybutyrate, triglycerides, glycerol, and O_2) were measured as described previously (Banta et al. 2005; Yamaguchi et al. 1997). Urea content in the perfusate was measured based on its specific reaction with diacetyl monoxime using a commercial assay kit (Stanbio Laboratory, Boerne, TX). Glucose concentrations were determined using enzymatic and colorimetric methods with commercially available assay kits (Sigma Chemical Co., St. Louis, MO). The concentrations of β-hydroxybutyrate in the perfusate samples were measured by means of an enzymatic assay using a Stanbio Diagnostic Kit (Stanbio Laboratory, Boerne, TX). Lactate was quantified using a commercial kit (Trinity Biotech, Berkeley Heights, NJ). Glutamine, glutamate, triglycerides and glycerol kits were purchased from Sigma (Sigma Chemical Co., St. Louis, MO). Amino acid

measurements (except glutamine and glutamate) were performed using HPLC system. LDH activity measurements from perfusate samples were carried out using a cytotoxicity detection kit (Roche, Indianapolis, IN).

The dissolved O_2 and total hemoglobin concentrations were immediately measured using blood gas analyzer during the perfusion experiments (Bayer Rapidlab 855, Diamond Diagnostics, MA). The oxygen concentration is calculated using the equation described in the results section. Since the liver inlet and outlet oxygen concentrations are known, the difference multiplied by the perfusate flow rate gives the oxygen uptake rate.

Metabolite concentrations were multiplied by the total perfusate volume at the time of sampling to obtain the total amount of each metabolite remaining at the time of sampling. This quantity changed linearly with time, indicating that the perfused liver was metabolically stable for the duration of the perfusion, consistent with prior observations (Arai et al. 2001; Banta et al. 2005; Lee et al. 2000; Lee et al. 2003). The slope was determined to obtain the rate of production or consumption of each metabolite. Multiple comparisons among the groups were performed using analysis of variance (ANOVA) followed by Tukey's studentized range test. The criterion for statistical significance was chosen as $P<0.05$.

5.2.2 Metabolic Network

The liver metabolic network used in this work was originally developed for perfused livers and hepatocyte cultures (Banta et al. 2007; Chan et al. 2003; Lee et al. 2000; Lee et al. 2003) and was modified to simultaneously include both glycolytic and gluconeogenic pathways, fatty acid synthesis and oxidation, as well as glycogenesis and glycogenolysis (see "APPENDIX" for details). Given the physiological properties of the liver and the perfusate composition, the network involves all major liver-specific pathways involved in central carbon and nitrogen metabolism such as gluconeogenesis, glycolysis, urea cycle, fatty acid metabolism, pentose phosphate pathway, TCA cycle, glycogen metabolism and amino acid metabolism. Given that protein metabolism only accounts for a small portion of the nitrogen metabolism in the liver during perfusion (Orman et al. 2010), a detailed description of protein metabolism was not considered herein.

5.2.3 Metabolic Network Model

The flux distribution was calculated using the mass balances of internal metabolites by assuming that internal metabolites are at pseudo steady state due to the insignificant intracellular accumulation rates. Therefore, steady state flux space is described by the following formulation:

$$\begin{aligned} &\sum_{j}^{n_r} S_{kj} v_j = 0, \quad \forall k \in n_m, \\ &v_j^{\min} \le v_j \le v_j^{\max}, \ \forall j \in n_r, \\ &v_m \ge 0, \quad \forall m \in \{\text{irreversible fluxes}\}. \end{aligned} \tag{5.1}$$

where S_{kj} is the stoichiometric coefficient of metabolite k in reaction j; v_j is the flux of reaction j; n_m and n_r are the total number of metabolites, and total number of reactions, respectively.

Any flux vector $\boldsymbol{v}$ in a metabolic network can be also expressed as a linear combination of elementary modes as given in **Figure 5.2** (Wiback et al. 2003), therefore a weight can be assigned for each pathway:

$$v_j = \sum_i^{n_p} P_{ji} w_i, \quad \forall j \in n_r. \tag{5.2}$$

where w_i is the weight of pathway i; P_{ji} corresponds to the relative flux level (normalized) of reaction j in pathway i; and n_p is the total number of pathways. Note that each pathway also satisfies the reaction reversibility constraint given in Equation (5.1). Substituting Equation (5.2) into Equation (5.1) results in the following set of constraints:

$$\begin{aligned} &\sum_j^{n_r} S_{kj} \left(\sum_i^{n_p} P_{ji} w_i \right) = 0, \quad \forall k \in n_m, \\ &v_j^{\min} \le \sum_i^{n_p} P_{ji} w_i \le v_j^{\max}, \quad \forall j \in n_r, \\ &w_i \ge 0, \quad \forall i \in n_p. \end{aligned} \tag{5.3}$$

Thus, the flux space can be described by elementary modes with their corresponding weight values as shown in Equation (5.3). Since reversible pathways are split into two irreversible pathways, the system is defined as a non-negative linear combination of irreversible elementary modes.

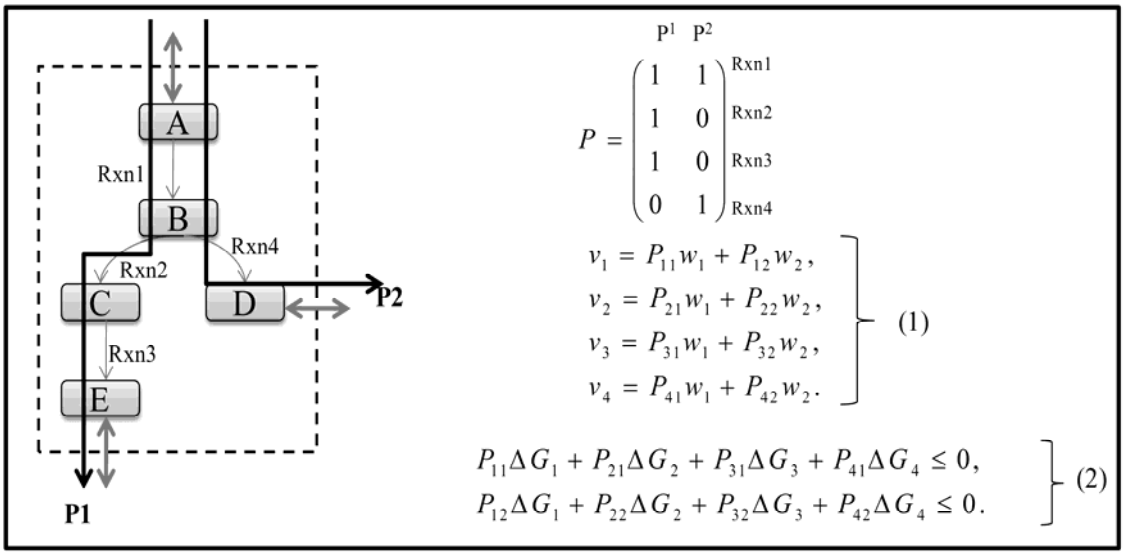

Figure 5.2. A simplified metabolic network example with its reactions (v_1, v_2, v_3 and v_4) and pathways (P^1 and P^2).

Each pathway is represented by a normalized flux distribution vector. A linear combination of the weighted pathways gives the net flux distribution in the network (Equation 1). The rate of heat dissipation of each pathway should be less than zero so that the pathway can be thermodynamically feasible (Equation 2).

5.2.3.1 Pathway based thermodynamic constraints

The model described by Equation (5.3) is further modified by incorporating additional constraints such as thermodynamic constraints. Recently, pathway based energy balance has been commonly applied to reduce the steady state flux space (Boghigian et al. 2010; Iyer et al. 2010a; Iyer et al. 2010b; Nolan et al. 2006; Yang et al. 2011; Yoon et al. 2007). The underlying assumption behind the energy balance analysis is that an exergonic

reaction can be a “driving-force” for an endergonic reaction if these two reactions are coupled in the same pathway.

Thermodynamic feasibility condition of a reaction determined by Gibbs free energy change of that reaction is given as follows:

$$\begin{aligned} &\text{A ==> B} \\ &\Delta G_{rxn} \le 0 \end{aligned} \tag{5.5}$$

where ΔG_{rxn} is the Gibbs free energy of the reaction and v_{rxn} is the reaction’ flux. The condition $\Delta G_{rxn} \le 0$ implies that the product $v_{rxn}.\Delta G_{rxn}$ should negative or equal to zero ($v_{rxn} \ge 0$). The product $v_{rxn}.\Delta G_{rxn}$ corresponds to the rate of heat dissipation of the reaction in non-equilibrium steady state (Qian and Beard 2005; Qian et al. 2003).

As proposed by Xu and co-workers (Xu et al. 2008), a pathway can be also regarded as a macroscopic reaction which should satisfy the thermodynamic constraint, i.e. the rate of heat dissipation of the pathway should be less or equal to zero, similar to the constraint represented by Equation (5.5). A very simple example of a metabolic network with its pathway based thermodynamic constraints is illustrated in **Figure 5.2**. The Gibbs free energy of the pathway *i*, ΔG_i^P, is the summation of the Gibbs free energies of reactions involved in that pathway which should be less than or equal to zero:

$$\Delta G_i^P = \sum_j^{n_r} \Delta G_j P_{ji} \le 0, \qquad \forall i \in n_p \tag{5.6}$$

where ΔG_j is the Gibbs free energy of reaction *j* and is calculated by using the standard Gibbs free energy of the reaction and metabolite concentrations involved in that reaction as follows:

$$\begin{aligned} &\Delta G_j = \sum_{k}^{n_m} S_{kj} \Delta G^o_{f,k} - RT \sum_{k}^{n_m} S_{kj} L_k, \quad \forall j \in n_r, \\ &L_k^{\min} \le L_k \le L_k^{\max}, \quad \forall k \in n_m. \end{aligned} \tag{5.7}$$

where L_k is the logarithmic concentration of metabolite *k*, and $\Delta G^o_{f,k}$ is the standard Gibbs free energy of metabolite *k*. Given that we can identify a range of values for each ΔG_i^P using the maximum and minimum values of logarithmic concentrations of metabolites (Yang et al. 2011), and considering the weight values, we formulated the pathway based thermodynamic constraints as follows:

$$\begin{aligned} &\Delta G_i^P w_i \le 0, \quad \forall i \in n_p, \\ &\Delta G_i^{P,\min} \le \Delta G_i^P \le \Delta G_i^{P,\max}, \quad \forall i \in n_p. \end{aligned} \tag{5.8}$$

The condition $\Delta G_i^P w_i \le 0$ implies that the pathway *i* can be active ($w_i \ge 0$) if its Gibbs free energy is less than zero ($\Delta G_i^P \le 0$), otherwise it is not active ($w_i = 0$). Equation (5.8) is nonlinear due the bilinear term $\Delta G_i^P w_i$. Since w_i is a positive variable as explained before, any w_i satisfying the inequality $\Delta G_i^{P,\max} w_i \le 0$ also satisfies $\Delta G_i^P w_i \le 0$ and $\Delta G_i^{P,\min} w_i \le 0$. Thus, the constraint described in Equation (5.8) is replaced by $\Delta G_i^{P,\max} w_i \le 0$ which further tightens the solution space although this can cause the elimination of certain solutions.

The proposed method has certain advantages compared to traditional metabolic flux analysis method. The proposed thermodynamic constraint not only reduces the solution space, but also eliminates thermodynamically infeasible pathways. Considering the overall free energy of a pathway also decreases the number of unknown parameters since the concentrations of internal or transient metabolites are not required.

5.2.3.2 Integration of enzymatic regulatory constraints for futile cycles

When two metabolic reactions or pathways in opposite directions are active simultaneously, a futile cycle is formed, which results in energy waste. In general, reciprocal control between the enzymes inhibits the formation of futile cycles. We proposed a mathematical formulation by introducing binary variables to prevent futile cycle from occurring:

$$\begin{aligned} &0 \le V_A \le \beta(1-y), \\ &0 \le V_B \le \beta y, \\ &y \in \{0,1\} \end{aligned} \tag{5.9}$$

The constraint given by Equation (5.9) describes the reciprocal control between two reactions (such as the reaction of glucokinase and the reaction of glucose-6-phosphatase) forming a futile cycle. This constraint allows the two reactions (V_A and V_B) to inhibit each other and prevent the formation of the cycle. y is a binary variable, and β is a very large number which forces y to be 0 (thus V_B is zero) if the reaction V_A is active. If the reaction V_A is zero, then V_B can take any value. Note that another advantage of this formulation is that it provides a net flux in the futile cycle with a direction in case the

cycle is active. Constraint (5.9) can be also described by the elementary modes with their weight values:

$$\begin{aligned} &0 \le \sum_{i}^{n_p} P_{Ai} w_i \le \beta(1-y), \\ &0 \le \sum_{i}^{n_p} P_{Bi} w_i \le \beta y, \\ &y \in \{0,1\} \end{aligned} \tag{5.10}$$

The metabolic network used in this study includes both glycolytic and gluconeogenic pathways, fatty acid synthesis and oxidation, as well as glycogenesis and glycogenolysis. Three reactions calatalyzed by glucokinase, phosphofructokinase and pyruvate kinase in glycolysis (reactions 10, 9 and 8 respectively in "APPENDIX") are replaced by three gluconeogenic reactions in the opposite direction which are catalyzed by glucose-6-phosphatase, fructose-1,6-bisphosphatase and pyruvate carboxylase (reactions 1, 3 and 7 respectively). These reaction pairs form three different futile cycles. It has been assumed that, due to the reciprocal regulatory mechanisms of these enzyme complexes, gluconeogenesis and glycolysis are mutually exclusive (Chan et al. 2003). The lumped reactions 44 and 45 (see "APPENDIX") represent fatty acid oxidation and fatty acid synthesis, which form another cycle. Reactions 49 and 50 corresponding to glycogen synthesis and glycogen breakdown (these reactions are also lumped) are reaction pairs forming a futile cycle too. One of the main forms of control in these complex systems is the allosteric regulatory properties of some key substrates, such as glucose-6-phosphate which is an activator of the glycogen synthase. The constraint described by Equation (5.10) was independently applied for each futile cycle in this study.

5.2.3.3 Determining Weight and Flux Vectors

The decomposition of a steady state flux vector into pathways is not always unique, because the number of pathways (more than 130000 in this study) is not usually equal to the dimension of the null space of the stoichiometric matrix of larger networks. An objective function should be used in order to resolve this system. Some objective functions including maximization of the number of elementary modes, minimization of the elementary mode activity and the entropy maximization principle have been proposed in the literature (Nookaew et al. 2007; Schwartz and Kanehisa 2005; Schwartz and Kanehisa 2006; Zhao and Kurata 2009). We previously published a comprehensive analysis exploring different objective functions of perfused livers' metabolism in order to decompose the flux vector into pathways uniquely and it was observed that short pathways always had higher weight values (Orman et al. 2011a). Considering the thermodynamic constraints and enzymatic regulatory constraints for the futile cycles, we formulated a mixed integer quadratic programming (MIQP) to identify the weight values and fluxes simultaneously by maximizing the activity of short pathways (Orman et al. 2011a):

$$
\begin{aligned}
&\text{minimize } \sum_{i}^{n_p}\left(l_i w_i\right)^2 \\
&\text{subject to } \sum_{j}^{n_r} S_{kj}\left(\sum_{i}^{n_p} P_{ji} w_i\right) = 0, \quad \forall k \in n_m, \\
&\qquad v_j^{\min} \le \sum_{i}^{n_p} P_{ji} w_i \le v_j^{\max}, \quad \forall j \in n_r, \\
&\qquad w_i \ge 0, \quad \forall i \in n_p, \\
&\qquad \Delta G_i^{P,\max} w_i \le 0, \quad \forall i \in n_p, \\
&\qquad 0 \le \sum_{i}^{n_p} P_{Ai} w_i \le \beta\left(1-y\right), \\
&\qquad 0 \le \sum_{i}^{n_p} P_{Bi} w_i \le \beta y, \\
&\qquad y \in \left\{0,1\right\} \\
&\qquad l_i = \sum_{j=1}^{n_r} F_{ji}, \quad \forall i \in n_p, \\
&\qquad F_{ji} = \begin{cases} 1 & if \quad P_{ji} \ne 0, \\ 0 & if \quad P_{ji} = 0. \end{cases}
\end{aligned}
\tag{5.11}
$$

The length (*l)* of any pathway is equal to the number of reactions involved in that pathway and is calculated using the binary matrix of elementary modes, F, where F_{ji} is equal to 1 if P_{ji} is different than zero, otherwise F_{ji} is zero. The indices A and B represent any two reactions forming a futile cycle.

In this work, elementary modes were used to analyse the topology of the metabolic network. Since, extreme pathways are a subset of elementary modes, analyzing a biological system through a set of extreme pathways can result in the exclusion of possibly important modes (Klamt and Stelling 2003; Trinh et al. 2009). Elementary

modes were calculated using a MATLAB package, *CellNetAnalyzer* (Klamt et al. 2007). The mixed integer quadratic programming problem was solved using GAMS/CPLEX.

We used the data for the intracellular metabolite concentrations and standard Gibbs free energies that have been presented by Yang et al. (Yang et al. 2011). They have already explained the calculation of Gibbs free energies in details. Based on a very comprehensive literature survey, they also provided concentration ranges for the metabolites involved in the central carbon metabolism of hepatic cells. The constraints for the ranges of extracellular flux rates (known fluxes) were previously provided (Orman et al. 2010). Based on an extensive analysis of published perfused liver studies (Arai et al. 2001; Banta et al. 2007; Banta et al. 2005; Lee et al. 2000; Lee et al. 2003), the upper and lower limit of each unknown flux was typically assumed to be ±500 μmol/g liver/h.

5.3 Results

5.3.1 Metabolic Response of Perfused Livers to Various Oxygenation Conditions

5.3.1.1 Extracellular Fluxes

In this study, we investigated the impact of the oxygen delivery mode, namely 21% O_2, 95% O_2, and 95% O_2 + 10% Hct, on the metabolic activity of perfused livers, for a constant flow rate of 3 mL/min/g liver. Increasing the oxygen concentration in the gas phase from 21% to 95%, and then adding 10% Hct RBCs to the perfusate, significantly

increased the oxygen content of the fluid entering the liver (**Table 5.1**). Interestingly, the oxygen partial pressure of the fluid exiting the liver was similar in all three groups. Computing the oxygen consumption rate of the livers showed a parallel increase in oxygen utilization rate (**Figure 5.3**).

The concentrations of other metabolites (glucose, lactate, urea, β-hydroxybutyrate, glycerol, triglyceride, glutamate and glutamine) in the perfusate reservoir were found to change linearly as a function of time; for example, urea and β-hydroxybutyrate are shown in **Figure 5.4**, panels A and C. The data were fitted with lines to estimate the average uptake/release rates of these metabolites (**Figure 5.4**, panels B and D). Both urea and β-hydroxybutyrate production were significantly elevated by increasing oxygen partial pressure, and in turn, adding 10% Hct. Conversely, triglyceride and glycerol production rates, which were measurable in the 21% O_2 and 95% O_2 groups, decreased to near-zero values upon the addition of 10% Hct (**Figure 5.5**). A similar observation was made for lactate release from the perfused livers (**Figure 5.5**). In the 95% O_2 + 10% Hct group, some animals showed a net consumption of lactate, although on average the rate was close to zero. Glucose output was also affected by the oxygen delivery mode, increasing when going from 21% O_2 to 95% O_2, but then decreasing to a value between these two groups after adding 10% Hct. Glutamate and glutamine release/uptake rates were also measured but no significant difference among the groups was observed.

Table 5.1. Pre- and post-liver oxygen content of perfusate solutions.

Animal Groups	*Group 21%O_2*	*Group 95% O_2*	*Group 95% O_2+10% Hct*
Liver inlet			
pO_2 (mmHg)	184.3±36.1	612.3±6.1	610.3±9.2
O_2-Hb (µmole/L)	-	-	2.0±0.1
Total O_2 (µmole/L)	0.315±0.062	1.047±0.01	3.05±0.1
Liver outlet			
pO_2 (mmHg)	26.1±6.4	42.84.8	24.2±2.4
O_2-Hb (µmole/L)	-	-	0.78±0.005
Total O_2 (µmole/L)	0.045±0.01	0.073±0.008	0.83±0.005

pO_2: Partial pressure of O_2.

O_2-Hb: O_2 concentration carried by hemoglobin, which is calculated from the first part of the equation for total oxygen shown below.

Total O_2: Total oxygen concentration calculated using the equation:

$$ctO_2 = 1.39 \times FO_2Hb \times ctHb + 0.00314 \times pO_2$$

and then Total $O_2 = ctO_2 \times 0.00314^{-1} \times 0.00171$

where ctO_2 (ml/dL) and ctHb (g/dL) are the concentrations of oxygen and hemoglobin, respectively. FO_2Hb is the fraction of hemoglobin occupied by oxygen, and pO_2 (mmHg) is the partial pressure. The value 1.39 represents the oxygen binding factor of hemoglobin and 0.00314 is the oxygen solubility coefficient which is a conversion factor for mmHg O_2 perfusate to ml O_2/dL perfusate. Value of 0.00171 is the Henry constant (mmol /mmHg-L).

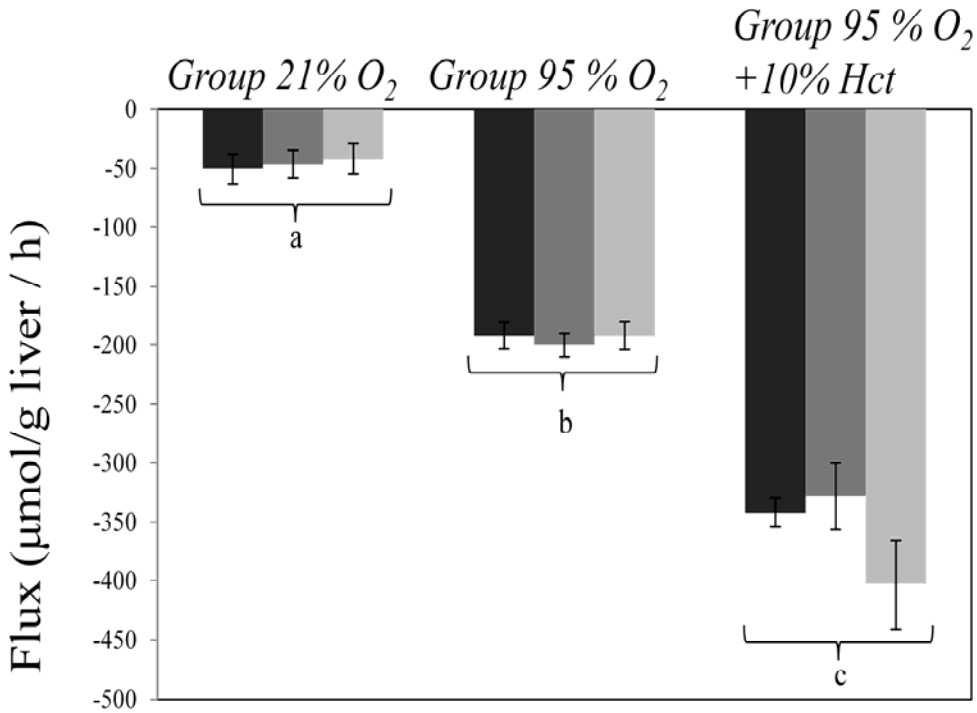

Figure 5.3. Perfused liver oxygen uptake rates (-) as a function of oxygen delivery mode at 20 min (black bar), 40 min (dark grey), and 60 min (light grey) after the beginning of perfusion.

All rats were in a fed state (n=4 per group). Note: Letters indicate statistically significant (P<0.05) differences among groups: ***a*** *is significantly different than either* ***b*** *or* ***c****; and* ***b*** *is significantly different than* ***c****. No significant difference is observed within the groups.*

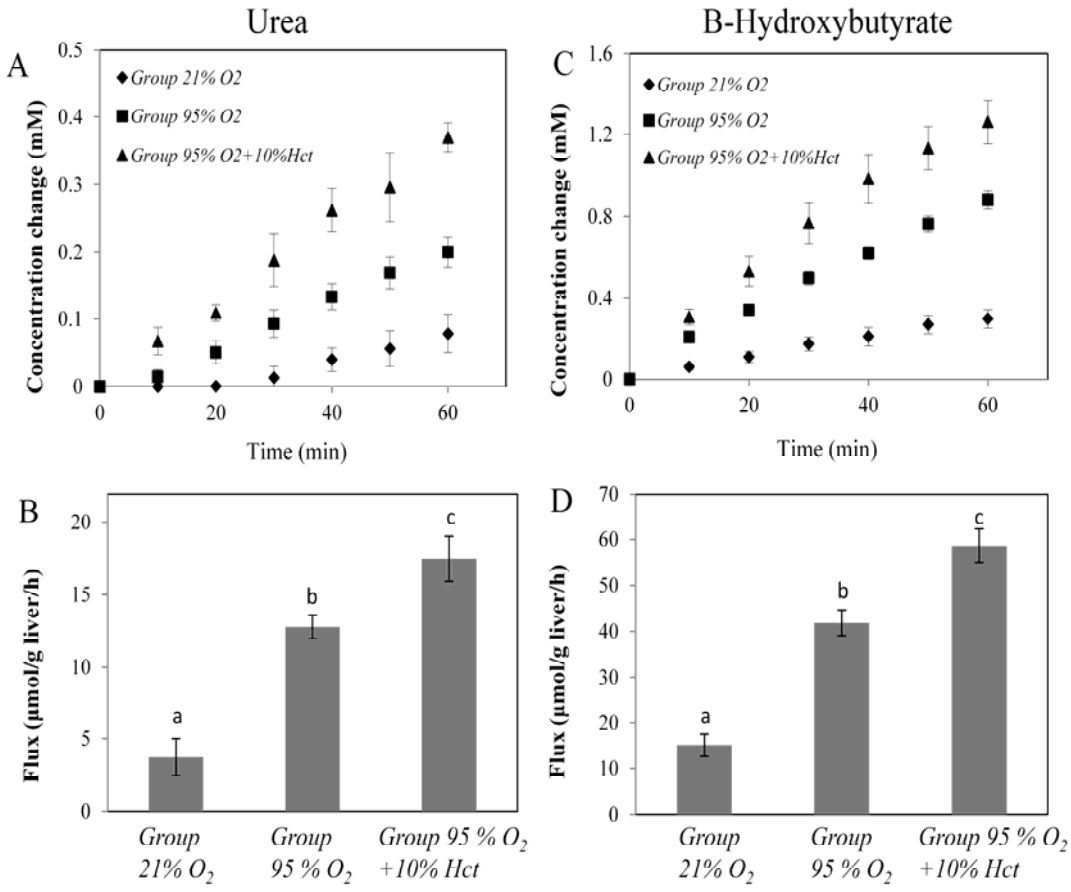

Figure 5.4. Urea and β-hydroxybutyrate production during perfusion as a function of oxygen delivery mode.

__A__. Urea accumulation as a function of time. __B__. Urea production rate, calculated from slope of panel __A__. __C__. β-hydroxybutyrate accumulation as a function of time. __D__. β-hydroxybutyrate production rate, calculated from slope of panel __C__. All rats were in a fed state (n=4 per group). Note: Letters indicate statistically significant (P<0.05) differences among groups: __a__ is significantly different than either __b__ or __c__; and __b__ is significantly different than __c__.

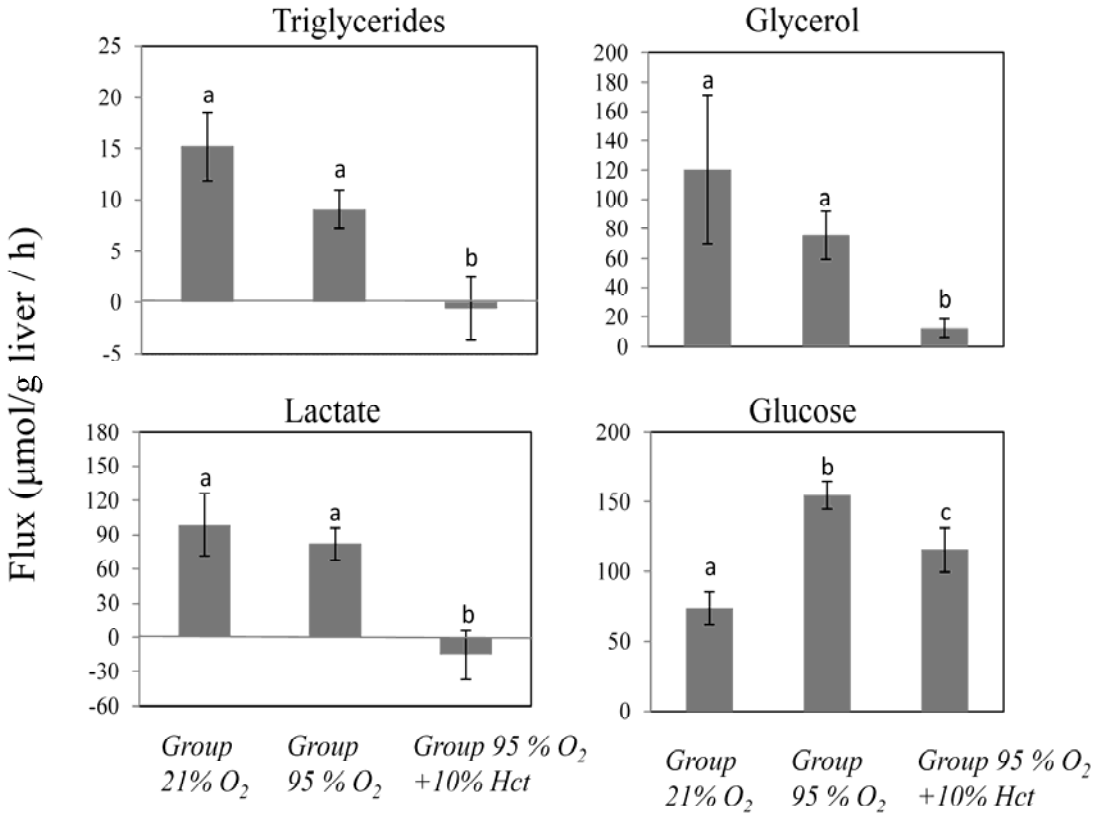

Figure 5.5. Glucose, lactate, TG and glycerol uptake (-) or production rates (+) during perfusion. All rats were fed.

n=4 per group. Note: Letters indicate statistically significant (P<0.05) differences among groups: ***a*** *is significantly different than either* ***b*** *or* ***c****; and* ***b*** *is significantly different than* ***c****. For example, lactate secretion rates in Group 21%O_2 (a) and Group 95%O_2 (a) are not significantly different, whereas Group 95%O_2+10%Hct (b) is significantly different than either Group 21%O_2 (a) or Group 95%O_2 (a).*

5.3.1.2 Steady State Flux Distribution

Flux vectors were uniquely determined by implementing the optimization method described by Equation 5.11 in the Materials and Methods section (note that thermodynamic and futile cycle associated constraints were not included). Since the perfused liver was metabolically stable for the duration of the perfusion, the pseudo steady-state assumption used to formulate the Equation 5.11 is reasonably valid. The calculated fluxes are shown in **Figure 5.6**. Reactions 1-7 are those in the gluconeogenic pathway, although some of them are also used (in a reverse direction) by the glycolysis pathway. For example, reaction 2 (generation of glucose-6-P from fructose-6-P), and reactions 4-5 (generation of phosphoenolpyruvate [PEP] from glyceraldehyde-3-P), had negative fluxes in the 21% O_2 and 95% O_2 groups, implying that they were operating in a glycolytic mode. Conversely, these reactions had positive fluxes, indicating a gluconeogenic pattern, in the 95% O_2 + 10% Hct group. Interestingly, flux values for reaction 1 (converting glucose-6-P to glucose) were positive, consistent with a gluconeogenic pattern, while flux values for reaction 8 (glucose-6-P generation from glucose), which is strictly glycolytic, were near zero in all groups. However, glycolytic reactions 9 and 10 (generation of pyruvate from PEP and fructose-1,6-P2 from fructose-6-P, respectively) were found to be active in all groups, which results in the futile cycles with the gluconeogenic reactions 3, 6-7 which are the opposite of reactions 9-10. Reaction 11 (conversion of pyruvate into acetyl-coA) had a significantly higher flux in the 95% O_2 + 10% Hct group compared to other groups.

Reaction 12 (a lumped reaction term representing the PPP) had a higher flux value in the 95% O_2 + 10% Hct group compared to other groups. Reaction 13 is catalyzed by lactate dehydrogenase, and represents the inter-conversion of pyruvate and lactate. A negative value, as was the case for the 21% O_2 and 95% O_2 groups, indicates that the reaction was producing lactate from pyruvate, while the opposite (net conversion of lactate to pyruvate) was true in the 95% O_2 + 10% Hct group.

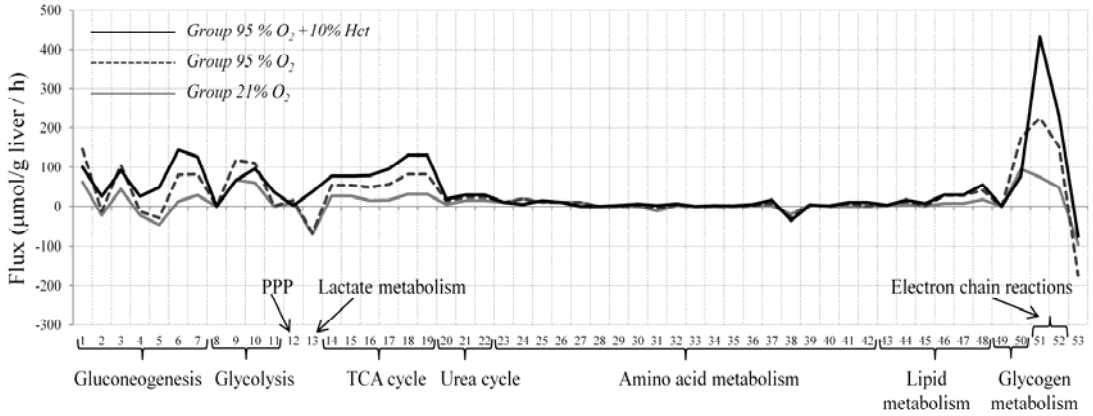

Figure 5.6. Calculated internal fluxes using Equation (5.11).

Reactions 14-19, which account for the TCA cycle, had their lowest fluxes in the 21% O_2 group, and increased in unison in the 95% O_2 group, and subsequently even more in the 95% O_2+10% Hct group. These changes largely reflect the observed changes in oxygen uptake rates (**Figure 5.3**), and not surprisingly parallel observed increases in the electron

transport reaction fluxes (reactions 51-52). These changes are also consistent with the increased production of pyruvate and acetyl-coA by reactions 11 and 13 in the 95% O_2+10%Hct group, which are the direct precursors entering the TCA cycle.

Fluxes in the urea cycle (reactions 20-22 in **Figure 5.6**) were higher when perfusate oxygen partial pressure was increased from 21% to 95%, and then by addition of 10% Hct. Fluxes in amino acid metabolism, represented by reactions 23-42, were not significantly different and relatively lower when compared to other fluxes, as previously observed (Arai et al. 2001; Banta et al. 2007; Banta et al. 2005; Lee et al. 2000; Lee et al. 2003).

Fatty acid oxidation and ketone body production (reactions 43-48) were generally lower in the 21%O_2 group compared to the other groups, but there was little difference between the 95%O_2 and 95%O_2+10%Hct groups. In all three groups, glycogen production (reaction 49) was essentially zero, while glycogen degradation (reaction 50) was very active; interestingly, this flux was significantly higher in the 95%O_2 group, but there was no difference between the 21%O_2 and 95%+10% Hct groups.

The predicted values of CO_2 generation from the various relevant pathways which were calculated by the optimization method are reported in **Table 5.2**. The predictions show the quantitative productions from the TCA cycle, amino acid metabolism, and PPP, and usage in gluconeogenesis and the urea cycle for each group. CO_2 production from the

TCA cycle in the 95% O_2+10% Hct group were found to be significantly higher consistent with the increased TCA cycle fluxes. Due to the increased fluxes in PPP in 95% O_2 group, CO_2 production from the PPP was the highest in this group.

Table 5.2. Predicted CO2 utilization and production rates (μmole/g liver/h) by key pathways in the perfused liver.

	21 % O_2	95 % O_2	95 % O_2+10 % Hct
TCA cycle	41.1	102.4	155.8
PPP	58.9	84.7	13.6
Amino acid metabolism	10.0	5.6	6.3
Gluconeogenesis	-28.5	-80.9	-90.1
Urea	-15.1	-23.6	-29.1
Overall CO2 production	66.4	88.2	56.5

5.3.1.3 Pathway Analysis

Elementary modes were used to analyse the topology of the metabolic network. The number of all possible elementary modes of the hepatic metabolic network was found to be 134175. Among them, only 6 pathways are reversible (note that in this article we use the term “pathways” to denote the “elementary modes”). The optimization problem (Equation 5.11) identified possible important pathways with their weight values that characterize their importance in hepatic metabolism (**Figure 5.7**). It was observed that increasing the oxygen partial pressure from 21% to 95%, the number of active pathways whose weight values are greater than zero increased from 176 to 199. Adding 10% Hct then increased this number to 410. Furthermore, relatively longer pathways were found to

be active in the 95%O_2+10% Hct group when compared to other groups, although these pathways were generally with low weight values.

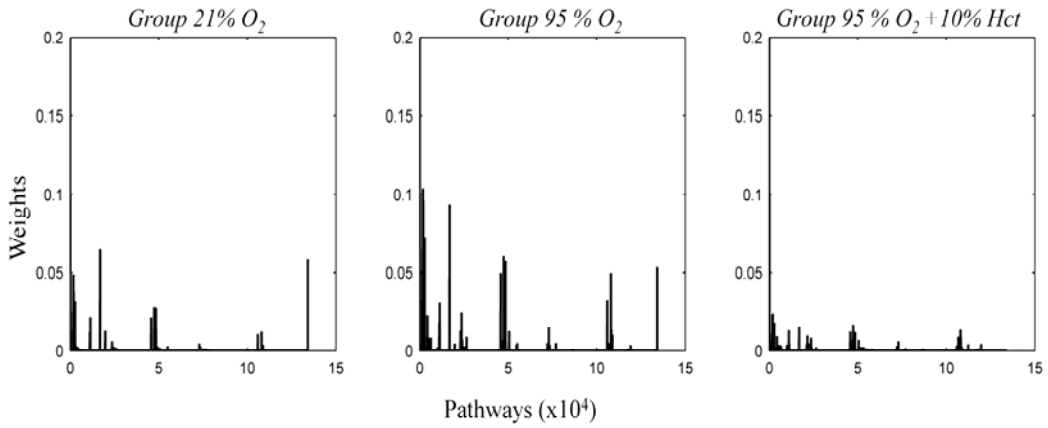

Figure 5.7. Weight values of pathways. A: *Group 21%O_2*; B: *Group 95%O_2;* C: *Group 95%O_2+10%Hct.*

Note that in each method all weights values are normalized to the largest one observed among the groups. Only P7, which is not shown in this figure, has a weight value greater than 0.2 in the three experimental groups (see Table 6 for details).

Table 5.3. Important elementary modes having larger weight values (w > 0.01 for each group).

Pathways	Explanation	Weights *Group 21%O_2*	Weights *Group 95%O_2*	Weights *Group 95%O_2+10%Hct*
P7	This is a very short pathway including glycogen breakdown, and glucose production and secretion.	0.45237	1	0.208647
P10	This pathway includes glycogen breakdown, glycolysis and lactate production.	0.079201	0.118951	0
P12	This includes glucose production from lactate through gluconeogenesis.	0	0.06365	0.026165
P23	This pathway includes glucose production from cysteine through gluconeogenesis.	0.031115	0.07476	0.07476
P237	This is related to aspartate production from gluconeogenic glucose through glycolysis.	0.02224	0.057114	0.012991
P2026	This is a very short pathway related to glycine and serine interconversion.	0.037758	0.096202	0.023511
P2094	This includes glucose production from glutamate through gluconeogenesis.	0	0.039033	0.011868
P2830	This represents energy metabolism including glycolysis, TCA cycle and electron transport reactions.	0	0	0.017946
P2842	This represents energy metabolism including fatty acid oxidation and electron transport reactions.	0	0	0.016352
P16876	This pathway includes glycogenolysis, glycolysis and PPP.	0.032322	0.084866	0.015341
P16897	This pathway includes lactate production from glycogenic glucose in addition to PPP.	0.064988	0.093428	0
P108052	This elementary mode includes two distinct extreme pathways. One represents serine and glycine inter-conversion. The other includes glucose production from aspartate through gluconeogenesis.	0	0.049932	0.013575
P134172	This pathway is related to cysteine and lactate inter-conversion.	0.058845	0.05362	0

In order to gain a better comprehensive understanding of the metabolic response of the liver to the oxygen delivery mode, dominant pathways (having larger weight values) were further examined and listed in **Table 5.3**. P7, a very short pathway describing glucose production from glycogen stores, was found to be active with a very high weight value in all groups. The highest weight for P7 was in the 95%O_2 group, consistent with the experimental observation that glucose output (reaction 1) was highest in that group as

well. P10 is also a short pathway, linking glycogen breakdown, glycolysis, and lactate production. This pathway was nonexistent in the 95%O_2+10%Hct group, but was significant in the other two groups. P12 and P13 represent glucose production through gluconeogenesis from lactate and cysteine, respectively. These pathways were found to be more active in the 95%O_2 and 95%O_2+10%Hct groups. P237, which was found to be active in all conditions, involves the production of aspartate from glucose. P2026 represents serine and glycine inter-conversion by glycine dehydrogenase and aminomethyltransferase, and had a higher weight value in the 95%O_2+10%Hct group when compared to the other groups.

P2094 involves glutamate uptake (including glutamine uptake followed by deamination to glutamate), formation of oxaloacetate by an anaplerotic route via the TCA cycle and gluconeogenesis. The activity of this pathway was increased when perfusate oxygen content was increased. P2830 and P2842 were only active in the 95%O_2+10%Hct group and are related to energy metabolism (**Table 5.3**). They represent ATP production through electron transport chain reactions from high energy metabolites (e.g. NADH) produced by glycolysis, the TCA cycle, or fatty acid oxidation. P16876 and P16897 had higher weights in the 21%O_2 and 95% O_2 groups. These pathways show the possible paths for metabolizing intracellular glucose (generated from glycogen), namely either via the PPP or via glycolysis towards lactate. P10852 has two different pathways. One is related to glucose production from aspartate through the gluconeogenic pathway, and the other shows the inter-conversion of serine and glycine. P134172 involves lactate

production from cysteine by lactate dehydrogenase, and cysteine transaminase. This pathway was upregulated in the 21% O_2 and 95% O_2 groups (**Table 5.3**). Similarly, there were other pathways (such as P47434 and P48418, not shown) involving lactate production through glycolysis, which were also significantly upregulated in the 21% O_2 and 95% O_2 groups.

5.3.2 Liver Metabolic Response to Experimental Burn Injury Associated with Fasting

5.3.2.1 Extracellular Fluxes

In this study, we investigated the metabolic response of liver to fasting and/or burn systemic injury in rats. Totally, four different animal groups, *Sham+Fed*, *Sham+Fasted*, *Burn+Fed*, *Burn+Fasted*, were compared. The average uptake and release rates of major metabolites, including glucose, urea, lactate, β-hydroxybutyrate, oxygen, and amino acids were obtained from livers isolated 4 days post injury and perfused for 1 hr (Orman et al. 2011b). For fasted groups, fasting was applied 24 h prior to perfusion.

Figure 5.8 shows glucose, lactate, urea and β-hydroxybutyrate production or utilization rates in the four different groups. Note that positive values indicate net release rates whereas negative values represent net uptake rates. Following fasting, glucose production rates were significantly decreased in both the burn and sham-burn groups. Interestingly, glucose production increased as a result of burn injury in the fed groups (*Burn+Fed* vs.

Sham+Fed), while the opposite (i.e. glucose production decreased as a result of burn injury) was observed in the sham groups (*Burn+Sham* vs. *Sham+ Sham*). The uptake of lactate, a typical substrate for the gluconeogenic pathway, was increased over 5 fold by fasting in the sham groups, but not in the burn groups. As expected, burn injury significantly increased urea production when evaluated in both fed and fasted conditions. Of note is that the magnitude of the increase was less than 2 fold in the fed groups, but more than 3.5 fold in the fasted groups. In addition, fasting reduced urea production in sham animals but increased it in burn animals. Beta-hydroxybutyrate production, on the other hand, was significantly – albeit slightly - increased after fasting in the sham animals, as well as in both burn groups.

Among the amino acids, the uptake or release rates of glutamine, ornithine, arginine, glycine and methionine showed significant variations among the groups (**Figure 5.9**). Glutamate production rates were higher in the *Burn+Fasted* and *Burn+Fed* groups when compared to the *Sham+Fed* group; however, there was no statistically significant difference between the *Sham+Fed* and *Sham+Fasted* groups. Glutamine, arginine, and methionine utilization rates were significantly higher in the *Burn+Fasted* group, whereas no significant differences were observed among the other groups. Ornithine production was also significantly elevated in the *Burn+Fasted* group compared to the other groups.

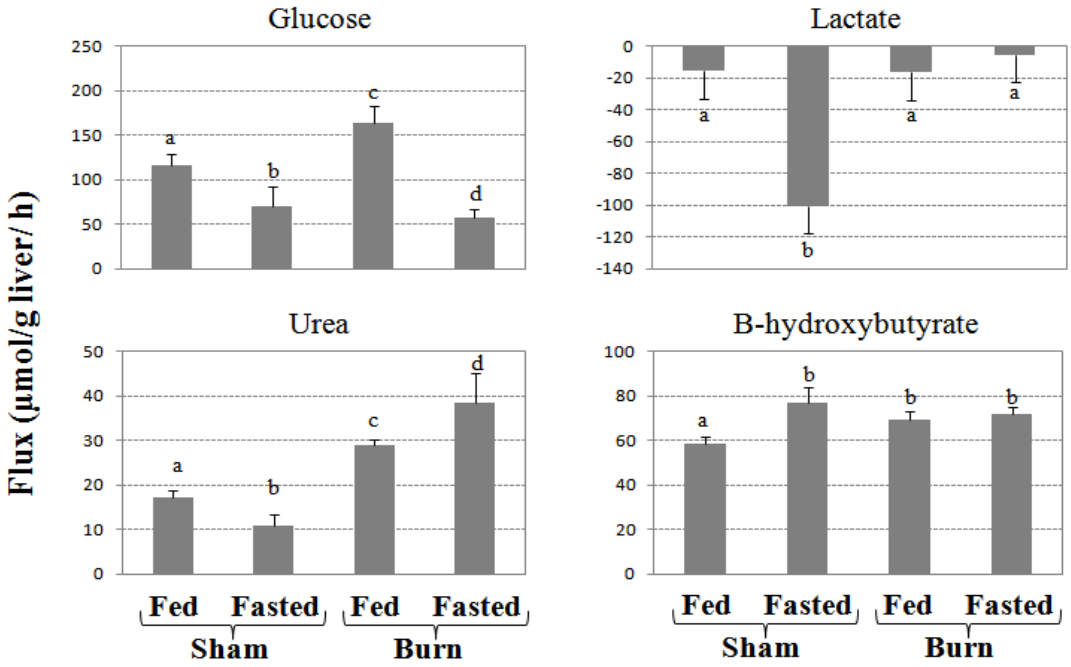

Figure 5.8. Glucose, lactate, urea and β-hydroxybutyrate uptake (-) or production rates (+) during perfusion.

Bars are labeled with letters to indicate statistically significant ($P<0.05$; $N\geq3$) differences among groups: ***a*** *is significantly different than* ***b***, ***c*** *and* ***d****; and* ***b*** *is significantly different than* ***c*** *and* ***d****. For example, lactate secretion rates in Sham+Fed group (a), Burn+Fed group (a) and Burn+Fasted group (a) are not significantly different, whereas Sham+Fasted (b) is significantly different than other groups.*

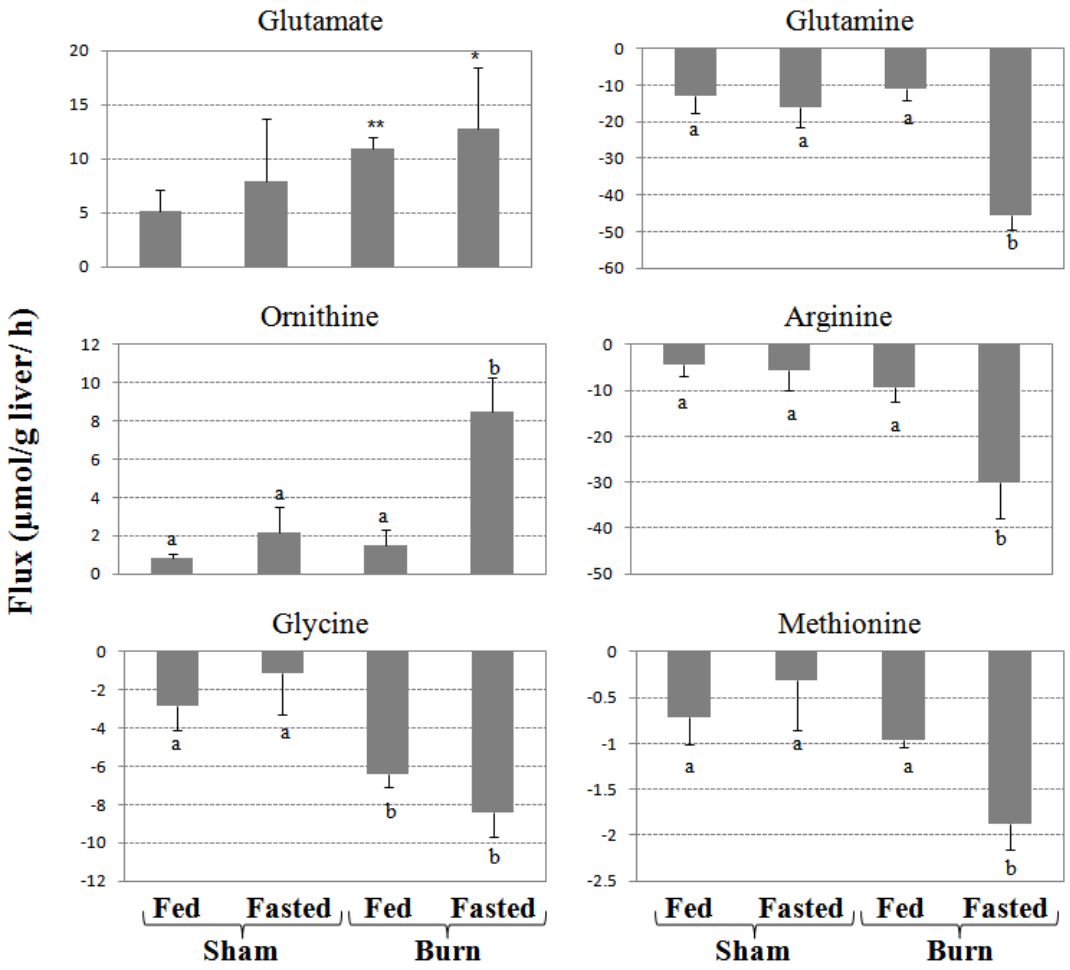

Figure 5.9. Uptake (-) or production rates (+) of important amino acids during perfusion.

Bars are labeled with letters to indicate statistically significant (P<0.05; N≥3) differences among groups: a is significantly different than b, c and d; and b is significantly different than c and d.

** Glutamate uptake rate in burn+fasted group was found to be significantly higher than that of sham+fed group (P<0.05).*

*** Glutamate uptake rate in burn+fed group was found to be significantly higher than that of sham+fed group (P<0.05).*

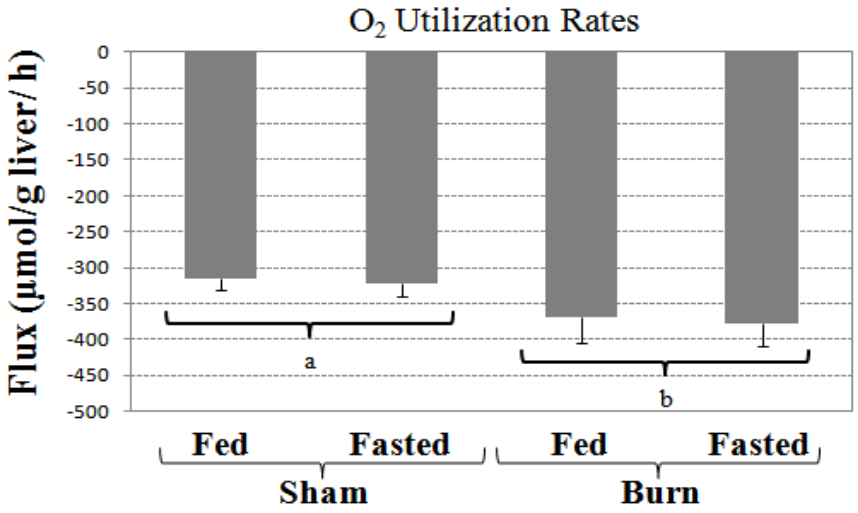

Figure 5.10. Oxygen utilization rates.

Bars are labeled with letters to indicate statistically significant (P<0.05; N≥3) differences among groups: ***a*** *is significantly different than* ***b.***

Oxygen consumption rates were slightly but significantly elevated in response to burn injury when comparing all the burn groups vs. all the sham groups (**Figure 5.10**). To assess tissue damage, we monitored the release of intracellular lactate dehydrogenase (LDH) during the perfusion (**Figure 5.11**). All groups showed an increase in LDH activity as a function of time. By the end of the 1 hr perfusion, LDH accumulation was greater in both burn groups compared to the sham groups. These results indicate that prior burn injury results in evidence of greater tissue damage during perfusion.

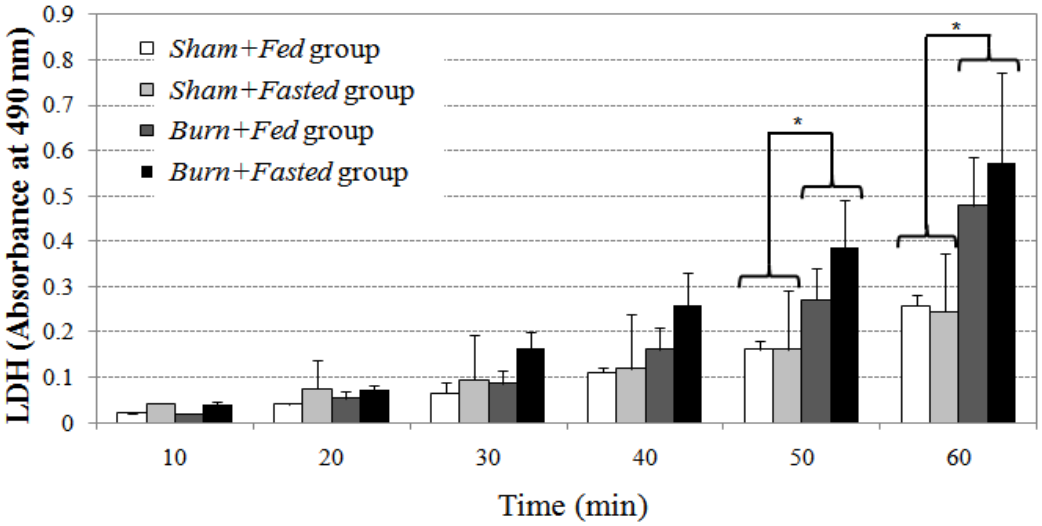

Figure 5.11. Lactate dehydrogenase (LDH) activity in perfusate as a function of time during the perfusion.

N≥3 for each group.

**LDH activity in burn groups were significantly different than that of sham groups (P<0.05).*

5.3.2.2 Intracellular Fluxes

Flux vectors were uniquely determined by utilizing the optimization methodology based on elementary mode analysis which is summarized in equation 5.11 and described in greater detail in the Materials and Methods section. Since the perfused liver was metabolically stable for the duration of the perfusion as observed previously (Arai et al. 2001; Banta et al. 2007; Banta et al. 2005; Lee et al. 2000; Lee et al. 2003; Orman et al. 2010; Yokoyama et al. 2005), it is quite reasonable to assume that the metabolic fluxes

were at pseudo steady-state. Given that the metabolic network utilized in this study simultaneously accounts for the glycolytic and gluconeogenic pathways, fatty acid synthesis and oxidation, as well as glycogenesis and glycogenolysis, we used a mixed integer quadratic programming to prevent futile cycle from occurring. The binary variables in this formulation allow the reactions (forming a futile cycle) to inhibit each other. The model further includes thermodynamic constraints to reduce the solution space. A flux distribution vector was uniquely determined by maximizing the activity of short pathways (Orman et al. 2011a; Orman et al. 2011b). The calculated fluxes for all four groups are shown in **Figure 5.12**. Fluxes exhibiting significant differences among the groups are described in further detail in **Figures 5.13** and **5.14**. The modeling results suggest that gluconeogenesis, glycogenolysis and fatty acid oxidation were active in all groups (**Figure 5.12**).

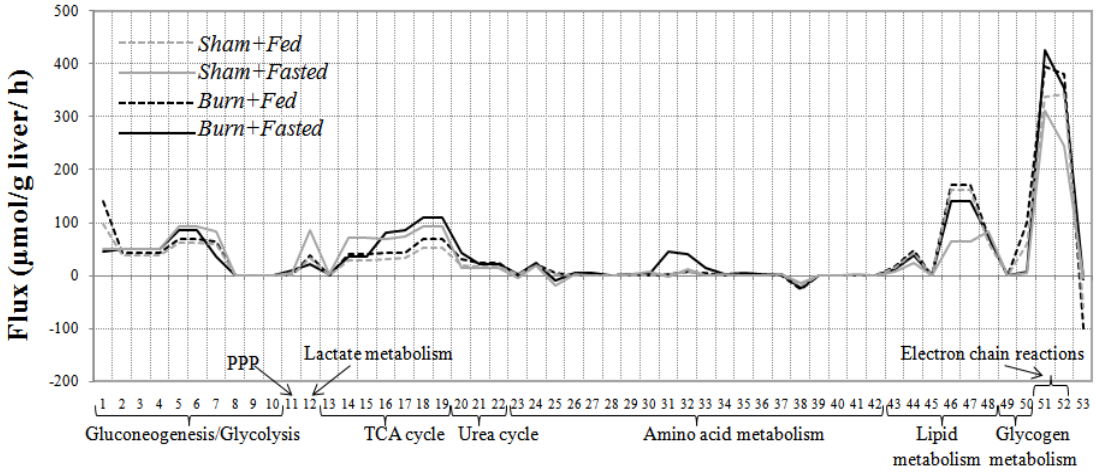

Figure 5.12. Calculated internal fluxes using the optimization method (equation 5.11).

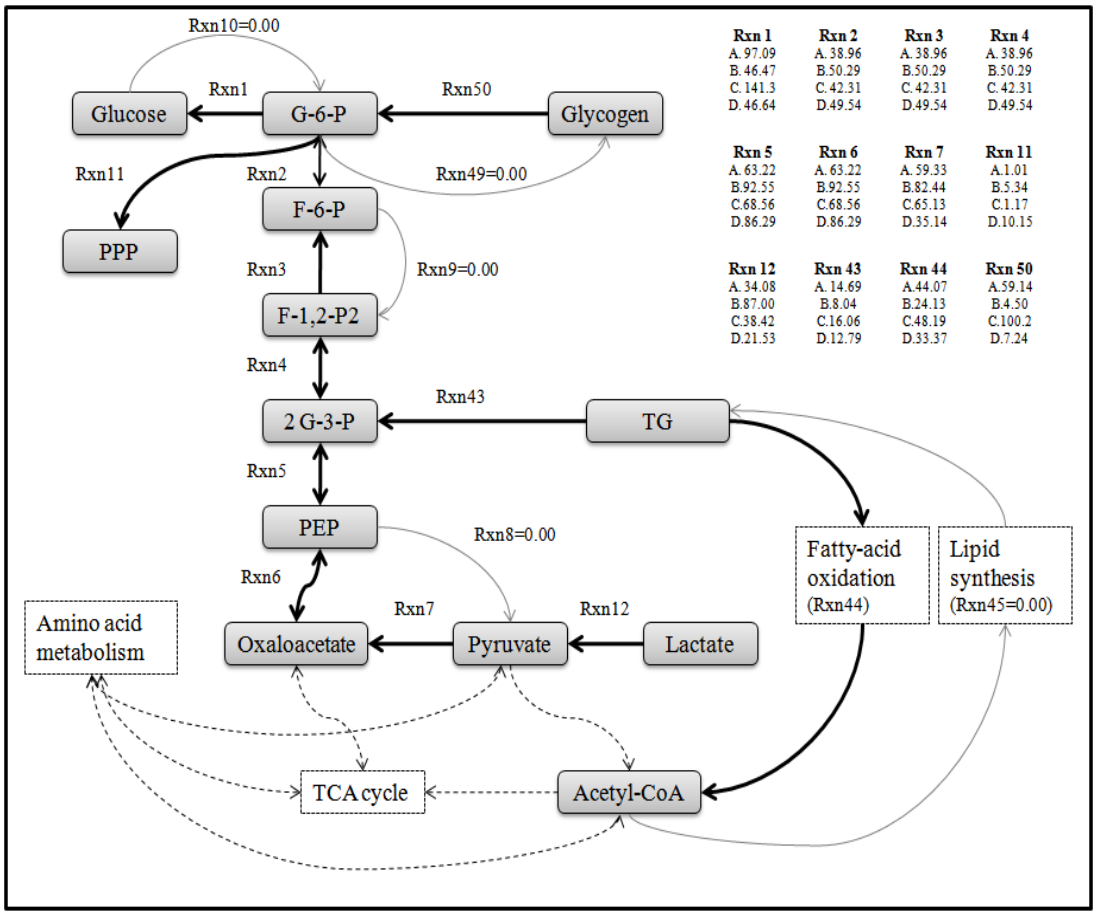

Figure 5.13. Calculated fluxes of most important reactions.

Note that several reaction pairs (Rxn 1 vs. Rxn 10; Rxn 3 vs. Rxn 9; Rxn 6 vs. Rxn 8; Rxn 49 vs. Rxn 50; and Rxn 44 vs. Rxn 45) form futile cycles. Black straight lines indicate active (or dominant) reactions whereas gray lines represent inactive (i.e. flux = 0) reactions. Dashed lines are used to depict reaction steps not shown in detail. Flux units are µmol/g liver/h. A: Sham+Fed group; B: Sham+Fasted group; C: Burn+Fed group; D: Burn+Fasted group.

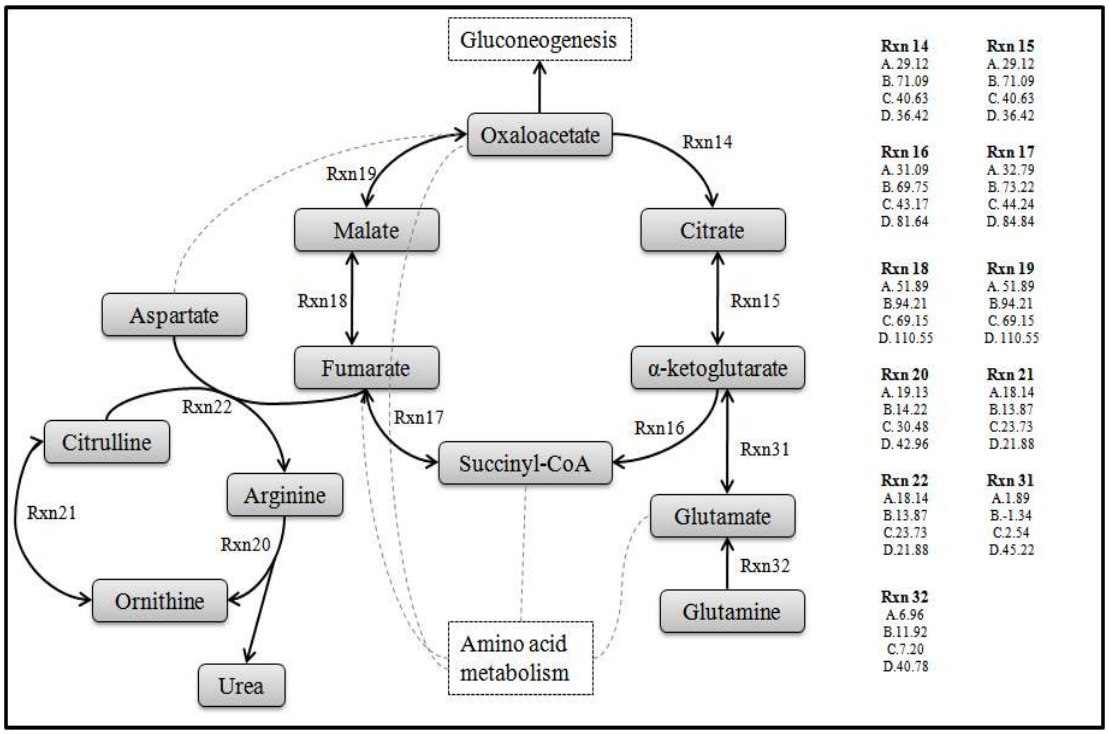

Figure 5.14. Calculated fluxes of important reactions in TCA and urea cycles.
Dashed lines are used to depict reaction steps not shown in detail. Flux units are μmol/g liver/h. A: Sham+Fed group; B: Sham+Fasted group; C: Burn+Fed group; D: Burn+Fasted group.

The rate of reaction 1 (generation of glucose from glucose-6-P) was significantly up-regulated in fed groups due to the increased rate of glycogen breakdown (reaction 50). Reaction 11 (a lumped reaction term representing the PPP) had a slightly higher flux value in the *Burn+Fasted* group (group A). Fatty acid oxidation (reaction 44) and fatty acid synthesis (reaction 45) also form a futile cycle, although our analysis suggests that fatty acid synthesis was negligible in all groups. Fatty acid oxidation was generally higher in the fed groups (groups A and B).

Figure 5.14 provides the overall picture of the changes in the TCA cycle and urea cycle fluxes. Reactions 14 and 15 fluxes were higher in the *Sham+Fasted* group (group C) compared to other groups, which likely reflects the contribution of pyruvate to oxaloacetate as a result of increased lactate uptake rate in the same group. Reactions 16-19 fluxes, where oxaloacetate is generated from α-ketoglutarate, were higher in the fasted groups (groups B and D) compared to the fed groups (groups A and C). In the case of the *Burn+Fasted* group (group D), there was a dramatic increase in reaction fluxes 31 and 32, indicating an increased supply of α-ketoglutarate through glutamine and glutamate. The rate of reaction 20, where urea is generated from arginine, was also higher in the *Burn+Fasted* group (group D), consistent with the previously measured increase in urea output (**Figure 5.9**). Electron chain reactions (**Figure 5.12**) were increased in the burn groups (groups C and D), which correlates with the increased TCA fluxes in *Burn+Fasted* group and increased fatty acid oxidation in the *Burn+Fed* group. In spite of the increased TCA fluxes in the *Sham+Fasted* (group B) group, the electron chain reactions were not elevated compared to the other groups, which might be the result of decreased fatty acid oxidation in that particular group.

5.3.3 Metabolic Flux Distributions in the Liver Following Burn or Sepsis

5.3.3.1 Steady State Flux Distribution

In this section, we investigated the effects of burn or CLP on liver metabolism. The livers were isolated for perfusion experiments 24 h after the treatments. Flux vectors were

uniquely determined using the weights of pathways calculated from the optimization problem described by Equation (5.11). Detailed description of flux distribution of gluconeogenic and glycolytic pathways for different groups are given in **Figure 5.15**. Reactions 1-7 are gluconeogenic reactions, although some of them are also used (in a reverse direction) by the glycolysis pathway. Application of optimization programming revealed that gluconeogenic pathway was active or dominant in four groups. The fluxes in gluconeogenic reactions 2-6 had higher values in burn animals compared to other groups. However these fluxes had the lowest values in SCLP group. Reaction 11 (a lumped reaction term representing the PPP) had a slightly higher flux value in the burn group, and it was found to be almost zero in CLP group during 1-h of liver perfusion. Reaction 12 is catalyzed by lactate dehydrogenase, and represents the inter-conversion of pyruvate and lactate. A significant amount of lactate was taken in Burn group. This was significantly decreased in SCLP group, which explains the decrease of gluconeogenic reactions rates in SCLP group. Fatty acid oxidation (reaction 44) and fatty acid synthesis (reaction 45) also form a potential futile cycle, and our method identified that fatty acid oxidation was dominant in all conditions. Glycogen production (reaction 49) was essentially zero, while glycogen degradation (reaction 50) was found to be active. Interestingly, in SCLP group, the glucose production from glycogen was significantly lower compared to other groups.

We did not observed significant differences between the groups in TCA cycle reactions. Similarly, fluxes in amino acid metabolismwere not significantly different and relatively

lower when compared to other fluxes, as previously observed (Arai et al. 2001; Banta et al. 2007; Banta et al. 2005; Lee et al. 2000; Lee et al. 2003)

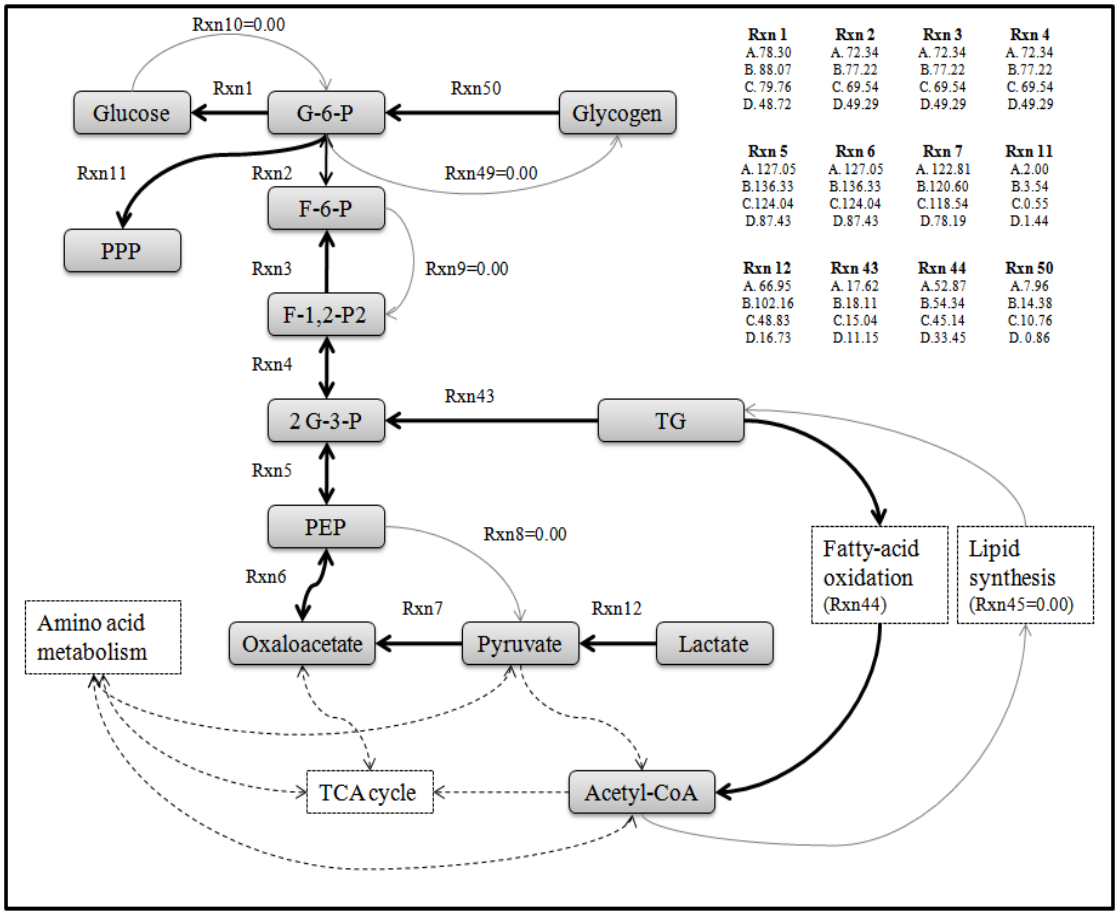

Figure 5.15. Calculated fluxes of most important reactions.

Note that several reaction pairs (Rxn 1 vs. Rxn 10; Rxn 3 vs. Rxn 9; Rxn 6 vs. Rxn 8; Rxn 49 vs. Rxn 50; and Rxn 44 vs. Rxn 45) form futile cycles. Black straight lines indicate active (or dominant) reactions whereas gray lines represent inactive (i.e. flux = 0) reactions. Dashed lines are used to depict reaction steps not shown in detail. Flux units are µmol/g liver/h. A: Sham group; B: Burn group; C: CLP group; D: SCLP group.

.

5.3.3.2 Pathway analysis

Application of optimization programming (Equation 5.11) identified the weight values of 134175 different pathways found in the network. The pathways with the highest weight values in all conditions were given in **Table 5.4**. P4 is a very short pathway representing the urea production from arginine (**Figure 5.16**). The weight of this pathway was increased in burn group. P7, a pathway describing glucose production from glycogen stores, was found to be active in all groups. Its weight value is significantly higher in burn group compared to others. However, its value is the lowest in SCLP group. P1802 and P1817 are related to lactate metabolism (**Figure 5.16**), and their weight values were slightly increased in burn group. P1802 represents alanine production whereas P1817 cysteine from lactate. P2026 represents serine and glycine inter-conversion by glycine dehydrogenase and aminomethyltransferase, and had a higher weight value following the burn injury. P106764 is long pathway which has the lowest weight value in SCLP group. This pathway (not shown in **Figure 5.16**) represents glucose production from glycerol moiety of triglycerides. P107249 represent glucose production from lactate through gluconeogenic pathway. P108052 includes glucose production from aspartate. These two pathways were found to have highest weight values in burn group while they had lowest values in SCLP group. There are also other pathways which have been found to be slightly up-regulated following the burn injury including modes where glucose production from glutamine, acetyl-coA from ketone bodies, and other amino acids takes place. These metabolites are generally converted to glucose through an anaplerotic route via the TCA cycle.

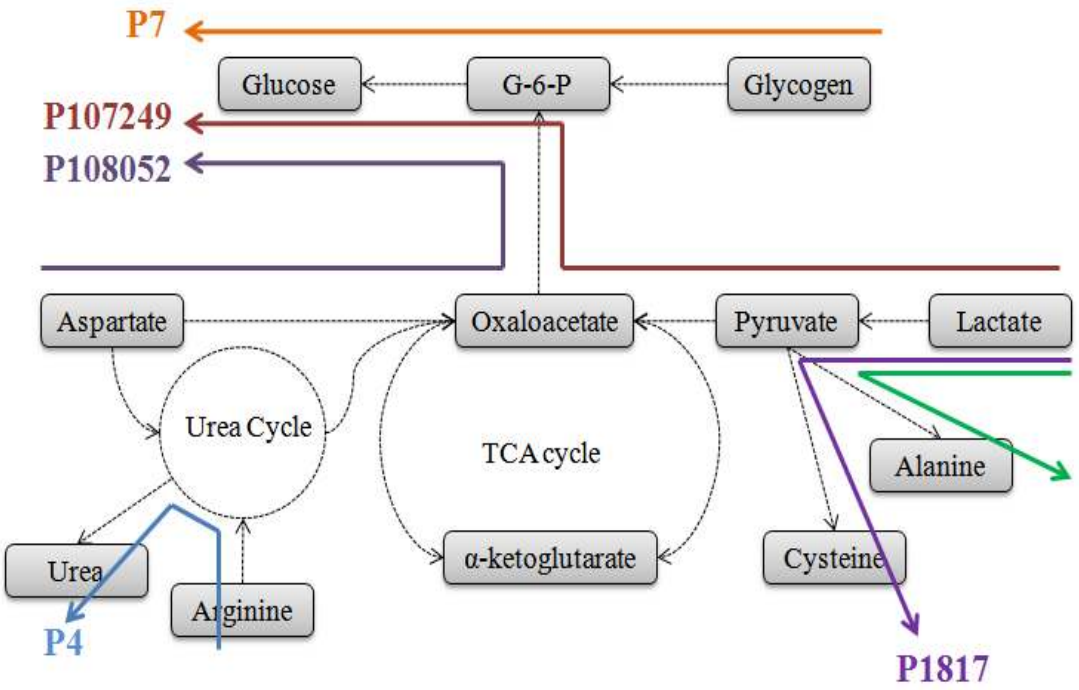

Figure 5.16. Important pathways.

Table 5.4. Pathways and their weight values.

Pathways	Sham	Burn	CLP	SCLP
P4	1.158159	7.374255	3.379989	0.484268
P7	7.656045	14.08193	10.36079	0.667422
P1802	0.611389	1.004788	0.566645	0.084998
P1817	0.611389	1.447353	0.543593	0.084998
P2026	0.677453	1.324446	0.551893	0.060123
P106764	0.586166	0.984844	0.495505	0.084342
P107249	0.823529	1.020031	0.722303	0.181982
P108052	0.949969	1.334128	0.670894	0.159344

5.4 Discussion

In this study we used a medium scale metabolic network that has been extensively used to characterize the flux distribution of central carbon metabolism in perfused rat livers (Arai et al. 2001; Banta et al. 2007; Banta et al. 2005; Lee et al. 2000; Lee et al. 2003). It has been well established that there is a consistency between the perfused liver-measurements and assumed biochemistry of the network (Lee et al. 2000; Lee et al. 2003). Thermodynamic properties of this network has been also extensively characterized in literature (Iyer et al. 2010a; Iyer et al. 2010b; Nolan et al. 2006; Yang et al. 2011; Yoon et al. 2007). In this study, a metabolic network analysis based on elementary modes was used. In order to determine the flux distribution vector and weights of pathways simultaneously, activity of short pathways was maximized.

Thermodynamic constraints were applied to further narrow and refine the flux and activity of elementary mode predictions. Although thermodynamics have been applied to many areas of biological systems, many studies have been performed on relatively small scale pathways or networks with non detailed thermodynamic models. Incomplete knowledge regarding the intracellular conditions, lack of thermodynamic data on metabolic reactions obviously the main reasons of these problems. Maskow and Stockar (Maskow and von Stockar 2005) emphasized that intracellular conditions should be known for thermodynamic feasibility of unknown pathways. In this study, we assumed that each pathway can be represented as a macroscopic reaction which should satisfy the thermodynamic constraint. Underlying assumption behind this formulation is based on

the fact that a reaction can be a driving force for its subsequent reaction given the Gibbs free energies they have. Based on a very comprehensive analysis regarding the standard Gibbs free energies of reactions and hepatic metabolic concentrations provided by Yang and co-workers (Yang et al. 2011), we determined the upper and lower limits of free energies of pathways. Solving the nonlinear inequality term, $\Delta G_i^P w_i \le 0$ where two variables are multiplied, is quite difficult in the model given the total number of variables. Therefore we introduced the inequality constraint, $\Delta G_i^{P,\max} w_i \le 0$, to the model in order to eliminate the nonlinear inequality terms in the model and further tighten the solution space as it has been justified in the Materials and Method section. In our study, elementary modes were calculated considering the stoichiometric matrix and well known reaction reversibility constraints; therefore each pathway satisfies the mass balance and reaction reversibility constraints that have been imposed. However this does not mean that the overall Gibbs free energy of each pathway is less than zero. In this very redundant system (134175 pathways were analyzed in this study), imposing energy balance eliminates thermodynamically infeasible pathways in the networks and thus reduces the feasible solution space.

In most of the perfused liver studies, some certain assumptions such as lack of glycogen and lipid storage and inhibition of all strictly glycolytic enzymes have been made since the animals have typically been fasted prior to liver perfusion experiments. Eliminating these reactions or pathways results in relatively small scale network without futile cycles so that the intracellular fluxes can be easily calculated. On the other hand, for non-fasted

animals, these major reactions or pathways should be considered in the model, which causes an underdetermined system. In some cases, a different metabolic model was used for the fed state, and both the fed and fasted models were fitted to the data; the best fitting model was then used to calculate the fluxes (Arai et al. 2001; Banta et al. 2007; Banta et al. 2005; Lee et al. 2000; Lee et al. 2003; Yokoyama et al. 2005). Therefore, there is a need to develop a "unified" metabolic flux analysis approach that could be similarly applied to both fed and fasted states. We applied a mathematical formulation (including binary variables preventing the formation of futile cycles) to each reaction pair forming a cycle in glycolysis/gluconeogenesis pathways, glycogen metabolism and fatty acid metabolism. We identified that gluconeogenic reactions, glycogen breakdown and fatty acid oxidation were found to be active in all perfusion experiments.

First, we investigated the effect of increasing oxygen delivery by increasing oxygen partial pressure and adding bovine RBCs to the perfusate on rat liver metabolism in an ex vivo perfusion system. Increasing oxygen delivery enhanced oxygen uptake rate and fluxes through the TCA cycle and electron transport chain, suggesting an upregulation of oxidative phosphorylation and intrahepatic energy production. Concomitantly, we observed increased β-hydroxybutyrate production, and decreased lipogenesis and lactate production, consistent with an upregulation of lipid oxidation pathways and a downregulation of anaerobic glycolysis. We also found that increasing oxygen delivery increased urea cycle fluxes.

Animal-based perfusion systems using hyperoxic oxygen but without oxygen carriers have been extensively used to characterize the hepatic response to various injury models (Arai et al. 2001; Banta et al. 2007; Banta et al. 2005; Lee et al. 2000; Lee et al. 2003). Herein we aimed to analyze the effect of oxygen carriers on perfused liver metabolism, and our results suggest that greater oxygen uptake is achieved in this experimental system. Normothermic liver perfusion systems are being developed as an alternative to cold preservation techniques in the context of liver transplantation, and the perfusates used typically contain oxygen carriers. A better understanding of the metabolic pattern in such systems may be helpful to assess the status of a liver graft before transplantation.

Perfusion parameters critically impact on liver viability and function during ex vivo perfusion. Oxygen delivery is a particularly challenging problem due to the low solubility of oxygen in perfusion media. Supraphysiological flow rates are often used to compensate for that low solubility. For example, Bessems et al. (Bessems et al. 2006) claimed that a flow rate of 3 mL/min/g liver will adequately oxygenate a 10-12 g rat liver as long as the inlet pO_2 is greater than 500 mmHg without using any oxygen carrier. Numerous other studies have used similar flow rates (Arai et al. 2001; Banta et al. 2007; Banta et al. 2005; Lee et al. 2000; Lee et al. 2003). The data presented herein suggest that with a similar flow rate, an inlet pO_2 of ~600 mmHg results in an oxygen uptake rate of ~200 μmol/h/g liver (**Table 5.1** and **Figure 5.3**). In contrast, in vivo measurements show that the rat liver oxygen demand can be up to 400 μmol/h/g liver after experimental burn injury (Izamis et al. 2011). Since more than 90 % of the oxygen available in the perfusate

of the 95% O_2 group was used (**Table 5.1**), it would not possible to ever match this rate without roughly doubling the flow rate, which would likely cause shear stress damage to the liver. This is consistent with other literature data suggesting that hepatic functions (e.g. bile production) and histological appearance are improved when perfusate is supplemented with RBCs or diluted blood (Alexander et al. 1995; Cheung et al. 1996; Rupenko et al. 2008). It is interesting to note, however, that the outlet oxygen partial pressure did not go below ~20 mmHg in any of the groups (**Table 5.1**), and a similar observation was made in vivo (Izamis et al. 2011). Further studies to establish whether or not this represents the lower limit for oxygen extraction by the liver are warranted.

The addition of red blood cells to the perfusate at a hematocrit level of 10% is expected to increase perfusate viscosity by as much as a factor of 2, although in vivo measurements such as those carried out in the classical work of Whittaker & Winton (Whittaker and Winton 1933) show little effect of hematocrit on apparent viscosity at hematocrits below 20%. Since perfusion pressure did not increase significantly (remaining around 15 cm H_2O) with the addition of red blood cells, it is indeed possible that some vasodilation occurred, and one could speculate that it may be due to shear stress induced nitric oxide production (Paniagua et al. 2001). Incidentally red blood cells can carry nitric oxide and the impact on vasoactivity could be propagated throughout the liver. We did not measure nitric oxide production rate or include its metabolism in the network model because the expected flux is too small to impact on the metabolic flux

distribution map. However, this is an intriguing possibility that could explain the increased oxygen consumption observed upon the addition of red blood cells.

Another purpose of this research was to investigate the effect of preexisiting systemic injury (20% TBSA scald burn) on the fasting response of liver in a rat model, as well as to identify metabolic changes in response to burn injury that are sensitive to the feeding state of the animal. The data show that burn injury significantly up-regulated glycine and oxygen uptake as well as urea production irrespective of the feeding status of the animal; however, the increases were more dramatic fasted animals. Interestingly, fasting decreased urea production in sham-burned control animals, but increased it in burned animals. In addition, fasting significantly increased glutamine, arginine, and methionine uptake in burned animals but not in sham-burned controls. Conversely, fasting increased lactate uptake in sham-burned controls but not burned animals. Our flux analysis also determined that gluconeogenesis, glycogenolysis and fatty acid oxidation were active in all conditions. The results suggest that the main substrate for fasting-induced gluconeogenesis in sham-burned controls is lactate, but switches to glutamine and arginine in the burned animals.

Several prior studies have reported on the response of isolated perfused livers (albeit in the absence of oxygen carriers) to a systemic burn injury similar to that applied in the current study evaluated under fasting conditions. The experimental data for fasted animals herein are largely consistent with those of Lee and Banta (Banta et al. 2007; Lee

et al. 2000; Lee et al. 2003). Notably, the uptake of oxygen and lactate, and the production of urea increased while net glucose output and glutamine utilization did not change. However, in these studies, RBCs were not used to facilitate the oxygen uptake rate of liver. Our results showed that perfusate with RBCs significantly increased the oxygen uptake rate and ketone body formation when compared to previous observations (Banta et al. 2007; Lee et al. 2000; Lee et al. 2003). On the other hand, in-vivo measurements published by Izamis and co-workers (Izamis et al. 2011) showed lactate and glutamine uptake rates by the liver were insignificant in burn rats which have been fasted prior to perfusion. It should be kept in mind that the liver is not exposed to circulating factors such as insulin, glucagon and other hormones in perfusion system. Moreover, the metabolite concentrations in the circulating system are not constant, which might affect the in-vivo flux-rates in the liver.

Furthermore, we elucidated that fasting further increased the urea production in burn animals, but it slightly down-regulated the urea secretion in sham animals. It is well known that initial response of a healthy body to fasting is the breakdown of liver and muscle glycogen stores to produce glucose required by the body. Consequently, the metabolites are mainly used for glucose production (Orman et al. 2011a), which might reduce urea secretion after a short period of fasting (24 h) in control animals as previously observed (Orman et al. 2010). Typical response of the body to burn injury is accelerated protein breakdown and increased amino acid concentration in the circulation. 24 h fasting might further up-regulate protein catabolism in burn animals. Consequently

this might result in up-regulation of urea production to remove the ammonia (the toxic byproduct of protein catabolism). Moreover, increased amino acids including glutamine (the most abundant free amino acid) and arginine in the circulation of the burn animals further up-regulate the urea production. In addition to continual presence of elevated stress hormones and substrate loads during the inflammation, the persistent intrinsic changes caused by gene expression and enzyme protein levels might also up-regulate the urea metabolism.

Finally, we used our network model and experimental methodologies to identify flux distribution in the liver following the burn injury or CLP. The animals were not fasted and all perfusion experiments were performed by utilizing RBCs in order to eliminate fasting and inadequate oxygenation-related metabolic alterations. Our analysis showed that following the burn injury, gluconeogenic fluxes and glucose production from glycogen were found to be increased whereas these were significantly decreased in SCLP group. Moreover, pathway analysis elucidated that some pathways representing glucose production from glycogen, lactate and aspartate were found to be important. We also identified the pathways where alanine and cysteine are produced from lactate. It was shown that these pathways had highest weight values in burn group whereas they had lowest weight values following the SCLP.

There are also other dominant pathways in all conditions which are generally related to glycogen breakdown (P7), urea and ornithine production from arginine (P4), serine-

glycine interconversion (P2026) and glucose production from glycerol and ketone bodies resulted from fatty acid oxidation (P106764). Attribution of higher weight to P7 indicates a strong relationship between arginine uptake and urea secretion. Nolan and his co-workers (Nolan et al. 2006) also identified that urea and ornithine exchange reactions are important properties of hepatic metabolic network. Liver likely plays a critical role in regulating the serine concentration in the body (De Koning et al. 2003) since it is a precursor for neurotransmitters glycine, and taurine. Ketone bodies are also important metabolites produced by the liver. They reduce proteolysis during periods of glucose deficiency, and stimulate insulin release (Laffel 1999). They are also important as alternative energy sources.

Although livers were harvested from animals in a fed state, we measured a net glucose output (as opposed to consumption) and the model predicted glycogen breakdown (as opposed to glycogen synthesis), which is more typical of a fasted pattern. These findings are in fact similar to that reported in a prior study using perfused livers isolated from fed rats (Orman et al. 2010). A plausible explanation is that in the perfusion system, the liver is not exposed to circulating factors such as insulin and glucagon that control glucose production and utilization in vivo. Moreover, our analysis showed that the PPP is up-regulated in burn group. The oxidative branch of the PPP produces NADPH, which is used in cells to recycle anti-oxidants and thus may indicate the presence of the oxidative stress caused by burn (Lee et al. 2003). The increased PPP flux in this group is a

significant draw from the glucose 6-phosphate pool and could also explain the increased glycogen breakdown.

5.5 Conclusions

In this study, first we explored a methodology based on elementary mode analysis where thermodynamic as well as other metabolic constraints for the formation of futile cycles are integrated. This "unified" metabolic network analysis that could be simultaneously applied to both fed and fasted states successfully identified internal fluxes and active pathways. This analysis was further used to identify the paths of main metabolites in the hepatic metabolic network and essential extracellular fluxes required to characterize the perfused liver.

Second, this study shows that when perfusing rat livers ex vivo, it is essential to supplement the perfusate with oxygen carriers to meet the oxygen demand of the liver at typical flow rates of 3 mL/min/g liver. When using red blood cells, we found that a 10% hematocrit was adequate to meet the oxygen demand, and livers perfused under these conditions consumed oxygen at in vivo rates. Even when using 95% O_2, in the absence of oxygen carriers, oxygen uptake was only half the in vivo rate, urea and ketone body production were significantly decreased, and pathway analysis suggests that significant anaerobic glycolysis occurred. Conversely, when RBCs were used, glucose production from lactate and glutamate, as well as pathways related to energy metabolism were upregulated. The improved physiological relevance of a perfusion system using oxygen

carriers makes it a more attractive tool to investigate the effect of various perturbations on liver metabolism, including the response to toxicants and drugs, as well as disease conditions known to alter liver metabolism, such as burns and trauma leading to systemic hypermetabolism.

Then we analyzed the effect of fasting on the hepatic metabolic functions in animal groups receiving a 20 % TBSA scald burn or sham-burn treatment. It was revealed that hepatic metabolic response is more complicated in the present of multiple stresses (e.g. burn and fasting together). We observed fasting further up-regulated the urea production and amino acid uptake rates including glutamine, arginine, glycine, and methionine, which have been used for the gluconeogenesis and urea production. On the other hand, not very significant differences were observed between *Sham+Fed* and *Burn+Fed* groups. Altough previous studies concluded that burn injury increased the urea production and gluconeogenic fluxes (Banta et al. 2007; Lee et al. 2000; Lee et al. 2003), these studies were carried out by utilizing fasted animals, and perfusion experiments were performed without using oxygen carriers. However, these might result in misinterpretation of experimental observations analyzed to elucidate burn-induced effects. Our results showed that fasting resulted in distinct metabolic responses in sham and burn animal groups.

Finally, we investigated the effects of burn or CLP on liver metabolism. The animals were sacrificed 24 h following the treatment. They were not fasted and the livers were

perfused with perfusate solutions including RBCs at 10 % Htc. It was observed that burn injury up-regulated gluconeogenic reactions whereas these reactions were significantly down-regulated following the SCLP. Glucose production from glycogen was significantly reduced in SCLP group which indicates depletion of glycogen stores. Burn injury slightly increased the PPP implying burn induced oxidative stress, however PPP flux was found to be very low in CLP group. Moreover, most of pathways in burn and CLP groups had significantly higher weight values compared to other groups.

CHAPTER VI

6 CONCLUDING REMARKS AND FUTURE DIRECTIONS

In this study, a systematic analysis of short term (24 h) local and systemic responses, including the measurements of inflammatory mediators, gene expression and metabolic profiles of liver, in rat models receiving 20% total body surface area (TBSA) scald burn injury or cecal ligation and puncture (CLP) treatment was performed. Consistent with physiological alterations in burn and septic patients characterized by accelerated breakdown of skeletal muscle protein as well as significant alterations in the utilization of amino acids, glucose, fatty acids, and nitrogen balance, similar observations were monitored in our animal models. All animal groups had 100% survival for at least 10 days following treatments. The time course of whole body weight changes was also monitored. CLP caused a ~10% weight loss indicating an accelerated breakdown of skeletal muscle protein. It was found that a certain number of cytokines and chemokines, such as MCP-1, GROK/KC, IL-12, IL-18, and IL-10, were changed following the treatments including SCLP which is a sterile surgical treatment where cecum is not ligated and punctured. This is also consistent with the observations related to abdominal surgeries resulting in systemic inflammation in human. Gene expression analysis also showed that hepatic transcriptional response to burn injury was mainly related to pro-inflammatory and anti-inflammatory gene groups and genes involved in lipid biosynthesis and central carbon metabolism. Shortly after the CLP treatment, genes

related to Toll like receptors and MAPK signaling pathway were significantly up-regulated. Furthermore, perfusion experiments elucidated that hepatic metabolic response to burn injury and CLP was characterized by a significant up-regulation of pathways including gluconeogenic reactions (sources of which are mainly lactate, aspartate, glycerol and glutamine), urea production from arginine, and serine-glycine inter-conversion. On the other hand, weight values of these pathways were significantly decreased following the SCLP treatment.

In order to propose therapeutic approaches to modulate the abnormal inflammatory response, it is essential to analyze the physiological behaviors of important players during the inflammation including circulatory cytokines/chemokines concentrations as well as metabolic and gene expression profiles in the liver controlling the metabolic activity of the body and production of acute phase proteins. Proposing a therapeutic strategy for burn and septic patients by interfering with circulatory inflammatory mediators is quite challenging due to the complex interactions of cytokines or chemokines through a very redundant and interconnected network. Therefore, a comprehensive understanding of the behaviors of inflammatory mediators following various injuries is essential. Unfortunately, the results from experimental researches and clinical trials of immunomodulatory therapies are quite controversial. As suggested by Vincent et al., the timing and dose of these interventions are critical, and single therapy might not be ineffective (Vincent et al. 2002). Moreover, variations in experimental procedures, and size and severity of injuries and utilizing different species might also result in different

outcomes. Holzheimer et al. investigated the relationship between the circadian rhythm and cytokine production (Holzheimer et al. 2002). They showed that cytokines' production was altered by the time of injury. These quantitative and temporal differences in the secretion of endotaxins by the damaged tissues as well as the physiological dynamics of host body result in more complex and unpredictable responses to the injuries. Herein, we used non-lethal animal models which eventually recover from the injuries. Therefore, it can be speculated that the inflammatory response of host body to the injuries should be protective and under control. We have observed that IL-18 and MCP-1 have been significantly up-regulated in our animal groups, which might be essential to induce cell mediated immunity. It has been shown that administration of IL-18 significantly improved the survival rates of animals (Kinoshita et al. 2011). MCP-1 is also known as an important mediator for the development of burn associated type 2 T-cell response (Furukawa et al. 2002). Another interesting observation in this study is that IP-10 and Leptin concentrations were down-regulated in both CLP and SCLP groups. Leptin is playing an important role in regulating energy metabolism and reducing the food intake. Although it has been shown that Leptin reduced elevated tissue associated myeloperoxidase activity in burn animals (ÇakIr et al. 2005), the reason of down-regulation of Leptin in this study may be to reverse the CLP or surgery induced anorexia, which might be a protective response. Similarly, down-regulation of IP-10, a chemo-tactic cytokine, can be also a protective response in order to balance the excessive up-regulation of other chemokines. Anti-Leptin and anti-IP-10 treatment strategies should be further investigated to elucidate their therapeutic effects. Interfering with IL10, IL6,

TNF-alpha cytokines has been relatively disappointing with regard to identifying treatments to improve the survival (Angele and Faist 2002; Blackwell and Christman 1996; Vincent et al. 2002). These cytokines play key roles therefore these treatments may inhibit the host defense functions or result in inadequate inflammatory response. However, administration of a moderate mediator exhibiting both pro and anti inflammatory behaviors (such as IL-12) might balance the system and improve the host immune functions. In our study, IL-12 was observed in burn and CLP models. This cytokine can activate both pro and anti-inflammatory pathways and treatment of burn animals with IL-12 have significantly improved the survival rates in previous studies (Göebel et al. 2000; Osuilleabhain et al. 1996). It is essential to further analyze the effects of these cytokines/chemokines' treatments on the injury models to gain a more comprehensive understanding of these complex physiological changes and to propose medical treatments.

Nutrional supplementation is another approach to eliminate the metabolic stress caused by injuries or infections. It has been previously observed that the hepatic response to severe injury is described by a significant up-regulation of glucose, and amino acid turnover (Lee et al. 2000; Lee et al. 2003; Yarmush et al. 1999) and up-regulation in the expression levels of genes involved in the urea cycle, gluconeogenesis, and the metabolism of several amino acids, with specific transporters for glutamine and arginine (Banta et al. 2007; Vemula et al. 2004). It is also known that burn injury leads to a negative nitrogen balance with accelerated hepatic amino acid metabolism in patients. It

is estimated that 80-90% of urinary nitrogen loss in burn patients occurs as urea (Tredget and Yu 1992). Therefore, glutamine and arginine serving as substrates in urea production might play a critical role (Pan et al. 2004; Pawlik et al. 2000). Arginine and glutamine have already been proposed as a dietary supplement to enhance hepatic functions during catabolic state (Espat et al. 1996). Besides these amino acids, our analysis showed that serine and asparagine are also other important amino acids found to be main sources for the production of urea (Orman et al. 2011a). Moreover, these amino acids as well as lactate are also used for the production of glucose which is needed to maintain a fuel supply required for other organs during the catabolic state. Therefore, these metabolites could be potential nutrients which might be utilized to manipulate biochemical environment in order to reduce physiologic stress caused by burn.

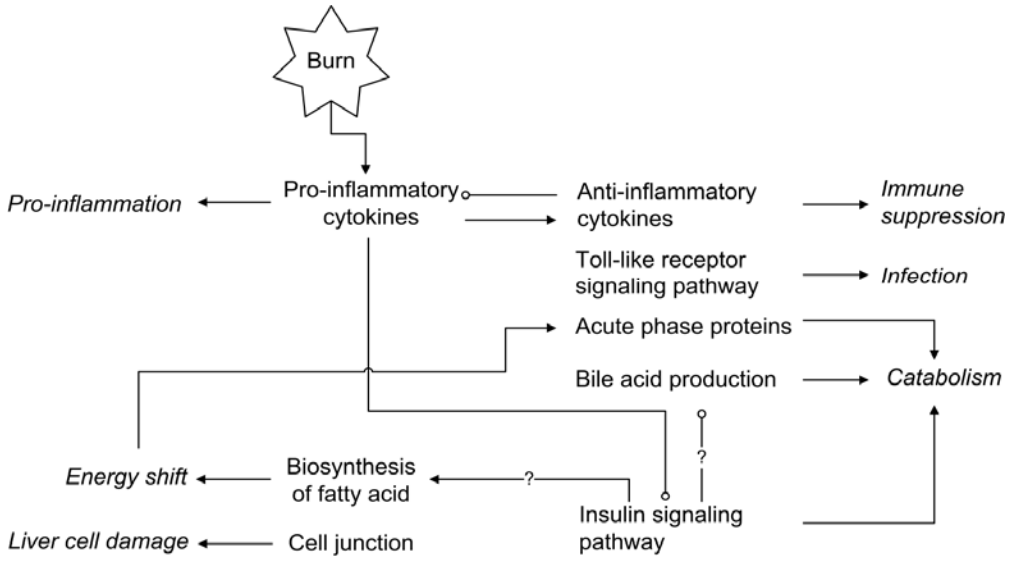

Figure 6.1. Proposed network of changes in the liver following burn injury.
Italics represent outcomes following burn-induced gene expression alterations. Arrows indicate activation and/or induction, and circles indicate inhibition.

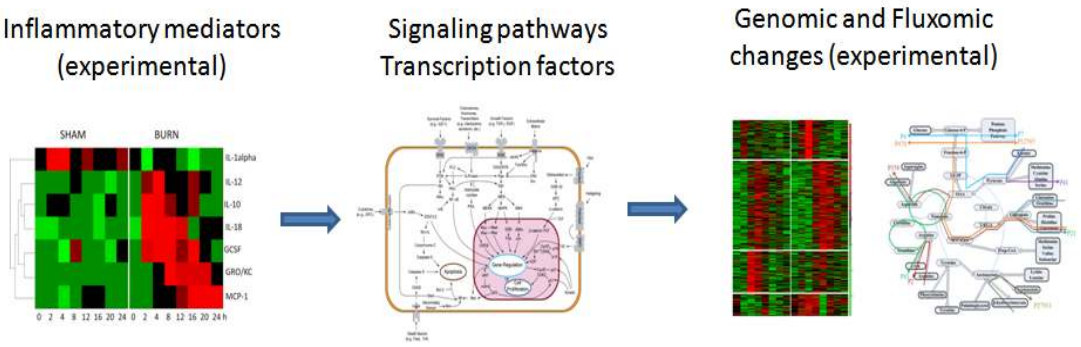

Figure 6.2. Interaction between different systems.

Due to the high interdependency of physiological processes from whole body level to organ level, integrating multiple sources together with the computational methodologies provide an overview of the global regulation in attempt to answer the question to what extend a change in circulatory inflammatory mediators affect the gene expression profiles of a regulatory organ, liver, and to what extend these genomic alterations consequently impact on the metabolic alterations. For example, **Figure 6.1** depicts a network of temporally coordinated changes in the liver in response to burn injury, which has been interpreted from our results. Italics represent outcomes following burn-induced gene expression alterations. Arrows indicate activation and/or induction, and circles indicate inhibition. The early upregulation of pro-inflammatory cytokines and chemokines, and their corresponding receptors in Cluster 1 indicates the activation of the immune system and a pro-inflammatory response. Then, the suppression of fatty acid biosynthesis associated genes in Cluster 2 implies an enhanced energy demand. In Cluster 3, the

downregulation of the genes functioning as cell-cell junctions and providing membrane structural integrity indicate possible damage caused by the injury. Around 8 h following the injury, activation of the expression of well known anti-inflammatory cytokines (including IL-4 and IL-13) may suggest the upcoming immune suppression. The activation of the Toll-like receptor signaling pathway, also in the Cluster 3, has been reported to have a priming effect to a subsequent secondary stimulus, i.e., infection. The most significant feature of Cluster 3 is the enhanced production of positive APPs, which is correlated to hyper-catabolism in muscle. In the same cluster, the enhanced expression of bile acid synthesis related genes may also be an indication of enhanced energy demand from nutrition supply. Finally, the late downregulation of the insulin signaling pathway-associated genes in Cluster 4 leads to the catabolism and insulin resistance. Our model analyzing the metabolic network of liver has already predicted that central carbon metabolism was increased in perfused livers from the animals 24h after being exposed to burn injury. Similarly, a number of cytokines and chemokines were activated in the early stage of 24 h post-injury period, which would affect the signaling network (including MAPK and Toll like receptor signaling pathways) in the liver cells. However, a complete analysis to establish the interactions between these physiological changes at systemic and cellular level is warranted (**Figure 6.2**). This can be achieved by characterizing the possible signaling pathways which have been activated by the inflammatory mediators that have been already monitored. This eventually affects the expression levels of a certain number of genes, consequently the metabolic reaction rates.

APPENDIX: Hepatic Metabolic Network

Reaction no	Enzymes and explanations	Glycolysis & Gluconeogenesis
Reaction 1	Glucose-6-Pase	Glucose-6-P + H2O ==> Glucose + Pi
Reaction 2	Phosphoglucose isomerase	Fructose-6-P <==> Glucose-6-P
Reaction 3	Fructose-1,6-Pase-1	Fructose-1,6-P2 + H2O ==> Fructose-6-P + Pi
Reaction 4	Triose P-isomerase, fructose biphosphate aldolase	2 Glyceraldehyde-3-P <==> Fructose-1,6-P2
Reaction 5	Glyceraldehyde-P dehydrogenase, 3-phosphoglycerate kinase, phosphoglyceromutase, enolase	ATP + NADH + PEP + H+ + H2O <==> Glyceraldehyde-3-P + Pi + NAD+ + ADP
Reaction 6	PEPCK	Oxaloacetate + GTP <==> CO2 + PEP + GDP
Reaction 7	Pyruvate carboxylase	CO2 + ATP + Pyruvate + H2O ==> Pi + ADP + Oxaloacetate
Reaction 8	Hexokinase	Glucose + ATP ==> Glucose-6-P + ADP
Reaction 9	PFK-1	Fructose-6-P + ATP ==> Fructose-1,6-P2 + ADP
Reaction 10	Pyruvate kinase	ADP + PEP ==> ATP + Pyruvate
Reaction 11	PDH	NAD+ + Pyruvate + CoA-SH ==> CO2 + NADH + Acetyl-CoA + H+
		PPP
Reaction 12	Glucose-6-P dehydrogenase and 3 additional steps	Glucose-6-P + 12 NADP+ + 7 H2O ==> 6 CO2 + 12 NADPH + Pi + 12 H+
		Lactate
Reaction 13	Lactate dehydrogenase	NAD+ + Lactate <==> NADH + Pyruvate + H+
		TCA
Reaction 14	Citrate synthase	Oxaloacetate + Acetyl-CoA + H2O ==> Citrate + CoA-SH + H+
Reaction 15	Aconitase, isocitrate dehydrogenase	NAD+ + Citrate <==> CO2 + NADH + a-ketoglutarate
Reaction 16	a-ketoglutarate dehydrogenase	NAD+ + CoA-SH + a-ketoglutarate ==> CO2 + NADH + Succinyl-CoA + H+
Reaction 17	Succinyl-CoA synthase and succinate dehydrogenase	Pi + GDP + Succinyl-CoA + FAD <==> GTP + CoA-SH + Fumarate + FADH2
Reaction 18	Fumarase	Fumarate + H2O <==> Malate
Reaction 19	Malate dehydrogenase	NAD+ + Malate <==> NADH + Oxaloacetate + H+
		Urea
Reaction 20	Arginase	Arginine + H2O ==> Urea + Ornithine
Reaction 21	Carbonate dehydratase, carbamoyl-P synthase, ornithine transcarbamylase	CO2 + 2 ATP + Ornithine + NH4+ + H2O <==> 2 Pi + 2 ADP + Citrulline + 3 H+
Reaction 22	Argininosuccinate synthetase, argininosuccinase.	ATP + Citrulline + Aspartate ==> Fumarate + Arginine + AMP + PPi
		Amino acid metabolism
Reaction 23	Alanine aminotranferase	NAD+ + Alanine + H2O <==> NADH + Pyruvate + NH4+ + H+
Reaction 24	Serine dehydratase	Serine ==> Pyruvate + NH4+
Reaction 25	Transaminase, 3-mercaptopyruvate sulfurtransferase	NAD+ + Cysteine + H2SO3 + H2O <==> NADH + Pyruvate + NH4+ + H2S2O3 + H+
Reaction 26	Threonine 3-dehydrogenase, acetyl-CoA ligase	NAD+ + CoA-SH + Threonine ==> NADH + Acetyl-CoA + Glycine
Reaction 27	Glycine hydroxymethyltranferase, glycine cleavage system	NAD+ + 2 Glycine <==> CO2 + NADH + NH4+ + Serine
Reaction 28	Lysine metabolism (8	5 NAD+ + CoA-SH + FAD + Lysine + 3 H2O ==> 2 CO2 + 5 NADH + FADH2 + 2

	steps)	NH4+ + Acetoacetyl-CoA + 5 H+
Reaction 29	Phenylalanine hydroxylase	Phenylalanine + Tetrahydrobiopterin + O2 ==> Dihydrobiopterin + Tyrosine + H2O
Reaction 30	Tyrosine metabolism (5 steps)	NAD+ + 2 O2 + Tyrosine + H2O ==> CO2 + NADH + Fumarate + NH4+ + H+ + Acetoacetate
Reaction 31	Glutamate dehydrogenase	NAD+ + Glutamate + H2O <==> NADH + a-ketoglutarate + NH4+ + H+
Reaction 32	Glutaminase	Glutamine + H2O ==> NH4+ + Glutamate
Reaction 33	Ornithine metabolism (2 steps)	NADP+ + NAD+ + Ornithine + H2O ==> NADPH + NADH + NH4+ + Glutamate + H+
Reaction 34	Proline oxidase, 1-pyrroline-5-carboxylate dehydrogenase	0.5 NADP+ + 0.5 NAD+ + 0.5 O2 + Proline ==> 0.5 NADPH + 0.5 NADH + Glutamate + H+
Reaction 35	Histidine metabolism (4 steps)	Histidine + THF + 2 H2O ==> NH4+ + Glutamate + 2-formimino-THF
Reaction 36	Methionine metabolism (5 steps)	ATP + NAD+ + CoA-SH + Serine + Methionine ==> CO2 + Pi + NADH + NH4+ + Cysteine + PPi + Adenosine + Propinoyl-CoA
Reaction 37	Propinoyl-CoA carboxylase, Methylmalonyl-CoA epimerase, Methylmalonyl-CoA mutase	CO2 + ATP + Propinoyl-CoA ==> Succinyl-CoA + AMP + PPi
Reaction 38	Aspartate aminotransferase	NAD+ + Aspartate + H2O <==> NADH + Oxaloacetate + NH4+ + H+
Reaction 39	Asparaginase	Asparagine + H2O ==> NH4+ + Aspartate
Reaction 40	Valine metabolism (7 steps)	0.5 NADP+ + 3.5 NAD+ + FAD + 2 H2O + valine ==> 2 CO2 + 0.5 NADPH + 3.5 NADH + FADH2 + NH4+ + Propinoyl-CoA + 3 H+
Reaction 41	Isoleucine Metabolism (6 steps)	0.5 NADP+ + 2.5 NAD+ + FAD + 2 H2O + isoleucine ==> CO2 + 0.5 NADPH + 2.5 NADH + Acetyl-CoA + FADH2 + NH4+ + Propinoyl-CoA + 3 H+
Reaction 42	Leucine Metabolism (6 steps)	0.5 NADP+ + ATP + 1.5 NAD+ + FAD + H2O + leucine ==> 0.5 NADPH + Pi + ADP + 1.5 NADH + Acetyl-CoA + FADH2 + NH4+ + 2 H+ + Acetoacetate
		Lipid
Reaction 43	Hepatic Lipase, Glycerol-3-P dehydrogenase	Palmitoylglycerol + NAD+ + 3 H2O <==> Glyceraldehyde-3-P + 3 Palmitate + NADH + 4 H+
Reaction 44	Fatty acid oxidation (7x4 steps)	ATP + 7 NAD+ + Palmitate + 8 CoA-SH + 7 FAD ==> 2 Pi + 7 NADH + 8 Acetyl-CoA + 7 FADH2 + AMP
Reaction 45	Fatty acid synthesis (7x4 steps)	14 NADPH + 7 ATP + 8 Acetyl-CoA + 14 H+ ==> 14 NADP+ + 7 Pi + Palmitate + 7 ADP + 6 H2O
Reaction 46	Thiolase (Ketogenesis)	2 Acetyl-CoA <==> 2 CoA-SH + Acetoacetyl-CoA
Reaction 47	HMG-CoA synthase and lyase (Ketogenesis)	Acetoacetyl-CoA + H2O ==> CoA-SH + Acetoacetate
Reaction 48	B-OH-butyrate dehydrogenase (Ketogenesis)	NADH + H+ + Acetoacetate <==> NAD+ + B-OH-butyrate
		Glycogen
Reaction 49	Glycogenolysis	Glucose-6-P + ATP + H2O + Glycogen(n-1) ==> ADP + Glycogen
Reaction 50	Glycogenesis	Pi + Glycogen ==> Glucose-6-P + Glycogen(n-1)
		Electron
Reaction 51	Electron transport system	3 ADP + NADH + 0.5 O2 + H+ ==> 3 ATP + NAD+ + H2O
Reaction 52	Electron transport system	2 ADP + FADH2 + 0.5 O2 ==> 2 ATP + FAD + H2O
		Exchange Reactions
Reaction 53		Glycogen <==>
Reaction 54		Palmitoylglycerol <==>
Reaction 55		valine <==>
Reaction 56		isoleucine <==>
Reaction 57		leucine <==>
Reaction 58		Glucose <==>
Reaction 59		Lactate <==>
Reaction 60		Urea <==>
Reaction 61		NH4+ <==>
Reaction 62		Ornithine <==>
Reaction 63		Arginine <==>

Reaction 64		Alanine <==>
Reaction 65		Serine <==>
Reaction 66		Cysteine <==>
Reaction 67		Threonine <==>
Reaction 68		Glycine <==>
Reaction 69		Glutamate <==>
Reaction 70		Glutamine <==>
Reaction 71		Proline <==>
Reaction 72		Histidine <==>
Reaction 73		Methionine <==>

REFERENCES

Abel S, Hundhausen C, Mentlein R, Schulte A, Berkhout TA, Broadway N, Hartmann D, Sedlacek R, Dietrich S, Muetze B and others. 2004. The transmembrane CXC-chemokine ligand 16 is induced by IFN-gamma and TNF-alpha and shed by the activity of the disintegrin-like metalloproteinase ADAM10. J Immunol 172(10):6362-72.

Alexander B, Aslam M, Benjamin IS. 1995. Hepatic function during prolonged isolated rat liver perfusion using a new miniaturized perfusion circuit. Journal of Pharmacological and Toxicological Methods 34(4):203-210.

Almon RR, Yang E, Lai W, Androulakis IP, DuBois DC, Jusko WJ. 2008. Circadian variations in rat liver gene expression: relationships to drug actions. J Pharmacol Exp Ther 326(3):700-16.

Andrejko KM, Chen JD, Deutschman CS. 1998. Intrahepatic STAT-3 activation and acute phase gene expression predict outcome after CLP sepsis in the rat. American Journal of Physiology-Gastrointestinal and Liver Physiology 275(6):G1423-G1429.

Angele M, Faist E. 2002. Clinical review: Immunodepression in the surgical patient and increased susceptibility to infection. Critical Care 6(4):298 - 305.

Antoniewicz MR, Kelleher JK, Stephanopoulos G. 2007. Elementary metabolite units (EMU): A novel framework for modeling isotopic distributions. Metabolic Engineering 9(1):68-86.

Arai K, Lee K, Berthiaume F, Tompkins RG, Yarmush ML. 2001. Intrahepatic amino acid and glucose metabolism in a D-galactosamine-induced rat liver failure model. Hepatology 34(2):360-371.

Arend WP, Palmer G, Gabay C. 2008. IL-1, IL-18, and IL-33 families of cytokines. Immunological Reviews 223:20-38.

Baes M, Huyghe S, Carmeliet P, Declercq PE, Collen D, Mannaerts GP, Van Veldhoven PP. 2000. Inactivation of the peroxisomal multifunctional protein-2 in mice impedes the degradation of not only 2-methyl-branched fatty acids and bile acid intermediates but also of very long chain fatty acids. J Biol Chem 275(21):16329-36.

Banta S, Vemula M, Yokoyama T, Jayaraman A, Berthiaume F, Yarmush ML. 2007. Contribution of gene expression to metabolic fluxes in hypermetabolic livers induced through burn injury and cecal ligation and puncture in rats. Biotechnology and Bioengineering 97(1):118-137.

Banta S, Yokoyama T, Berthiaume F, Yarmush ML. 2005. Effects of dehydroepiandrosterone administration on rat hepatic metabolism following thermal injury. Journal of Surgical Research 127(2):93-105.

Barber RC, Maass DL, White DJ, Horton JW. 2008. Increasing percent burn is correlated with increasing inflammation in an adult rodent model. Shock 30(4):388-393.

Bartz F, Kern L, Erz D, Zhu M, Gilbert D, Meinhof T, Wirkner U, Erfle H, Muckenthaler M, Pepperkok R and others. 2009. Identification of cholesterol-regulating genes by targeted RNAi screening. Cell Metab 10(1):63-75.

Beal AL, Cerra FB. 1994. Multiple Organ Failure Syndrome in the 1990s - Systemic Inflammatory Response and Organ Dysfunction. Jama-Journal of the American Medical Association 271(3):226-233.

Beard DA, Qian H. 2005. Thermodynamic-based computational profiling of cellular regulatory control in hepatocyte metabolism. American Journal of Physiology-Endocrinology and Metabolism 288(3):E633-E644.

Benjamini Y, Hochberg Y. 1995. CONTROLLING THE FALSE DISCOVERY RATE - A PRACTICAL AND POWERFUL APPROACH TO MULTIPLE TESTING. Journal of the Royal Statistical Society Series B-Methodological 57(1):289-300.

Berndorff D, Gessner R, Kreft B, Schnoy N, Lajous-Petter AM, Loch N, Reutter W, Hortsch M, Tauber R. 1994. Liver-intestine cadherin: molecular cloning and characterization of a novel Ca(2+)-dependent cell adhesion molecule expressed in liver and intestine. J Cell Biol 125(6):1353-69.

Bessems M, t'Hart NA, Tolba R, Doorschodt BM, D Leuvenink HG, Ploeg RJ, Minor T, van Gulik TM. 2006. The isolated perfused rat liver: standardization of a time-honoured model. Laboratory Animals 40(3):236-246.

Bessey PQ, Jiang ZM, Johnson DJ, Smith RJ, Wilmore DW. 1989. Posttraumatic Skeletal-Muscle Proteolysis - the Role of the Hormonal Environment. World Journal of Surgery 13(4):465-471.

Bjarnason I, MacPherson A, Hollander D. 1995. Intestinal permeability: an overview. Gastroenterology 108(5):1566-81.

Blackwell TS, Christman JW. 1996. Sepsis and cytokines: Current status. British Journal of Anaesthesia 77(1):110-117.

Boghigian B, Shi H, Lee K, Pfeifer B. 2010. Utilizing elementary mode analysis, pathway thermodynamics, and a genetic algorithm for metabolic flux determination and optimal metabolic network design. BMC Systems Biology 4(1):49.

Bohn E, Sing A, Zumbihl R, Bielfeldt C, Okamura H, Kurimoto M, Heesemann J, Autenrieth IB. 1998. IL-18 (IFN-gamma-inducing factor) regulates early cytokine production in, and promotes resolution of, bacterial infection in mice. Journal of Immunology 160(1):299-307.

Bonarius HPJ, Özemre A, Timmerarends B, Skrabal P, Tramper J, Schmid G, Heinzle E. 2001. Metabolic-flux analysis of continuously cultured hybridoma cells using 13CO2 mass spectrometry in combination with 13C-lactate nuclear magnetic resonance spectroscopy and metabolite balancing. Biotechnology and Bioengineering 74(6):528-538.

Bonarius HPJ, Timmerarends B, de Gooijer CD, Tramper J. 1998. Metabolite-balancing techniques vs. 13C tracer experiments to determine metabolic fluxes in hybridoma cells. Biotechnology and Bioengineering 58(2-3):258-262.

ÇakIr B, Çevik H, Contuk G, Ercan F, Eksioglu-Demiralp E, Yegen BÇ. 2005. Leptin ameliorates burn-induced multiple organ damage and modulates postburn immune response in rats. Regulatory Peptides 125(1-3):135-144.

Cakir T, Tacer CS, Ulgen KO. 2004. Metabolic pathway analysis of enzyme-deficient human red blood cells. Biosystems 78(1-3):49-67.

Çalik P, Akbay A. 2000. Mass flux balance-based model and metabolic flux analysis for collagen synthesis in the fibrogenesis process of human liver. Medical Hypotheses 55(1):5-14.

Cannon JG, Friedberg JS, Gelfand JA, Tompkins RG, Burke JF, Dinarello CA. 1992. Circulating Interleukin-1-Beta and Tumor Necrosis Factor-Beta Concentrations after Burn Injury in Humans. Critical Care Medicine 20(10):1414-1419.

Carninci P, Kasukawa T, Katayama S, Gough J, Frith MC, Maeda N, Oyama R, Ravasi T, Lenhard B, Wells C and others. 2005. The transcriptional landscape of the mammalian genome. Science 309(5740):1559-63.

Chan C, Berthiaume F, Lee K, Yarmush ML. 2003. Metabolic flux analysis of cultured hepatocytes exposed to plasma. Biotechnology and Bioengineering 81(1):33-49.

Chan MM, Chan GM. 2009. Nutritional therapy for burns in children and adults. Nutrition 25(3):261-269.

Charo IF, Ransohoff RM. 2006. Mechanisms of disease - The many roles of chemokines and chemokine receptors in inflammation. New England Journal of Medicine 354(6):610-621.

Cheung K, Hickman PE, Potter JM, Walker NI, Jericho M, Haslam R, Roberts MS. 1996. An Optimized Model for Rat Liver Perfusion Studies. Journal of Surgical Research 66(1):81-89.

Chinnaiyan AM, Huber-Lang M, Kumar-Sinha C, Barrette TR, Shankar-Sinha S, Sarma VJ, Padgaonkar VA, Ward PA. 2001. Molecular signatures of sepsis: multiorgan gene expression profiles of systemic inflammation. Am J Pathol 159(4):1199-209.

Cho K, Adamson LK, Jeong J, Crivello SD, Vanhook TG, Palmieri T, Greenhalgh DG. 2004a. CD14-dependent alterations in c-Jun expression in the liver after burn injury. Journal of Surgical Research 122(1):36-42.

Cho K, Pham TN, Crivello SD, Jeong J, Green TL, Greenhalgh DG. 2004b. Involvement of CD14 and toll-like receptor 4 in the acute phase response of serum amyloid a proteins and serum amyloid P component in the liver after burn injury. Shock 21(2):144-150.

Christensen B, Nielsen J. 2000. Metabolic Network Analysis. In: Sonnleitner B, editor. Bioanalysis and Biosensors for Bioprocess Monitoring: Springer Berlin / Heidelberg. p 209-231.

Church D, Elsayed S, Reid O, Winston B, Lindsay R. 2006. Burn wound infections. Clinical Microbiology Reviews 19(2):403-+.

Cobb JP, Mindrinos MN, Miller-Graziano C, Calvano SE, Baker HV, Xiao W, Laudanski K, Brownstein BH, Elson CM, Hayden DL and others. 2005. Application of genome-wide expression analysis to human health and disease. Proc Natl Acad Sci U S A 102(13):4801-6.

Correa SG, Maccioni M, Rivero VE, Iribarren P, Sotomayor CE, Riera CM. 2007. Cytokines and the immune-neuroendocrine network: What did we learn from infection and autoimmunity? Cytokine & Growth Factor Reviews 18(1-2):125-134.

Covert MW, Palsson BO. 2002. Transcriptional regulation in constraints-based metabolic models of Escherichia coli. Journal of Biological Chemistry 277(31):28058-28064.

Covert MW, Schilling CH, Palsson B. 2001. Regulation of gene expression in flux balance models of metabolism. Journal of Theoretical Biology 213(1):73-88.

Damas P, Canivet JL, DeGroote D, Vrindts Y, Albert A, Franchimont P, Lamy M. 1997. Sepsis and serum cytokine concentrations. Critical Care Medicine 25(3):405-412.

Dasu MRK, Cobb JP, Laramie JM, Chung TP, Spies M, Barrow RE. 2004. Gene expression profiles of livers from thermally injured rats. Gene 327(1):51-60.

Dauner M. 2010. From fluxes and isotope labeling patterns towards in silico cells. Current Opinion in Biotechnology 21(1):55-62.

De Koning TJ, Snell K, Duran M, Berger R, Poll-The BT, Surtees R. 2003. L-serine in disease and development. Biochemical Journal 371:653-661.

Debandt JP, Cholletmartin S, Hernvann A, Lioret N, Duroure LD, Lim SK, Vaubourdolle M, Guechot J, Saizy R, Giboudeau J and others. 1994. Cytokine Response to Burn Injury - Relationship with Protein-Metabolism. Journal of Trauma-Injury Infection and Critical Care 36(5):624-628.

Dehne MG, Sablotzki A, Hoffmann A, Muhling J, Dietrich FE, Hempelmann G. 2002. Alterations of acute phase reaction and cytokine production in patients following severe burn injury. Burns 28(6):535-542.

Dinarello CA. 1989. Interleukin-1 and its biologically related cytokines. Adv Immunol 44:153-205.

Dong B, Zhou Q, Zhao J, Zhou A, Harty RN, Bose S, Banerjee A, Slee R, Guenther J, Williams BR and others. 2004. Phospholipid scramblase 1 potentiates the antiviral activity of interferon. J Virol 78(17):8983-93.

Doniger SW, Huh J, Fay JC. 2005. Identification of functional transcription factor binding sites using closely related Saccharomyces species. Genome Res 15(5):701-9.

Drost AC, Burleson DG, Cioffi WG, Jr., Jordan BS, Mason AD, Jr., Pruitt BA, Jr. 1993a. Plasma cytokines following thermal injury and their relationship with patient mortality, burn size, and time postburn. J Trauma 35(3):335-9.

Drost AC, Burleson DG, Cioffi WG, Mason AD, Pruitt BA. 1993b. Plasma Cytokines after Thermal-Injury and Their Relationship to Infection. Annals of Surgery 218(1):74-78.

Duntas LH. 2009. Selenium and inflammation: underlying anti-inflammatory mechanisms. Horm Metab Res 41(6):443-7.

Ertel W, Morrison MH, Wang P, Ba ZF, Ayala A, Chaudry IH. 1991. The Complex Pattern of Cytokines in Sepsis - Association between Prostaglandins, Cachectin, and Interleukins. Annals of Surgery 214(2):141-148.

Espat NJ, Watkins KT, Lind DS, Weis JK, Copeland EM, Souba WW. 1996. Dietary Modulation of Amino Acid Transport in Rat and Human Liver. Journal of Surgical Research 63(1):263-268.

Evers LH, Bhavsar D, Mailander P. 2010. The biology of burn injury. Experimental Dermatology 19(9):777-783.

Fang CW, Yao YM, Shi ZG, Yu Y, Wu Y, Lu LR, Sheng ZY. 2002. Lipopolysaccharide-binding protein and lipopolysaccharide receptor CD14 gene expression after thermal injury and its potential mechanism(s). J Trauma 53(5):957-67.

Fantuzzi G, Faggioni R. 2000. Leptin in the regulation of immunity, inflammation, and hematopoiesis. Journal of Leukocyte Biology 68(4):437-446.

Feezor RJ, Cheng A, Paddock HN, Baker HV, Moldawer LL. 2005. Functional Genomics and Gene Expression Profiling in Sepsis: Beyond Class Prediction. Clinical Infectious Diseases 41(Supplement 7):S427-S435.

Feterowski C, Mack M, Weighardt H, Bartsch B, Kaiser-Moore S, Holzmann B. 2004. CC chemokine receptor 2 regulates leukocyte recruitment and IL-10 production during acute polymicrobial sepsis. European Journal of Immunology 34(12):3664-3673.

Finnerty CC, Herndon DN, Przkora R, Pereira CT, Oliveira HM, Queiroz DMM, Rocha AMC, Jeschke MG. 2006. Cytokine expression profile over time in severely burned pediatric patients. Shock 26(1):13-19.

Finnerty CC, Przkora R, Herndon DN, Jeschke MG. 2009. Cytokine expression profile over time in burned mice. Cytokine 45(1):20-25.

Flo TH, Smith KD, Sato S, Rodriguez DJ, Holmes MA, Strong RK, Akira S, Aderem A. 2004. Lipocalin 2 mediates an innate immune response to bacterial infection by sequestrating iron. Nature 432(7019):917-21.

Foteinou PT, Yang E, Androulakis IP. 2009. Networks, biology and systems engineering: A case study in inflammation. Computers & Chemical Engineering 33(12):2028-2041.

Furukawa K, Kobayashi M, Herndon DN, Pollard RB, Suzuki F. 2002. Appearance of monocyte chemoattractant protein 1 (MCP-1) early after thermal injury - Role in the subsequent development of burn-associated type 2 T-cell responses. Annals of Surgery 236(1):112-119.

Gabay C, Kushner I. 1999. Acute-phase proteins and other systemic responses to inflammation. N Engl J Med 340(6):448-54.

Gallant S, Gilkeson G. 2006. ETS transcription factors and regulation of immunity. Archivum Immunologiae et Therapiae Experimentalis 54(3):149-163.

Gauglitz GG, Halder S, Boehning DF, Kulp GA, Herndon DN, Barral JM, Jeschke MG. 2009. Post-Burn Hepatic Insulin Resistance Is Associated with Er Stress. Shock.

Gauglitz GG, Song J, Herndon DN, Finnerty CC, Boehning D, Barral JM, Jeschke MG. 2008. Characterization of the Inflammatory Response During Acute and Post-Acute Phases after Severe Burn. Shock 30(5):503-507.

Gee K, Lim W, Ma W, Nandan D, Diaz-Mitoma F, Kozlowski M, Kumar A. 2002. Differential regulation of CD44 expression by lipopolysaccharide (LPS) and

TNF-alpha in human monocytic cells: distinct involvement of c-Jun N-terminal kinase in LPS-induced CD44 expression. J Immunol 169(10):5660-72.

Genomatix. http://www.genomatix.de.

Ghielmetti M, Bellis M, Spycher MO, Miescher S, Vergeres G. 2006. Gene expression profiling of the effects of intravenous immunoglobulin in human whole blood. Mol Immunol 43(7):939-49.

Göebel A, Kavanagh E, Lyons A, Saporoschetz IB, Soberg C, Lederer JA, Mannick JA, Rodrick ML. 2000. Injury Induces Deficient Interleukin-12 Production, But Interleukin-12 Therapy After Injury Restores Resistance to Infection. Annals of Surgery 231(2):253-261.

Gosain A, Gamelli RL. 2005. Role of the gastrointestinal tract in burn sepsis. Journal of Burn Care & Rehabilitation 26(1):85-91.

Goudar C, Biener R, Boisart C, Heidemann R, Piret J, de Graaf A, Konstantinov K. 2010. Metabolic flux analysis of CHO cells in perfusion culture by metabolite balancing and 2D [13C, 1H] COSY NMR spectroscopy. Metabolic Engineering 12(2):138-149.

Haimovich B, Calvano J, Haimovich AD, Calvano SE, Coyle SM, Lowry SF. 2010. In vivo endotoxin synchronizes and suppresses clock gene expression in human peripheral blood leukocytes. Crit Care Med 38(3):751-8.

Hardison RC. 2000. Conserved noncoding sequences are reliable guides to regulatory elements. Trends Genet 16(9):369-72.

Hasselgren PO, Pedersen P, Sax HC, Warner BW, Fischer JE. 1988. Current concepts of protein turnover and amino acid transport in liver and skeletal muscle during sepsis. Arch Surg 123(8):992-9.

Heideman M, Bengtsson A. 1992. The Immunological Response to Thermal-Injury. World Journal of Surgery 16(1):53-56.

Heino J, Tunyan K, Calvetti D, Somersalo E. 2007. Bayesian flux balance analysis applied to a skeletal muscle metabolic model. Journal of Theoretical Biology 248(1):91-110.

Heinzl H. 1996. A note on testing areas under the curve when using destructive measurement techniques. Journal of Pharmacokinetics and Pharmacodynamics 24(6):651-655.

Helenius A, Aebi M. 2001. Intracellular functions of N-linked glycans. Science 291(5512):2364-9.

Herndon DN, Wilmore DW, Mason JAD. 1978. Development and analysis of a small animal model simulating the human postburn hypermetabolic response. Journal of Surgical Research 25(5):394-403.

Holzheimer RG, Curley P, Saporoschetz IB, Doherty JM, Mannick JA, Rodrick ML. 2002. Circadian Rhythm of Cytokine Secretion Following Thermal Injury in Mice: Implications for Burn and Trauma Research. Shock 17(6):527-529.

Ibarra RU, Edwards JS, Palsson BO. 2002. Escherichia coli K-12 undergoes adaptive evolution to achieve in silico predicted optimal growth. Nature 420(6912):186-189.

Iyer VV, Ovacik MA, Androulakis IP, Roth CM, Ierapetritou MG. 2010a. Transcriptional and metabolic flux profiling of triadimefon effects on cultured hepatocytes. Toxicology and Applied Pharmacology 248(3):165-177.

Iyer VV, Yang H, Ierapetritou MG, Roth CM. 2010b. Effects of glucose and insulin on HepG2-C3A cell metabolism. Biotechnology and Bioengineering 107(2):347-356.

Izamis M-L, Sharma NS, Uygun B, Bieganski R, Saeidi N, Nahmias Y, Uygun K, Yarmush ML, Berthiaume F. 2011. In situ metabolic flux analysis to quantify the liver metabolic response to experimental burn injury. Biotechnology and Bioengineering 108(4):839-852.

Jayaraman A, Maguire T, Vemula M, Kwon DW, Vannucci M, Berthiaume F, Yarmush ML. 2009. Gene Expression Profiling of Long-Term Changes in Rat Liver Following Burn Injury. Journal of Surgical Research 152(1):3-17.

Jayaraman A, Yarmush ML, Roth CM. 2005. Evaluation of an in vitro model of hepatic inflammatory response by gene expression profiling. Tissue Engineering 11(1-2):50-63.

Jeong J, Adamson LK, Hatam R, Greenhalgh DG, Cho K. 2003. Alterations in the expression and modification of histones in the liver after injury. Experimental and Molecular Pathology 75(3):256-264.

Jeschke MG, Mlcak RP, Finnerty CC, Norbury WB, Gauglitz GG, Kulp GA, Herndon DN. 2007. Burn size determines the inflammatory and hypermetabolic response. Critical Care 11(4).

Jesmin S, Gando S, Zaedi S, Sakuraya F. 2006. Chronological expression of PAR isoforms in acute liver injury and its amelioration by PAR2 blockade in a rat model of sepsis. Thrombosis and Haemostasis 96(6):830-838.

Jung UJ, Lee MK, Park YB, Jeon SM, Choi MS. 2006. Antihyperglycemic and antioxidant properties of caffeic acid in db/db mice. J Pharmacol Exp Ther 318(2):476-83.

Kataranovski M, Magic Z, Pejnovic N. 1999. Early inflammatory cytokine and acute phase protein response under the stress of thermal injury in rats. Physiol Res 48(6):473-82.

Kauffman KJ, Prakash P, Edwards JS. 2003. Advances in flux balance analysis. Current Opinion in Biotechnology 14(5):491-496.

Keller M, Mazuch J, Abraham U, Eom GD, Herzog ED, Volk HD, Kramer A, Maier B. 2009. A circadian clock in macrophages controls inflammatory immune responses. Proceedings of the National Academy of Sciences of the United States of America 106(50):21407-21412.

Kelly-Scumpia KM, Scumpia PO, Delano MJ, Weinstein JS, Cuenca AG, Wynn JL, Moldawer LL. Type I interferon signaling in hematopoietic cells is required for survival in mouse polymicrobial sepsis by regulating CXCL10. J Exp Med 207(2):319-26.

Kelly JL, O'Suilleabhain CB, Soberg CC, Mannick JA, Lederer JA. 1999. Severe injury triggers antigen-specific T-helper cell dysfunction. Shock 12(1):39-45.

Kim HK, Kim JE, Chung J, Han KS, Cho HI. 2007. Surface expression of neutrophil CXCR4 is down-modulated by bacterial endotoxin. Int J Hematol 85(5):390-6.

King KR, Wang S, Irimia D, Jayaraman A, Toner M, Yarmush ML. 2007. A high-throughput microfluidic real-time gene expression living cell array. Lab Chip 7(1):77-85.

Kinoshita M, Miyazaki H, Ono S, Inatsu A, Nakashima H, Tsujimoto H, Shinomiya N, Saitoh D, Seki S. 2011. Enhancement of neutrophil function by IL-18 therapy protects burn-injured mice from MRSA infection. Infect. Immun.:IAI.01298-10.

Klamt S, Saez-Rodriguez J, Gilles ED. 2007. Structural and functional analysis of cellular networks with CellNetAnalyzer. Bmc Systems Biology 1.

Klamt S, Stelling J. 2003. Two approaches for metabolic pathway analysis? Trends in Biotechnology 21(2):64-69.

Klein A, Amigo L, Retamal MJ, Morales MG, Miquel JF, Rigotti A, Zanlungo S. 2006. NPC2 is expressed in human and murine liver and secreted into bile: potential implications for body cholesterol homeostasis. Hepatology 43(1):126-33.

Klein D, Einspanier R, Bolder U, Jeschke MG. 2003. Differences in the hepatic signal transcription pathway and cytokine expression between thermal injury and sepsis. Shock 20(6):536-543.

Kyriakis JM, Avruch J. 2001. Mammalian mitogen-activated protein kinase signal transduction pathways activated by stress and inflammation. Physiol Rev 81(2):807-69.

Kyrmizi I, Hatzis P, Katrakili N, Tronche F, Gonzalez FJ, Talianidis I. 2006. Plasticity and expanding complexity of the hepatic transcription factor network during liver development. Genes Dev 20(16):2293-305.

Laffel L. 1999. Ketone bodies: a review of physiology, pathophysiology and application of monitoring to diabetes. Diabetes-Metabolism Research and Reviews 15(6):412-426.

Lauw FN, Dekkers PEP, te Velde AA, Speelman P, Levi M, Kurimoto M, Hack CE, van Deventer SJH, van der Poll T. 1999. Interleukin-12 induces sustained activation of multiple host inflammatory mediator systems in chimpanzees. Journal of Infectious Diseases 179(3):646-652.

Lederer JA, Rodrick ML, Mannick JA. 1999. The effects of injury on the adaptive immune response. Shock 11(3):153-9.

Lee K, Berthiaume F, Stephanopoulos GN, Yarmush DM, Yarmush ML. 2000. Metabolic Flux Analysis of Postburn Hepatic Hypermetabolism. Metabolic Engineering 2(4):312-327.

Lee K, Berthiaume F, Stephanopoulos GN, Yarmush ML. 2003. Profiling of dynamic changes in hypermetabolic livers. Biotechnology and Bioengineering 83(4):400-415.

Leek JT, Monsen E, Dabney AR, Storey JD. 2006. EDGE: extraction and analysis of differential gene expression. Bioinformatics 22(4):507-8.

Li C, Wong WH. 2001. Model-based analysis of oligonucleotide arrays: expression index computation and outlier detection. Proc Natl Acad Sci U S A 98(1):31-6.

Li ZJ, Li YP, Gai HR, Xue YL, Feng XZ. 2007. [Research of gene expression profile of liver tissue in rat sepsis model]. Zhongguo Wei Zhong Bing Ji Jiu Yi Xue 19(3):156-9.

Lin E, Calvano SE, Lowry SF. 2000. Inflammatory cytokines and cell response in surgery. Surgery 127(2):117-126.

Litvak V, Ramsey SA, Rust AG, Zak DE, Kennedy KA, Lampano AE, Nykter M, Shmulevich I, Aderem A. 2009. Function of C/EBPdelta in a regulatory circuit that discriminates between transient and persistent TLR4-induced signals. Nat Immunol 10(4):437-43.

Llaneras F, Picó J. 2007. An interval approach for dealing with flux distributions and elementary modes activity patterns. Journal of Theoretical Biology 246(2):290-308.

Maejima K, Deitch E, Berg R. 1984. Promotion by burn stress of the translocation of bacteria from the gastrointestinal tracts of mice. Arch Surg 119(2):166-72.

Maier K, Hofmann U, Bauer A, Niebel A, Vacun G, Reuss M, Mauch K. 2009. Quantification of statin effects on hepatic cholesterol synthesis by transient 13C-flux analysis. Metabolic Engineering 11(4-5):292-309.

Maier K, Hofmann U, Reuss M, Mauch K. 2008. Identification of metabolic fluxes in hepatic cells from transient 13C-labeling experiments: Part II. Flux estimation. Biotechnology and Bioengineering 100(2):355-370.

Marshall JD, Aste-Amezaga M, Chehimi SS, Murphy M, Olsen H, Trinchieri G. 1999. Regulation of human IL-18 mRNA expression. Clinical Immunology 90(1):15-21.

Martens DE. 2007. Metabolic Flux Analysis of Mammalian Cells. In: Al-Rubeai M, Fussenegger M, editors. Systems Biology: Springer Netherlands. p 275-299.

Masaki T, Chiba S, Tatsukawa H, Noguchi H, Kakuma T, Endo M, Seike M, Watanabe T, Yoshimatsu H. 2005. The role of histamine H-1 receptor and H-2 receptor in LPS-induced liver injury. Faseb Journal 19(10):1245-1252.

Maskow T, von Stockar U. 2005. How reliable are thermodynamic feasibility statements of biochemical pathways? Biotechnology and Bioengineering 92(2):223-230.

Matsuda M, Yamashita JK, Tsukita S, Furuse M. abLIM3 is a novel component of adherens junctions with actin-binding activity. Eur J Cell Biol 89(11):807-16.

Mester M, Carter EA, Tompkins RG, Gelfand JA, Dinarello CA, Burke JF, Clark BD. 1994. Thermal injury induces very early production of interleukin-1 alpha in the rat by mechanisms other than endotoxemia. Surgery 115(5):588-96.

Metallo CM, Walther JL, Stephanopoulos G. 2009. Evaluation of 13C isotopic tracers for metabolic flux analysis in mammalian cells. Journal of Biotechnology 144(3):167-174.

Mizock BA. 1995. Alterations in Carbohydrate-Metabolism During Stress - a Review of the Literature. American Journal of Medicine 98(1):75-84.

Moran K, Munster AM. 1987. Alterations of the host defense mechanism in burned patients. Surg Clin North Am 67(1):47-56.

Motamed-Khorasani A, Jurisica I, Letarte M, Shaw PA, Parkes RK, Zhang X, Evangelou A, Rosen B, Murphy KJ, Brown TJ. 2007. Differentially androgen-modulated genes in ovarian epithelial cells from BRCA mutation carriers and control patients predict ovarian cancer survival and disease progression. Oncogene 26(2):198-214.

Munger J, Bennett BD, Parikh A, Feng X-J, McArdle J, Rabitz HA, Shenk T, Rabinowitz JD. 2008. Systems-level metabolic flux profiling identifies fatty acid synthesis as a target for antiviral therapy. Nat Biotech 26(10):1179-1186.

Murphy TJ, Paterson HM, Kriynovich S, Zang Y, Kurt-Jones EA, Mannick JA, Lederer JA. 2005. Linking the "two-hit" response following injury to enhanced TLR4 reactivity. Journal of Leukocyte Biology 77(1):16-23.

Nadler EP, Ford HR. 2000. Regulation of bacterial translocation by nitric oxide. Pediatric Surgery International 16(3):165-168.

Nagrath D, Avila-Elchiver M, Berthiaume F, Tilles A, Messac A, Yarmush M. 2007. Integrated Energy and Flux Balance Based Multiobjective Framework for Large-Scale Metabolic Networks. Annals of Biomedical Engineering 35(6):863-885.

Nagrath D, Avila-Elchiver M, Berthiaume F, Tilles AW, Messac A, Yarmush ML. 2010. Soft constraints-based multiobjective framework for flux balance analysis. Metabolic Engineering 12(5):429-445.

Ness TL, Carpenter KJ, Ewing JL, Gerard CJ, Hogaboam CM, Kunkel SL. 2004. CCR1 and CC chemokine ligand 5 interactions exacerbate innate immune responses during sepsis. Journal of Immunology 173(11):6938-6948.

Ness TL, Hogaboam CM, Strieter RM, Kunkel SL. 2003. Immunomodulatory role of CXCR2 during experimental septic peritonitis. J Immunol 171(7):3775-84.

Nguyen TT, Nowakowski RS, Androulakis IP. 2009. Unsupervised selection of highly coexpressed and noncoexpressed genes using a consensus clustering approach. Omics 13(3):219-37.

Niklas J, Schneider K, Heinzle E. 2010. Metabolic flux analysis in eukaryotes. Current Opinion in Biotechnology 21(1):63-69.

Nishiura T, Nishimura T, deSerres S, Godfrey V, Bradham CA, Nakagawa T, Brenner DA, Meyer AA. 2000. Gene expression and cytokine and enzyme activation in the liver after a burn injury. Journal of Burn Care & Rehabilitation 21(2):135-141.

Nolan RP, Fenley AP, Lee K. 2006. Identification of distributed metabolic objectives in the hypermetabolic liver by flux and energy balance analysis. Metabolic Engineering 8(1):30-45.

Nookaew I, Meechai A, Thammarongtham C, Laoteng K, Ruanglek V, Cheevadhanarak S, Nielsen J, Bhumiratana S. 2007. Identification of flux regulation coefficients from elementary flux modes: A systems biology tool for analysis of metabolic networks. Biotechnology and Bioengineering 97(6):1535-1549.

Obrzut S, Tiongson J, Jamshidi N, Phan H, Hoh C, Birgersdotter-Green U. 2010. Assessment of Metabolic Phenotypes in Patients with Non-ischemic Dilated Cardiomyopathy Undergoing Cardiac Resynchronization Therapy. Journal of Cardiovascular Translational Research 3(6):643-651.

Ogle CK, Kong FS, Guo XL, Wells DA, Aosasa S, Noel G, Horseman N. 2000. The effect of burn injury on suppressors of cytokine signalling. Shock 14(3):392-398.

Olofsson P, Nylander G, Olsson P. 1985. Endotoxin - Transport Routes and Kinetics in Intestinal Ischemia. Acta Chirurgica Scandinavica 151(7):635-639.

Olofsson P, Nylander G, Olsson P. 1986. Endotoxin - Routes of Transport in Experimental Peritonitis. American Journal of Surgery 151(4):443-447.

Ono I, Gunji H, Zhang JZ, Maruyama K, Kaneko F. 1995. A Study of Cytokines in Burn Blister Fluid Related to Wound-Healing. Burns 21(5):352-355.

Opal SM, DePalo VA. 2000. Anti-inflammatory cytokines. Chest 117(4):1162-1172.

Orman MA, Arai K, Yarmush ML, Androulakis IP, Berthiaume F, Ierapetritou MG. 2010. Metabolic Flux Determination in Perfused Livers by Mass Balance Analysis: Effect of Fasting. Biotechnology and Bioengineering 107(5):825-835.

Orman MA, Berthiaume F, Androulakis IP, Ierapetritou MG. 2011a. Pathway analysis of liver metabolism under stressed condition. Journal of Theoretical Biology 272(1):131-140.

Orman MA, Ierapetritou MG, Androulakis IP, Berthiaume F. 2011b. Metabolic response of perfused livers to various oxygenation conditions. Biotechnology and Bioengineering:n/a-n/a.

Osuilleabhain C, Osullivan ST, Kelly JL, Lederer J, Mannick JA, Rodrick ML. 1996. Interleukin-12 treatment restores normal resistance to bacterial challenge after burn injury. Surgery 120(2):290-296.

Otero-Anton E, Gonzalez-Quintela A, Lopez-Soto A, Lopez-Ben S, Llovo J, Perez LF. 2001. Cecal ligation and puncture as a model of sepsis in the rat: Influence of the puncture size on mortality, bacteremia, endotoxemia and tumor necrosis factor alpha levels. European Surgical Research 33(2):77-79.

Ovacik M, Sukumaran S, Almon R, DuBois D, Jusko W, Androulakis I. 2010. Circadian signatures in rat liver: from gene expression to pathways. Bmc Bioinformatics 11(1):540.

Ozbalkan Z, Aslar AK, Yildiz Y, Aksaray S. 2004. Investigation of the course of proinflammatory and anti-inflammatory cytokines after burn sepsis. International Journal of Clinical Practice 58(2):125-129.

Pahl HL. 1999. Activators and target genes of Rel/NF-kappa B transcription factors. Oncogene 18(49):6853-6866.

Pan M, Choudry HA, Epler MJ, Meng QH, Karinch A, Lin CM, Souba W. 2004. Arginine transport in catabolic disease states. Journal of Nutrition 134(10):2826S-2829S.

Paniagua OA, Bryant MB, Panza JA. 2001. Role of endothelial nitric oxide in shear stress-induced vasodilation of human microvasculature - Diminished activity in hypertensive and hypercholesterolemic patients. Circulation 103(13):1752-1758.

Parihar A, Parihar MS, Milner S, Bhat S. 2008. Oxidative stress and anti-oxidative mobilization in burn injury. Burns 34(1):6-17.

Park CH, Valore EV, Waring AJ, Ganz T. 2001. Hepcidin, a urinary antimicrobial peptide synthesized in the liver. J Biol Chem 276(11):7806-10.

Paterson HM, Murphy TJ, Purcell EJ, Shelley O, Kriynovich SJ, Lien E, Mannick JA, Lederer JA. 2003. Injury primes the innate immune system for enhanced Toll-like receptor reactivity. J Immunol 171(3):1473-83.

Paunovic V, Carroll HP, Vandenbroeck K, Gadina M. 2008. Signalling, inflammation and arthritis - Crossed signals: the role of interleukin (IL)-12,-17,-23 and-27 in autoimmunity. Rheumatology 47(6):771-776.

Pawlik TM, Lohmann R, Souba WW, Bode BP. 2000. Hepatic glutamine transporter activation in burn injury: role of amino acids and phosphatidylinositol-3-kinase. Am J Physiol Gastrointest Liver Physiol 278(4):G532-541.

Pearson R, Gonye G, Schwaber J. 2003. Outliers in microarray data analysis. Methods of Microarray Data Analysis III:41-55.

Peter FW, Schuschke DA, Barker JH, Fleishcher-Peter B, Pierangeli S, Vogt PM, Steinau HU. 1999. The effect of severe burn injury on proinflammatory cytokines and leukocyte behavior: its modulation with granulocyte colony-stimulating factor. Burns 25(6):477-486.

Pflanz S, Timans JC, Cheung J, Rosales R, Kanzler H, Gilbert J, Hibbert L, Churakova T, Travis M, Vaisberg E and others. 2002. IL-27, a heterodimeric cytokine composed of EBI3 and p28 protein, induces proliferation of naive CD4(+) T cells. Immunity 16(6):779-90.

Plackett TP, Colantoni A, Heinrich SA, Messingham KA, Gamelli RL, Kovacs EJ. 2007. The early acute phase response after burn injury in mice. J Burn Care Res 28(1):167-72.

Portais J-C, Schuster R, Merle M, Canioni P. 1993. Metabolic flux determination in C6 glioma cells using carbon-13 distribution upon [1-13C]glucose incubation. European Journal of Biochemistry 217(1):457-468.

Price ND, Reed JL, Papin JA, Wiback SJ, Palsson BO. 2003. Network-based analysis of metabolic regulation in the human red blood cell. Journal of Theoretical Biology 225(2):185-194.

Provost A, Bastin G. 2004. Dynamic metabolic modelling under the balanced growth condition. Journal of Process Control 14(7):717-728.

Qian H, Beard DA. 2005. Thermodynamics of stoichiometric biochemical networks in living systems far from equilibrium. Biophysical Chemistry 114(2-3):213-220.

Qian H, Beard DA, Liang S-d. 2003. Stoichiometric network theory for nonequilibrium biochemical systems. European Journal of Biochemistry 270(3):415-421.

Quek L-E, Dietmair S, Krömer JO, Nielsen LK. 2010. Metabolic flux analysis in mammalian cell culture. Metabolic Engineering 12(2):161-171.

Ramakrishna R, Edwards JS, McCulloch A, Palsson BO. 2001. Flux-balance analysis of mitochondrial energy metabolism: consequences of systemic stoichiometric constraints. American Journal of Physiology-Regulatory Integrative and Comparative Physiology 280(3):R695-R704.

Raman K, Chandra N. 2009. Flux balance analysis of biological systems: applications and challenges. Briefings in Bioinformatics 10(4):435-449.

Richens J, Fairclough L, Ghaemmaghami AM, Mahdavi J, Shakib F, Sewell HF. 2007. The detection of ADAM8 protein on cells of the human immune system and the demonstration of its expression on peripheral blood B cells, dendritic cells and monocyte subsets. Immunobiology 212(1):29-38.

Rittirsch D, Huber-Lang MS, Flierl MA, Ward PA. 2009. Immunodesign of experimental sepsis by cecal ligation and puncture. Nature Protocols 4(1):31-36.

Rosmorduc O, Housset C. 2010. Hypoxia: A Link between Fibrogenesis, Angiogenesis, and Carcinogenesis in Liver Disease. Seminars in Liver Disease 30(3):258-270.

Rupenko A, Kruglik O, Morgulis I. 2008. Oxygen supply of rat liver under the conditions of isolated perfusion. Doklady Biological Sciences 418(1):4-6.

Russell L, Garrett-Sinha LA. 2010. Transcription factor Ets-1 in cytokine and chemokine gene regulation. Cytokine 51(3):217-226.

Rutter MT, Zufall RA. 2004. Pathway length and evolutionary constraint in amino acid biosynthesis. Journal of Molecular Evolution 58(2):218-224.

Ryckman C, Vandal K, Rouleau P, Talbot M, Tessier PA. 2003. Proinflammatory activities of S100: proteins S100A8, S100A9, and S100A8/A9 induce neutrophil chemotaxis and adhesion. J Immunol 170(6):3233-42.

Saban MR, Hellmich H, Nguyen NB, Winston J, Hammond TG, Saban R. 2001. Time course of LPS-induced gene expression in a mouse model of genitourinary inflammation. Physiol Genomics 5(3):147-60.

Salkowski CA, Detore G, Franks A, Falk MC, Vogel SN. 1998. Pulmonary and hepatic gene expression following cecal ligation and puncture: monophosphoryl lipid A prophylaxis attenuates sepsis-induced cytokine and chemokine expression and neutrophil infiltration. Infect Immun 66(8):3569-78.

Saltiel AR, Kahn CR. 2001. Insulin signalling and the regulation of glucose and lipid metabolism. Nature 414(6865):799-806.

Santos SS, Leite SB, Sonnewald U, Carrondo MJT, Alves PM. 2007. Stirred vessel cultures of rat brain cells aggregates: Characterization of major metabolic pathways and cell population dynamics. Journal of Neuroscience Research 85(15):3386-3397.

Savinell J, Palsson B. 1992a. Network analysis of intermediary metabolism using linear optimization. II. Interpretation of hybridoma cell metabolism. J Theor Biol 154:455 - 473.

Savinell JM, Palsson BO. 1992b. Network analysis of intermediary metabolism using linear optimization. I. Development of mathematical formalism. Journal of Theoretical Biology 154(4):421-454.

Scheff J, Almon R, DuBois D, Jusko W, Androulakis I. 2011. Assessment of Pharmacologic Area Under the Curve When Baselines are Variable. Pharmaceutical Research:1-9.

Schilling CH, Letscher D, Palsson BO. 2000. Theory for the systemic definition of metabolic pathways and their use in interpreting metabolic function from? A pathway-oriented perspective. Journal of Theoretical Biology 203(3):229-248.

Schon MR, Kollmar O, Wolf S, Schrem H, Matthes M, Akkoc N, Schnoy NC, Neuhaus P. 2001. Liver transplantation after organ preservation with normothermic extracorporeal perfusion. Annals of Surgery 233(1):114-123.

Schwartz JM, Kanehisa M. 2005. A quadratic programming approach for decomposing steady-state metabolic flux distributions onto elementary modes. Bioinformatics 21:204-205.

Schwartz JM, Kanehisa M. 2006. Quantitative elementary mode analysis of metabolic pathways: the example of yeast glycolysis. Bmc Bioinformatics 7.

Schwarz R, Musch P, von Kamp A, Engels B, Schirmer H, Schuster S, Dandekar T. 2005. YANA - a software tool for analyzing flux modes, gene-expression and enzyme activities. Bmc Bioinformatics 6.

Segrè D, Vitkup D, Church GM. 2002. Analysis of optimality in natural and perturbed metabolic networks. Proceedings of the National Academy of Sciences of the United States of America 99(23):15112-15117.

Selleri S, Palazzo M, Deola S, Wang E, Balsari A, Marincola FM, Rumio C. 2008. Induction of pro-inflammatory programs in enteroendocrine cells by the Toll-like receptor agonists flagellin and bacterial LPS. Int Immunol 20(8):961-70.

Sharma NS, Ierapetritou MG, Yarmush ML. 2005. Novel quantitative tools for engineering analysis of hepatocyte cultures in bioartificial liver systems. Biotechnology and Bioengineering 92(3):321-335.

Shelley O, Murphy T, Paterson H, Mannick JA, Lederer JA. 2003. Interaction between the innate and adaptive immune systems is required to survive sepsis and control inflammation after injury. Shock 20(2):123-129.

Shilo S, Pardo M, Aharoni-Simon M, Glibter S, Tirosh O. 2008. Selenium supplementation increases liver MnSOD expression: molecular mechanism for hepato-protection. J Inorg Biochem 102(1):110-8.

Shlomi T, Berkman O, Ruppin E. 2005. Regulatory on/off minimization of metabolic flux changes after genetic perturbations. Proceedings of the National Academy of Sciences of the United States of America 102(21):7695-7700.

Soriano SF, Serrano A, Hernanz-Falcon P, de Ana AM, Monterrubio M, Martinez C, Rodriguez-Frade JM, Mellado M. 2003. Chemokines integrate JAK/STAT and G-protein pathways during chemotaxis and calcium flux responses. European Journal of Immunology 33(5):1328-1333.

Srikrishna G, Panneerselvam K, Westphal V, Abraham V, Varki A, Freeze HH. 2001. Two proteins modulating transendothelial migration of leukocytes recognize novel carboxylated glycans on endothelial cells. J Immunol 166(7):4678-88.

Stassen NA, Breit CM, Norfleet LA, Polk HC. 2003. IL-18 promoter polymorphisms correlate with the development of post-injury sepsis. Surgery 134(2):351-356.

Stelling J, Klamt S, Bettenbrock K, Schuster S, Gilles ED. 2002. Metabolic network structure determines key aspects of functionality and regulation. Nature 420(6912):190-193.

Storey JD, Xiao WZ, Leek JT, Tompkins RG, Davis RW. 2005. Significance analysis of time course microarray experiments. Proceedings of the National Academy of Sciences of the United States of America 102(36):12837-12842.

Struzyna J, Pojda Z, Braun B, Chomicka M, Sobiczewska E, Wrembel J. 1995. Serum Cytokine Levels (Il-4, Il-6, Il-8, G-Csf, Gm-Csf) in Burned Patients. Burns 21(6):437-440.

Summer GJ, Romero-Sandoval EA, Bogen O, Dina OA, Khasar SG, Levine JD. 2008. Proinflammatory cytokines mediating burn-injury pain. Pain 135(1-2):98-107.

Sun W, Hu W, Xu R, Jin J, Szulc ZM, Zhang G, Galadari SH, Obeid LM, Mao C. 2009. Alkaline ceramidase 2 regulates beta1 integrin maturation and cell adhesion. Faseb J 23(2):656-66.

Suzuki T, Hashimoto S, Toyoda N, Nagai S, Yamazaki N, Dong HY, Sakai J, Yamashita T, Nukiwa T, Matsushima K. 2000. Comprehensive gene expression profile of LPS-stimulated human monocytes by SAGE. Blood 96(7):2584-91.

Tamemoto H, Kadowaki T, Tobe K, Yagi T, Sakura H, Hayakawa T, Terauchi Y, Ueki K, Kaburagi Y, Satoh S and others. 1994. Insulin resistance and growth retardation in mice lacking insulin receptor substrate-1. Nature 372(6502):182-6.

Tan K, Tegner J, Ravasi T. 2008. Integrated approaches to uncovering transcription regulatory networks in mammalian cells. Genomics 91(3):219-31.

Tekir SD, Cakir T, Ulgen KO. 2006. Analysis of enzymopathies in the human red blood cells by constraint-based stoichiometric modeling approaches. Computational Biology and Chemistry 30(5):327-338.

Terzer M, Maynard ND, Covert MW, Stelling J. 2009. Genome-scale metabolic networks. Wiley Interdisciplinary Reviews-Systems Biology and Medicine 1(3):285-297.

Thomassen E, Bird TA, Renshaw BR, Kennedy MK, Sims JE. 1998. Binding of interleukin-18 to the interleukin-1 receptor homologous receptor IL-1Rrp1 leads to activation of signaling pathways similar to those used by interleukin-1. Journal of Interferon and Cytokine Research 18(12):1077-1088.

Tian L, White JE, Lin HY, Haran VS, Sacco J, Chikkappa G, Davis FB, Davis PJ, Tsan MF. 1998. Induction of Mn SOD in human monocytes without inflammatory cytokine production by a mutant endotoxin. Am J Physiol 275(3 Pt 1):C740-7.

Tong W, Cao X, Harris S, Sun H, Fang H, Fuscoe J, Harris A, Hong H, Xie Q, Perkins R. 2003. ArrayTrack--supporting toxicogenomic research at the US Food and Drug Administration National Center for Toxicological Research. Environmental health perspectives 111(15):1819-1826.

Tracey KJ. 2002. The inflammatory reflex. Nature 420(6917):853-859.

Tredget EE, Yu YM. 1992. The Metabolic Effects of Thermal-Injury. World Journal of Surgery 16(1):68-79.

Trinh CT, Wlaschin A, Srienc F. 2009. Elementary mode analysis: a useful metabolic pathway analysis tool for characterizing cellular metabolism. Applied Microbiology and Biotechnology 81(5):813-826.

Tsujimoto H, Ono S, Majima T, Kawarabayashi N, Takayama E, Kinoshita M, Seki S, Hiraide H, Moldawer LL, Mochizuki H. 2005. Neutrophil elastase, MIP-2, and TLR-4 expression during human and experimental sepsis. Shock 23(1):39-44.

Twigger S, Lu J, Shimoyama M, Chen D, Pasko D, Long H, Ginster J, Chen CF, Nigam R, Kwitek A and others. 2002. Rat Genome Database (RGD): mapping disease onto the genome. Nucleic Acids Res 30(1):125-8.

Uygun K, Matthew HWT, Huang Y. 2007. Investigation of metabolic objectives in cultured hepatocytes. Biotechnology and Bioengineering 97(3):622-637.

Valenti LM, Mathieu J, Chancerelle Y, De Sousa M, Levacher M, Tuan Dinh-Xuan A, Florentin I. 2005. High levels of endogenous nitric oxide produced after burn injury in rats arrest activated T lymphocytes in the first G1 phase of the cell cycle and then induce their apoptosis. Experimental Cell Research 306(1):150-167.

Varma A, Palsson BO. 1994. Metabolic Flux Balancing - Basic Concepts, Scientific and Practical Use. Bio-Technology 12(10):994-998.

Vemula M, Berthiaume F, Jayaraman A, Yarmush ML. 2004. Expression profiling analysis of the metabolic and inflammatory changes following burn injury in rats. Physiological Genomics 18(1):87-98.

Vincent JL, Sun QH, Dubois MJ. 2002. Clinical trials of immunomodulatory therapies in severe sepsis and septic shock. Clinical Infectious Diseases 34(8):1084-1093.

Vindenes HA, Ulvestad E, Bjerknes R. 1998. Concentrations of cytokines in plasma of patients with large burns: Their relation to time after injury, burn size, inflammatory variables, infection, and outcome. European Journal of Surgery 164(9):647-656.

Wagner A, Fell DA. 2001. The small world inside large metabolic networks. Proceedings of the Royal Society of London Series B-Biological Sciences 268(1478):1803-1810.

Wahl A, Sidorenko Y, Dauner M, Genzel Y, Reichl U. 2008. Metabolic flux model for an anchorage-dependent MDCK cell line: Characteristic growth phases and minimum substrate consumption flux distribution. Biotechnology and Bioengineering 101(1):135-152.

Wahl A, Sidorenko Y, Genzel Y, Reichl U. 2010. Metabolic Flux Distributions of Adherently Growing MDCK Cells in Different Media. In: Noll T, editor. Cells and Culture: Springer Netherlands. p 459-462.

Wallace JL, Ma L. 2001. Inflammatory mediators in gastrointestinal defense and injury. Experimental Biology and Medicine 226(11):1003-1015.

Walley ER, Lukacs NW, Standiford TJ, Strieter RM, Kunkel SL. 1996. Balance of inflammatory cytokines related to severity and mortality of murine sepsis. Infection and Immunity 64(11):4733-4738.

Wen AY, Sakamoto KM, Miller LS. 2010. The Role of the Transcription Factor CREB in Immune Function. Journal of Immunology 185(11):6413-6419.

Whittaker SRF, Winton FR. 1933. The apparent viscosity of blood flowing in the isolated hindlimb of the dog, and its variation with corpuscular concentration. The Journal of Physiology 78(4):339-369.

Wiback SJ, Mahadevan R, Palsson BØ. 2003. Reconstructing metabolic flux vectors from extreme pathways: defining the [alpha]-spectrum. Journal of Theoretical Biology 224(3):313-324.

Wiback SJ, Palsson BO. 2002. Extreme Pathway Analysis of Human Red Blood Cell Metabolism. Biophysical Journal 83(2):808-818.

Wichterman KA, Baue AE, Chaudry IH. 1980. Sepsis and septic shock--a review of laboratory models and a proposal. J Surg Res 29(2):189-201.

Wiechert W. 2001. 13C Metabolic Flux Analysis. Metabolic Engineering 3(3):195-206.

Williams DL, Ha T, Li C, Kalbfleisch JH, Schweitzer J, Vogt W, Browder IW. 2003. Modulation of tissue Toll-like receptor 2 and 4 during the early phases of polymicrobial sepsis correlates with mortality. Crit Care Med 31(6):1808-18.

Windsor JA, Hill GL. 1988. Weight loss with physiologic impairment. A basic indicator of surgical risk. Ann Surg 207(3):290-6.

Wolfe RR, Herndon DN, Jahoor F, Miyoshi H, Wolfe M. 1987. Effect of Severe Burn Injury on Substrate Cycling by Glucose and Fatty-Acids. New England Journal of Medicine 317(7):403-408.

Wolfsegger M. 2007. Establishing Bioequivalence in Serial Sacrifice Designs. Journal of Pharmacokinetics and Pharmacodynamics 34(1):103-113.

Wormald S, Hilton DJ. 2007. The negative regulatory roles of suppressor of cytokine signaling proteins in myeloid signaling pathways. Curr Opin Hematol 14(1):9-15.

Xu G, Sztalryd C, Lu X, Tansey JT, Gan J, Dorward H, Kimmel AR, Londos C. 2005. Post-translational regulation of adipose differentiation-related protein by the ubiquitin/proteasome pathway. J Biol Chem 280(52):42841-7.

Xu M, Smith R, Sadhukhan J. 2008. Optimization of Productivity and Thermodynamic Performance of Metabolic Pathways. Industrial & Engineering Chemistry Research 47(15):5669-5679.

Yamada Y, Endo S, Inada K. 1996. Plasma cytokine levels in patients with severe burn injury - With reference to the relationship between infection and prognosis. Burns 22(8):587-593.

Yamaguchi Y, Yu YM, Zupke C, Yarmush DM, Berthiaume F, Tompkins RG, Yarmush ML. 1997. Effect of burn injury on glucose and nitrogen metabolism in the liver: Preliminary studies in a perfused liver system. Surgery 121(3):295-303.

Yang E, Foteinou PT, King KR, Yarmush ML, Androulakis IP. 2007a. A novel non-overlapping bi-clustering algorithm for network generation using living cell array data. Bioinformatics 23(17):2306-13.

Yang E, Yarmush ML, Androulakis IP. 2009a. Transcription factor network reconstruction using the living cell array. J Theor Biol 256(3):393-407.

Yang H, Roth CM, Ierapetritou MG. 2009b. A rational design approach for amino acid supplementation in hepatocyte culture. Biotechnology and Bioengineering 103(6):1176-1191.

Yang H, Roth CM, Ierapetritou MG. 2011. Analysis of Amino Acid Supplementation Effects on Hepatocyte Cultures Using Flux Balance Analysis. OMICS: A Journal of Integrative Biology.

Yang J, Dong LW, Tang CS, Liu MS. 1999. Transcriptional and posttranscriptional regulation of beta(2)-adrenergic receptor gene in rat liver during sepsis. American Journal of Physiology-Regulatory Integrative and Comparative Physiology 277(1):R132-R139.

Yang S, Guo X, Yang YC, Papcunik D, Heckman C, Hooke J, Shriver CD, Liebman MN, Hu H. 2007b. Detecting outlier microarray arrays by correlation and percentage of outliers spots. Cancer Inform 2:351-60.

Yarmush DM, MacDonald AD, Foy BD, Berthiaume F, Tompkins RG, Yarmush ML. 1999. Cutaneous burn injury alters relative tricarboxylic acid cycle fluxes in rat liver. Journal of Burn Care & Rehabilitation 20(4):292-302.

Yoda E, Hachisu K, Taketomi Y, Yoshida K, Nakamura M, Ikeda K, Taguchi R, Nakatani Y, Kuwata H, Murakami M and others. 2010. Mitochondrial dysfunction and reduced prostaglandin synthesis in skeletal muscle of Group VIB

Ca2+-independent phospholipase A2gamma-deficient mice. J Lipid Res 51(10):3003-15.

Yokoyama T, Banta S, Berthiaume F, Nagrath D, Tompkins RG, Yarmush ML. 2005. Evolution of intrahepatic carbon, nitrogen, and energy metabolism in a D-galactosamine-induced rat liver failure model. Metabolic Engineering 7(2):88-103.

Yoon J, Si Y, Nolan R, Lee K. 2007. Modular decomposition of metabolic reaction networks based on flux analysis and pathway projection. Bioinformatics 23(18):2433-2440.

Youn BS, Jang IK, Broxmeyer HE, Cooper S, Jenkins NA, Gilbert DJ, Copeland NG, Elick TA, Fraser MJ, Jr., Kwon BS. 1995. A novel chemokine, macrophage inflammatory protein-related protein-2, inhibits colony formation of bone marrow myeloid progenitors. J Immunol 155(5):2661-7.

Zamboni N. 13C metabolic flux analysis in complex systems. Current Opinion in Biotechnology In Press, Corrected Proof.

Zhang P, Zhong Q, Bagby GJ, Nelson S. 2007. Alcohol intoxication inhibits pulmonary S100A8 and S100A9 expression in rats challenged with intratracheal lipopolysaccharide. Alcohol Clin Exp Res 31(1):113-21.

Zhao QY, Kurata H. 2009. Maximum entropy decomposition of flux distribution at steady state to elementary modes. Journal of Bioscience and Bioengineering 107(1):84-89.

Zhou X, Fragala MS, McElhaney JE, Kuchel GA. 2010. Conceptual and methodological issues relevant to cytokine and inflammatory marker measurements in clinical research. Current Opinion in Clinical Nutrition and Metabolic Care 13(5):541-547.